Department of Precision and Microsystems Engineering

Temperature variation effects on electrostrictive actuators and its quasi-static compensation

Aditya Singh

Report no : 2019.025
Coach : Hassan HosseinNia
Professor : Jo Spronck
Specialisation : Mechatronic System Design
Type of report : M.Sc. Thesis
Date : 26/08/2019

Temperature variation effects on electrostrictive actuators and its quasi-static compensation

Master of Science Thesis

For the degree of Master of Science in Mechanical Engineering at Delft University of Technology

Aditya Singh

Student Number: 4736354

Supervisors:	Ir. Bas Jansen	ASML
	Dr. Ir S. Hassan HosseinNia	TU Delft
	Ir. Ruben Vandervelden	ASML
	Dr. Ir. Andres Hunt	TU Delft
Thesis committee:	prof.ir. J.W. (Jo) Spronck	TU Delft
	Dr.Ir S. Hassan HosseinNia	TU Delft
	Ir. Bas Jansen	ASML
	Dr.Ir. Andres Hunt	TU Delft
	Dr.Ir. J.F.L. Goosen (Hans)	TU Delft

August 14, 2019

Faculty of Mechanical, Maritime and Materials Engineering (3mE) · Delft University of Technology

The work in this thesis was done at Optical Column Mechatronics Group at ASML, Veldhoven.

Abstract

Deformable mirrors are used for changing the wavefront of the reflected light by using one or more actuators behind the mirror to physically deform it. This application is widely used in telescopes to compensate for atmospheric aberrations using a feedback wavefront sensor. Recent advances in lithography process require more precise wavefront control than ever, and deformable mirrors are being considered as a suitable optical unit in the optical column of lithography systems. Using electrostrictive materials for the actuation provides benefits like less hysteresis, no creep, and fast response time. One major limiting factor in the use of such materials is the high sensitivity of strain response to temperature. Due to application constraints a position sensor is not available for the position control. This leads to a requirement of temperature dependent strain-field model in a feedforward control scheme to compensate for the temperature changes and predict the position to sufficient accuracy. In this thesis, different electrostrictive models are explored, and through high frequency impedance measurements and precise quasi-static strain-field experiments, actuator response is analyzed and model parameters are estimated. The parameters are then used in a feedforward control, with temperature sensor, to compensate for the temperature change resulting in decrease of temperature induced strain variation by 75%-87%. Furthermore, an optimum voltage region is identified for maximum actuation performance with compensation of temperature induced strain variation. Lastly, a novel temperature self-sensing approach is explored for which a patent application is filed.

Table of Contents

Symbols xi

Preface xiii

Acknowledgements xv

1 Introduction 1
1-1 Background . . . 1
1-1-1 Motivation . . . 3
1-2 State of the Art . . . 3
1-2-1 Outline . . . 3
1-2-2 Effect of Voltage . . . 6
1-2-3 Effect of Frequency of Voltage . . . 8
1-2-4 Effect of Material Composition . . . 10
1-2-5 Effect of Temperature . . . 11
1-2-6 Effect of Aging . . . 14
1-3 Measurement Methods . . . 16
1-4 Summary and Conclusions . . . 16
1-4-1 Research Gap . . . 17
1-4-2 Research Objective . . . 17

2 Model Analysis 19
2-1 Outline . . . 19
2-2 Linear Impedance Model . . . 19
2-2-1 Conclusions . . . 25
2-3 Nonlinear Analysis . . . 26
2-3-1 Models . . . 26
2-3-2 Linear analysis using Hyperbolic model . . . 30
2-3-3 Conclusions . . . 31
2-4 Summary . . . 32

3 Experiments and Analysis **35**
3-1 Outline . . . 35
3-2 Impedance Measurement . . . 35
3-2-1 Experiment Setup . . . 36
3-2-2 Experiment Results and Analysis . . . 37
3-2-3 Conclusions . . . 41
3-3 Quasi-static strain-electric field measurement . . . 42
3-3-1 Experiment Setup . . . 42
3-3-2 Experiment Results and Analysis . . . 44
3-3-3 Linearized hyperbolic model analysis using experiment data . . . 50
3-4 Feedforward Control . . . 54
3-4-1 Inverse Feedforward control scheme . . . 54
3-4-2 Observer based feedforward control scheme . . . 55
3-4-3 Linearized Hyperbolic model based feedforward control scheme . . . 56

4 Results **59**
4-1 Compensation of strain variation due to temperature change without DC bias . . . 59
4-2 Compensation of strain variation due to temperature change at DC bias . . . 61

5 Conclusions and Future Recommendations **65**

A Appendix A **69**

B Appendix B **75**
B-1 Measurement Instruments and Calibration . . . 75
B-1-1 Interferometer: Actuator displacement sensor . . . 75
B-1-2 Peltier Heating/Cooling device . . . 77
B-1-3 Speedgoat Data Acquisition system (Target PC+ I/O board) . . . 78
B-1-4 Amplifier . . . 78
B-1-5 Bode 100 Signal Generator . . . 79
B-2 Post-Processing . . . 80
B-2-1 Impedance Measurements . . . 80
B-2-2 Quasi-static strain-field measurements . . . 81

List of Figures

1-1 ASML machine . . . 1
1-2 Actuator heating . . . 2
1-3 Concept of temperature compensation with feedforward control . . . 2
1-4 Linear dielectric behavior . . . 4
1-5 Nonlinear dielectric response . . . 5
1-6 crystal structure of PMN . . . 5
1-7 PMN-PT crystal structure . . . 6
1-8 Linear dielectric,paraelectric, ferroelectric . . . 6
1-9 PMN-PT response to voltage . . . 7
1-10 permittivity variation with frequency . . . 8
1-11 variation of d with frequency . . . 9
1-12 Variation of dielectric constant with material composition . . . 10
1-13 effect of PT content composition . . . 11
1-14 variation of deformation with temperature . . . 12
1-15 thermal expansion table . . . 12
1-16 variation of depolarization temperature with composition . . . 13
1-17 polarization harmonic variation with aging . . . 14
1-18 polarization changes with field with aging . . . 15
1-19 reduction in d coeffficient with aging . . . 15

2-1 Electromechanical model of electrostrictive actuator . . . 20
2-2 impedance transfer function . . . 23
2-3 Effect of stiffness variation on impedance . . . 24
2-4 change in impedance thermal expansion . . . 24
2-5 Variation of impedance response frequency with changing DC bias . . . 25
2-6 Variation of resonance frequency with DC bias . . . 25

2-7 hyperbolic quadratic model . . . 28
2-8 Error between hyperbolic and quadratic model with varying k . . . 28
2-9 Response change with change in k and M . . . 29
2-10 Change in k vs same change in M . . . 29
2-11 Deformation voltage for different models . . . 30
2-12 Variation of slope with voltage . . . 31
2-13 Overview of electrostrictive models used in thesis . . . 33

3-1 Impedance test setup . . . 36
3-2 Transverse and thickness mode visualized . . . 37
3-3 impedance measurement full raw . . . 37
3-4 model parameter variation with temperature . . . 38
3-5 Variation of model parameters with DC bias . . . 39
3-6 Variation of resonance frequency with temperature at 100V DC bias . . . 40
3-7 Variation of resonance frequency with DC bias . . . 41
3-8 Experiment setup schematic quasi static experiment . . . 43
3-9 Side view of quasi static experiment setup . . . 43
3-10 Deformation vs Voltage for 100V amplitude . . . 44
3-11 Deformation vs Voltage curves with varying temperature for 150V amplitude . . . 44
3-12 Deformation vs Voltage curves with varying temperature for amplitude of 350V . . . 45
3-13 FFT with 100V amplitude . . . 45
3-14 FFT response with 150V amplitude . . . 46
3-15 FFT response with 350V amplitude . . . 46
3-16 100V harmonic contribution . . . 47
3-17 150V harmonic . . . 47
3-18 350V amplitude . . . 48
3-19 variation electrostrictive coefficient all voltage . . . 48
3-20 variation of relaxation coefficient with temperature . . . 49
3-21 Fitted lines of M with predictive bounds . . . 49
3-22 Compensation idea . . . 50
3-23 Linear and quadratic fit of M and k with temperature . . . 51
3-24 Variation of d with voltage and dmax variation . . . 52
3-25 variation of voltage at dmax with temperature . . . 52
3-26 Temperature variation compensation at Vmax . . . 53
3-27 Error with different AC voltages . . . 53
3-28 Error for assuming voltage invariant slope at 30V amplitude . . . 54
3-29 Feedforward control: Inverse model . . . 54
3-30 observer based control scheme . . . 56
3-31 Simulation result using observer based scheme and hyperbolic model . . . 56
3-32 linearized hyperbolic model control scheme . . . 57

4-1 uncompensated without DC bias 60
4-2 Compensated without DC bias 60
4-3 Error without DC bias 61
4-4 Uncompensated result with DC bias 62
4-5 Compensated result with DC Bias 63
4-6 Error with DC bias 63
4-7 temperature variation DC biased compensation 64

A-1 Electromechanical model 70

B-1 Interferometer working principle 76
B-2 Interferometer controller data acquisition 76
B-3 Amplifier gain frequency response 78
B-4 Impedance response calculation 80
B-5 deformation time data 81
B-6 Drift in the measurement 82
B-7 averaging error 82
B-8 Raw temperature and low pass filtered 83
B-9 step response 84
B-10 Triangle wave response 84
B-11 Front view experiment setup 85
B-12 Zoom in on the actuators and laser probes 85
B-13 Other instruments in the experiment setup 86

List of Tables

3-1 Sensitivity of model parameters to temperature and voltage 38
3-2 Sensitivity of resonance and anti-resonance frequencies to DC bias and temperature 41

Symbols

The list below defines the symbols used unless otherwise stated in the report.

z	Actuator displacement (m)
P	Polarization ($\frac{C}{m^2}$)
ϵ	Dielectric permittivity ($\frac{F}{m}$)
κ	Dielectric constant
x	Strain
M	Field based electrostrictive coefficient ($\frac{m^2}{V^2}$)
k	Relaxation parameter ($\frac{m}{V}$)
y	Fractional content in material composition
P_s	Satuaration polarization ($\frac{C}{m^2}$)
Q	Charge based electrostrictive coefficient ($\frac{m^4}{C^2}$)
T	Stress ($\frac{N}{m^2}$)
s	Compliance of actuator ($\frac{m}{N}$)
ϵ_{max}	Maximum permittivity ($\frac{F}{m}$)
T_m	Temperature at dielectric permittivity maximum ($^\circ C$)
ω	Angular frequency ($\frac{rad}{s}$)
T_F	Static freezing temperature at which remnant polarization tends to 0 ($^\circ C$)
d	Effective piezoelectric coefficient ($\frac{m}{V}$)
T_c	Curie temperature ($^\circ C$)
T_d	Depolarization temperature ($^\circ C$)
T_f	Dielectric frequency independence temperature ($^\circ C$)
s_E	Compliance at constant electric field ($\frac{m}{N}$)
D	Displacement Current ($\frac{C}{m^2}$)
f_p	Internal force generated in the actuator (N)
L	Actuator thickness (m)
C_p	Capacitance (F)
V_{ac}	AC voltage (V)
V_{dc}	DC bias (V)
c	Damping coefficient ($\frac{Ns}{m}$)
k^E	Stiffness at constant electric field ($\frac{N}{m}$)
d_{max}	Maximum effective piezoelectric coefficient ($\frac{m}{V}$)
V_{max}	Voltage at maximum effective piezoelectric coefficient value (V)

Preface

This document is part of the master programme and is dedicated towards complete fulfillment for the degree of Master of Science in Mechanical Engineering at Precision and Microsystems department at TU Delft with focus on Mechatronic System Design. The thesis has been done at the Optical Column Mechatronics Department and associated research labs at ASML Netherlands B.V, Veldhoven campus.

Acknowledgements

I would like to thank my daily supervisors, Bas Jansen and Ruben Vandervelden for being such excellent mentors throughout the duration of the thesis. I would also like to thank Hassan HosseinNia and Andres Hunt for their ever ready support and supervision throughout the year. Andres was especially helpful in providing critical feedback that helped me improve my work. My special thanks to Roland Valkenburg and Robert Van der Kall for providing sensors and heaters for the experiments, and Samer Abdelmoeti, along with other people in Optical Column Mechatronics Group, for providing help and support whenever it was needed. Last but not the least, I would like to thank my family and friends for their unwavering support and motivation during difficult times during this project.

"The more I see, the less I know for sure."
— *John Lennon*

Chapter 1

Introduction

1-1 Background

The growth in semiconductor chip industry has spawned a revolution in multiple sectors such as mobile phones, computers and IoT devices. The lithography process is one of the main steps in manufacturing chips with increasingly complex architecture and smaller size. With ever increasing demand of making these chips smaller, the requirement of high precision has never been more. Lithography process involves passing UV light through an array of lenses and mirrors in a precise way for chip manufacturing. To improve the control over the precision of light's wavefront, an additional optical element was needed. For this purpose a deformable mirror assembly (fig. 1-1) was deemed suitable to be installed in the machine by ASML.

Figure 1-1: ASML machine with lens arrangement. Figure adapted from [1]

The deformable mirror contains an actuator grid behind the mirror surface to control the topography of the mirror. By modifying the mirror topography, the reflected wavefront can be changed with a high degree of control. The actuator grid behind the mirror needs to deform in a precise manner in order to have a predictable mirror deformation. This in turn would help in correcting the error in wavefront, resulting in more precise chip manufacturing.

Due to multiple constraints in complex lithographic tools, it is often not possible to have local position sensing in the mirror assembly. The lack of position sensing meant that position-feedback control of these actuators was not possible. This means only the actuators having low hysteresis, low creep and having accurate and fast response, would work best in the current setup. One of the actuators that suits these needs is the PMN-PT based electrostrictive ceramic actuator [2]. Electrostrictive actuators have been also previously used for deformable mirror applications [3][4][5]. The main challenges in using PMN-PT electrostrictive actuator for position control are:

- The response of the actuator is highly nonlinear
- The actuator has high temperature sensitivity. This is a challegen as due to UV light, the mirror heats up and subsequently heats the actuator grid raising its temperature as shown in fig. 1-2.Consequently, the temperature induced strain variations are also high that affect the mirror deformation.

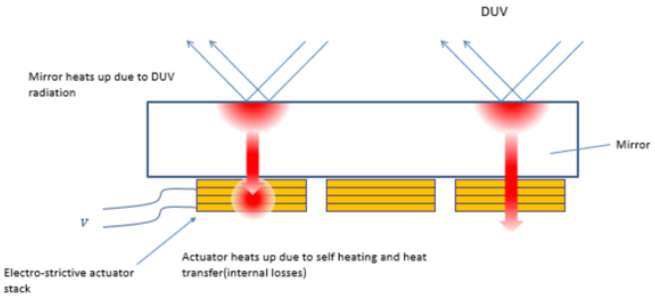

Figure 1-2: Actuator heating due to heat transfer from mirror

Despite the mentioned challenges, electrostrictor is a favorable type of actuator compared to piezoelectric actuator as it has extremely small hysteresis non-linearity above a certain temperature while having large strain energy. As the hysteresis type of non-linearity is challenging to compensate in open loop configuration, the absence of hysteresis above a certain temperature makes these electrostrictors suitable for a feedforward application. As it is possible to have temperature sensors on the actuator grid, a "feedback" with temperature sensing could be used to correct for the temperature induced variations in the actuator response.

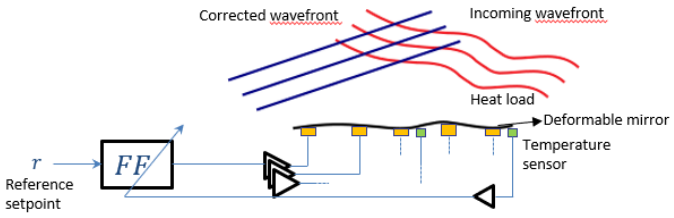

Figure 1-3: Temperature compensation with feedforward control concept

1-1-1 Motivation

The theory of electrostriction has been investigated quite well during the past few decades. Though many materials have been studied for actuator applications, PMN-PT (Lead Magnesium Niobate-Lead Titanate) has been found to be one of the most effective electrostrictors. The deformable mirror application at ASML requires these actuators to deliver precise position control without position sensing and in the presence of temperature disturbances. For such a requirement, a precise model of PMN-PT electrostrictive actuator is needed. The nonlinear behavior of this material has been researched well but its application to position control has only had preliminary research. Also, as temperature disturbances can cause substantial changes in the actuator response, an accurate actuator model, that contains temperature dependent parameters, has not yet been formulated for position control applications. This analysis and experimentation is needed due to the absence of position sensor in the deformable mirror system, because of which feedback control of the actuator is not possible. Therefore, there is also a need for suitable feedforward control schemes that achieve position control in real time with active temperature compensation as shown in fig. 1-3.

As the actuator response is nonlinear, a high performance region of working in the presence of temperature induced strain variation has not yet been identified where calibration and feedforward control could be implemented in the easiest way. For this high performance operation of the actuator, along with compensation of temperature induced strain variation, a suitable model must be formulated for devising appropriate feedforward scheme. Understanding and formulating this would lead to enabling real time temperature compensation of these actuators, that will help in achieving desired position control and therefore precision actuation of deformable mirror.

Thus, this thesis has broadly two-fold goals:

1.) To characterize the nonlinearities and performance in the electrostrictive response with varying voltage and temperature from the mindset of position control application.

2.) Model the response changes due to temperature change in the operating frequency band (0.1-100 Hz) and using the resultant model, devise a feedforward controller that can maintain a position.

The material is so far not been studied within ASML for position control application with high position accuracy. Therefore a thorough understanding of the state of the art is required. Through this knowledge, actuator response to composition, voltage, frequency and temperature changes would be understood and proper operating parameter bounds would be identified. Based on the literature review, a research gap would be identified.

1-2 State of the Art

1-2-1 Outline

This section is focused on discussing the relevant properties and models of electrostrictive PMN-PT actuator in the current state of the art. The dependency of strain on voltage, frequency of voltage, temperature, material composition and aging process is discussed and its importance on tuning the actuator behavior is also highlighted. As the analysis is done in

stress free conditions, the variation due to compression stress would not be discussed. The purpose of this study is to understand which actuator properties are most important for operation and how can they be tuned in order to get maximum performance under the given operating conditions. This in turn will help in devising an effective feedforward control.

Electrostriction is a property of any insulating material. In the most basic sense, it is the displacement of the charges in a dielectric. This displacement of charges translates to polarization of the overall material which translates into a displacement. The displacement is related to the polarization with a square law [6]. As the polarization increases with increasing dielectric constant, the strain is usually small for materials with low dielectric constants. Moreover, for linear dielectric materials, which includes almost all insulating materials, the induced polarization is directly proportional to the applied electric field.

$$P = \epsilon E \tag{1-1}$$

where P is the induced polarization ($\frac{C}{m^2}$), ϵ is the dielectric permittivity ($\frac{F}{m}$) and E is the applied electric field ($\frac{V}{m}$). This results in a quadratic strain-electric field curve as seen in eq. (1-1).

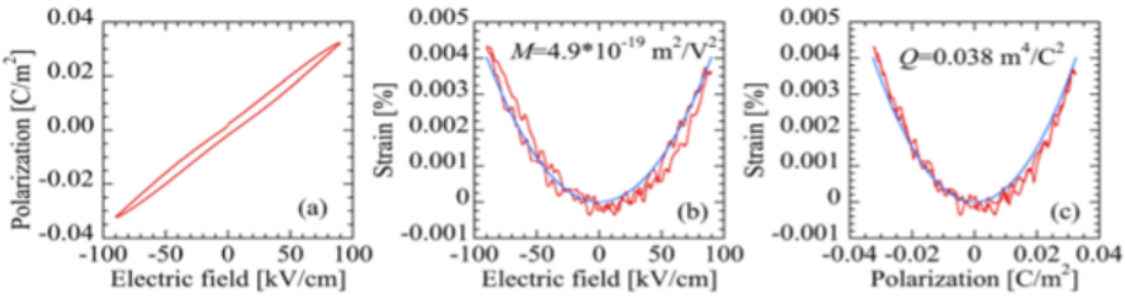

Figure 1-4: Linear dielectric characteristics [7]

The quadratic relation can be written as

$$x = ME^2 \quad [8] \tag{1-2}$$

where x is the strain and M is the electric field based electrostrictive coefficient ($\frac{m^2}{V^2}$). The strain response of a normal linear dielectric material is extremely small due to its small dielectric constant. Nonlinear dielectrics like PMN-PT and few others have a nonlinear relation between polarization and applied electric field. For a strain-field response this translates to a non-linearity different from quadratic non-linearity as seen in fig. 1-5.

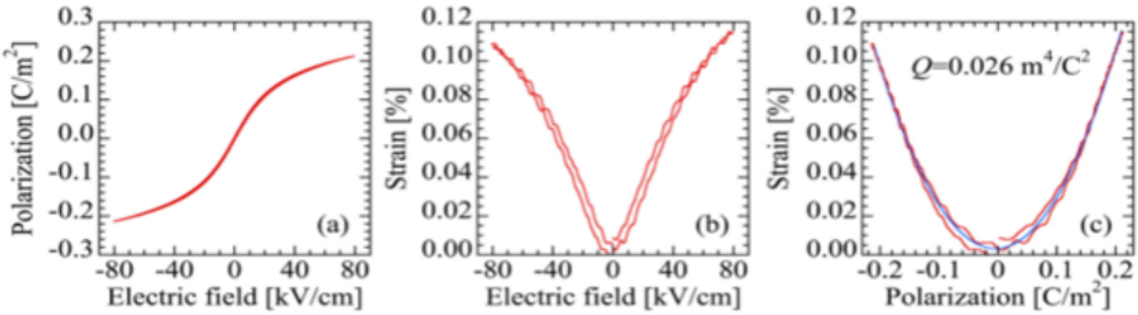

Figure 1-5: Nonlinear Dielectric response characteristics [7]

On the other hand, the strain has quadratic nonlinearity with induced polarization in both linear and nonlinear dielectric materials [9]. The higher order non-linearity in the nonlinear dielectric materials like PMN-PT is associated with its structure at nanometer level (PMN: fig. 1-7, PMN-PT: fig. 1-6). The compound PMN has rich Magnesium(Mg) and Niobium (Nb) regions [8]. These regions are highly inhomogenous which results in fluctuations in polarization due to temperature and electric field. Due to nanoscale size of these inhomogeneties, and due to strong coupling of the dipoles in Niobium rich region instead of lead dominated crystal lattice, an unstable structure is formed. This results in a system that responds strongly to temperature, stress and electric fields giving large strain and dielectric responses. Due to this unique feature of having polar nano-domains, these materials exhibit frequency dispersion of dielectric permittivity and loss. This dispersion is called dielectric relaxation and hence the materials are termed relaxor ferroelectrics [10].

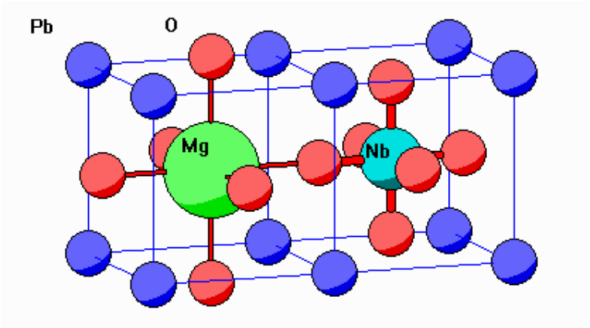

Figure 1-6: Crystal Structure of PMN material [11]

Above a certain temperature, depending on composition, relaxor ferroelectric are dominated by paraelectric phase (fig. 1-8). This results in low hysteresis, but large electrostrictive strains [13]. The low hysteresis again arises from the nano-domains associated with the paraelectric phase. As the domain size grows, hysteresis increases due to bigger domain wall motion [14]. Hysteresis creates servo-displacement problems which can be corrected in feedback systems, but in feed-forward systems hysteresis needs to be as small as possible in order to have good position control.

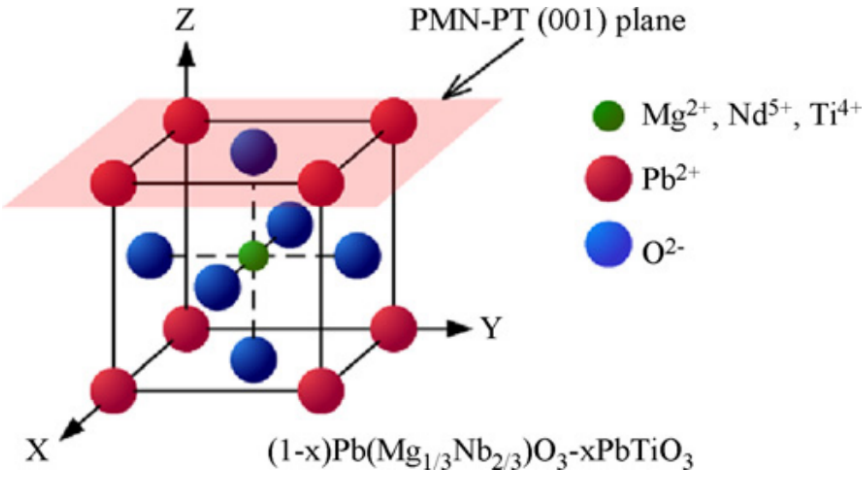

Figure 1-7: Crystal structure of PMN-PT [12]

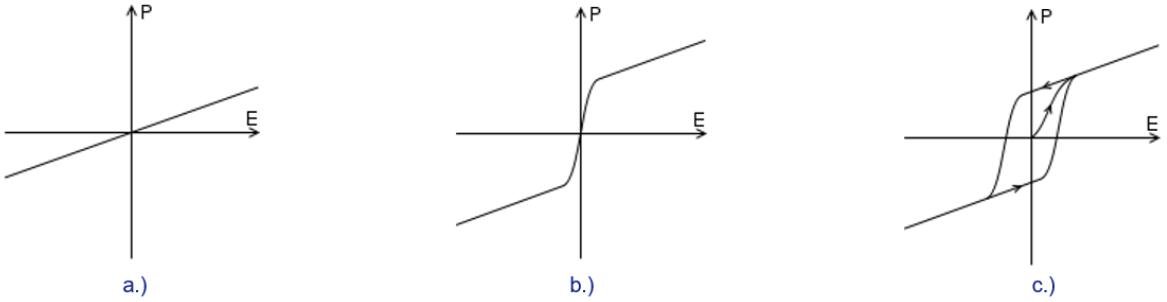

Figure 1-8: a.) Linear Dielectric, b.) Paraelectric, c.) Ferroelectric , polarization to field response [15]

In the subsequent sub-sections the state of the art on the variation of actuator parameters with voltage, frequency of the applied voltage, material composition and temperature is discussed.

1-2-2 Effect of Voltage

PMN-PT or specifically, (1-y)PMN-yPT ceramic (where y is the composition fraction), is electrostrictive in nature and hence has an even strain response to electric field [13] ,[16], [17]. Due to its abnormally large dielectric constant [18], the material is highly polarized on application of electric field/voltage. The domain re-alignment due to this high polarization translates into a macroscopic strain. Due to the un-poled nature of the material, domains re-align by the same amount irrespective of the direction of the applied electric field/voltage, resulting in net expansion of the material.
The PMN-PT has an approximate quadratic strain-field response at low electric field [19] as shown in eq. (1-2). As the applied electric field is increased, higher even-harmonics occur in the actuator response which eventually saturate [20] as shown in fig. 1-9.

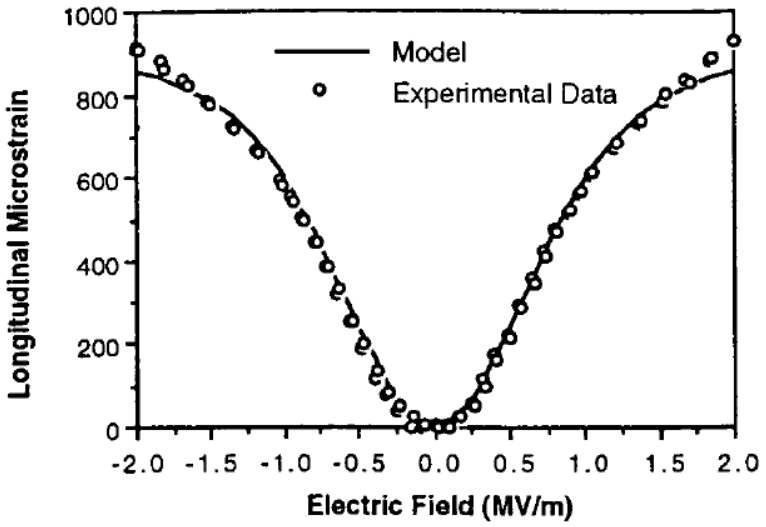

Figure 1-9: Response of PMN-PT to applied electric field [14]

As the response shows higher even harmonics, a model involving all the even harmonics was proposed by Hom and Shankar [21] in the form of hyperbolic relation. The relation is a charge based model of electrostriction (eq. (1-5)). The foundation for the model is based on nonlinear hyperbolic relation between induced polarization and applied electric field as described in eq. (1-3). The polarization has a saturation behavior with increasing electric field.

$$P = P_s tanh(kE) \tag{1-3}$$

Using 1-3 the constitutive equation under constant stress can be written in the form of implicit nonlinear relation between polarization and electric field,

$$E = -QPT + \frac{1}{k} tanh^{-1}(\frac{P}{P_s}) \tag{1-4}$$

$$x = sT + QP^2 \tag{1-5}$$

where Q is the charge based electrostrictive coefficient($\frac{m^4}{C^2}$), P_s is the saturation polarization ($\frac{C}{m}$), k is the relaxation parameter ($\frac{m}{V}$), s is the material compliance ($\frac{1}{Pa}$), T is the stress ($\frac{N}{m^2}$).

Using the stress free response and substituting polarization term from eq. (1-3) in eq. (1-5),

$$x = QP_s^2 tanh^2(kE) \tag{1-6}$$

The eq. (1-6) describes the variation of strain with electric field for the whole range of actuation for electrostrictive PMN-PT materials. The model does not describe hysteresis and assumes the parameters to be independent of voltage.

1-2-3 Effect of Frequency of Voltage

Relaxor ferroelectrics show frequency dispersion effects in dielectric permittivity and corresponding loss coefficient. The change in frequency affects the response characteristics as it shifts the permittivity vs temperature curves. Due to this effect, the maximum dielectric constant drops and the corresponding temperature, T_m shifts to higher temperatures as shown in fig. 1-10.

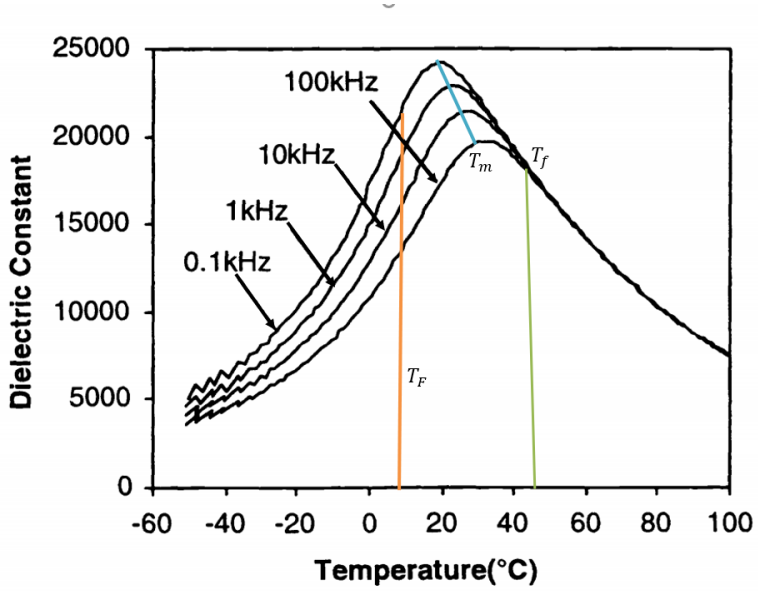

Figure 1-10: Variation of dielectric permittivity with frequency. Figure adapted from [6]

Changes in dielectric constant directly affect the strain response of the material. Increase in frequency of applied voltage results in T_m shifting to higher temperatures, where material becomes more normal ferroelectric at the reference temperature. This also results in increased hysteresis.
The frequency dispersion of the dielectric permittivity and its variation with temperature near T_m can be modeled using Smolensky's work [22].

$$\frac{1}{\epsilon(T,\omega)} = \frac{1}{\epsilon_{max}(\omega)}\left(1 + \frac{(T-T_m)^2}{2\delta^2}\right) \tag{1-7}$$

where, ϵ is the dielectric permittivity at the temperature T, ϵ_{max} is the maximum dielectric constant across the temperature range, T_m is the temperature at maximum dielectric constant and δ signifies the degree of dielectric relaxation or the broadness of the dielectric peak.

At a certain temperature above T_m, the frequency dependency of the dielectric constant, and therefore electrostrictive parameters, becomes negligible. This frequency dependence or dispersion is maximum at the maximum dielectric constant [18], ϵ_m, for temperatures lower than T_f, as shown in fig. 1-10. Operating the material above that temperature, T_f, makes the material parameters independent of operating frequency.

Earlier, the variation of dielectric constant with temperature was described using Smolensky's equation 1-7. The frequency of operation can be obtained using Volget-Fulcher equation

[23]that uses the Maximum dielectric temperature (T_m) and Freezing temperature (T_F) under low electric field conditions.

$$f = f_0 exp\Big(\frac{-E_A}{k_B(T_m - T_F)}\Big) \tag{1-8}$$

where, f is the applied frequency (Hz), f_0 is a pre-exponential factor, T_m is the maximum dielectric temperature (K), and T_F is the freezing temperature (K), E_A is the activation energy that describes relaxation process (J), k_B is the Boltzmann constant (JK^{-1})

The frequency invariance in the deformation is shown by the experiments done by Ren and Masys [24] using electromechanical properties. In the fig. 1-11, experiment is done at room temperature($\approx 20°C$) with materials that have T_m of 15°C (PMN-0.1PT or PMN-15), and T_m of 38°C (PMN-0.15PT or PMN-38). At room temperature, PMN-15 shows frequency independence with respect to electrostrictive parameters as room temperature is more than T_m . The effect of temperature is elaborated more clearly in the section 1-2-5.

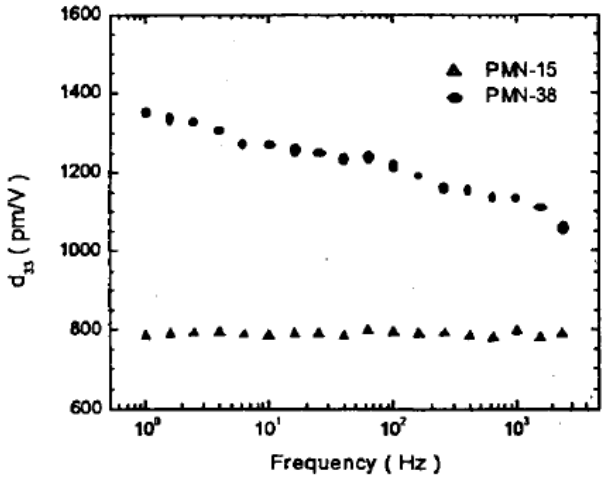

Figure 1-11: Variation of effective piezoelectric coefficient at a bias electric field [24]

In the fig. 1-11, the d_{33} is the effective piezoelectric coefficient for an electrostrictive material at DC bias in direction of the applied field and deformation (33). For electrostriction, d can be understood as effective piezoelectric coefficient at a certain DC bias. It can be shown that,

$$x = dE, \quad \text{Piezoelectric stress free equation} \tag{1-9}$$

$$x = ME^2, \quad \text{Electrostrictive stress free equation} \tag{1-10}$$

Differentiating eq. (1-10) with E at E_{dc} will give the response variation around the DC bias. With small enough actuating field, the strain response can be considered linear around the operating DC bias.

$$x_{dc} = \Big(2ME_{dc}\Big)E \tag{1-11}$$

Comparing eq. (1-9) with eq. (1-11),

$$d = 2ME_{dc} \tag{1-12}$$

This shows that the electrostrictive response can be tuned to piezoelectric response around a specific DC bias. The electromechanical coupling coefficient is voltage dependent in that case.

1-2-4 Effect of Material Composition

(1-y)PMN-yPT is a solid solution of relaxor ferroelectric PMN and normal ferroelectric material PT (Lead Titanate). Normal ferroelectric materials have a strong memory effect and operate far from their Curie Temperature (T_c). Relaxor ferroelectrics exhibit paraelectric effect and hence are hysteresis free. Addition of PT content increases the dielectric constant of the resulting solid solution but only up until 35% PT. The composition around 35 % is called morphotropic phase boundary in phase plot of the solid solution. Above that PT composition, the dielectric constant decreases and therefore strain response to electric field reduces [25] as shown in fig. 1-13. The ideal composition of the (1-y)PMN-yPT should be around the point when the dielectric constant is high enough to provide usable strain with minimal hysteresis. As shown in the fig. 1-13, that appears to be around 10-15% PT content [26].

The PT content fixes the T_m of the electrostrictive material at a certain frequency. This can be used to tune the T_m to be less than the operating temperature for the frequency range of operation. This effect is shown in the fig. 1-12

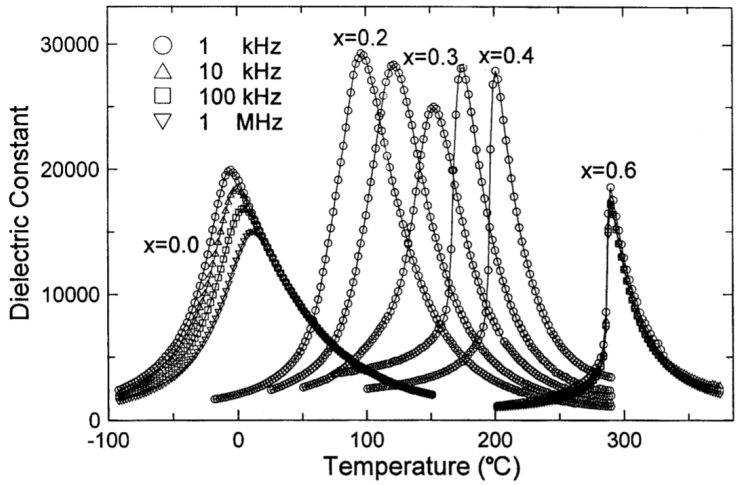

Figure 1-12: Variation of dielectric constant with material composition [26]. Here, x is the fraction of PT content in (1-y)PMN-yPT.

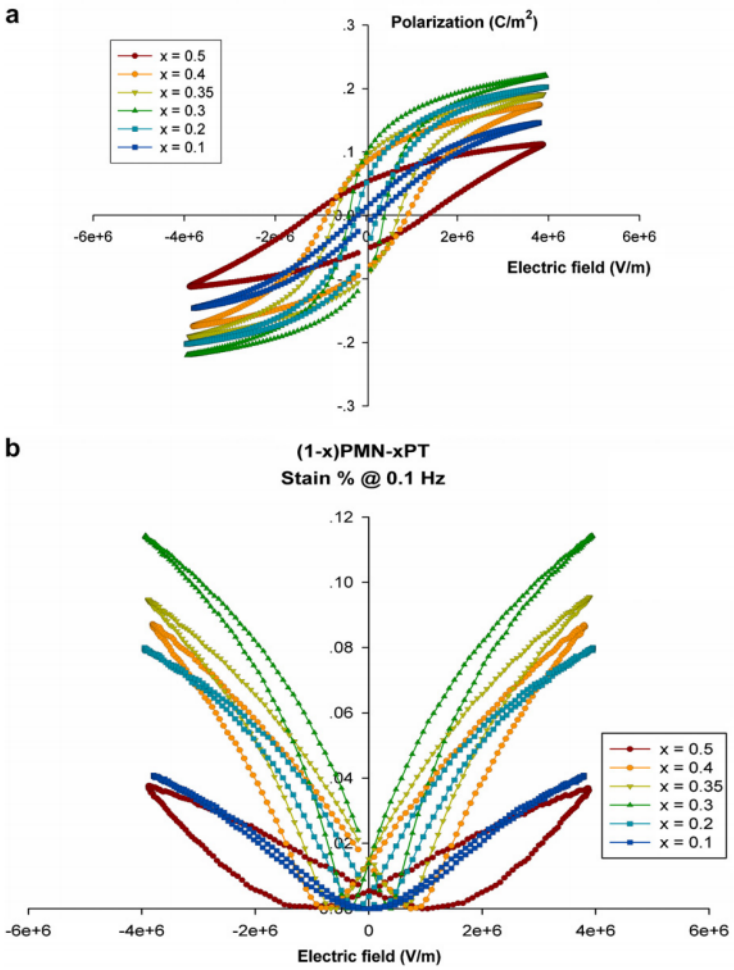

Figure 1-13: Effect of material composition [25] on a.) polarization and b.) strain response

1-2-5 Effect of Temperature

The study of temperature variation has been extensively studied in the domain of dielectric response [27], [28], strain response in quasi-static [29], [30] and high frequency sonar applications [31]. At quasi-static frequencies, due to changing temperatures, the strain response of the actuator changes as shown in fig. 1-14. For high frequency applications, a microscopic temperature model was created by Hom and Shankar [31] and the effect of hysteresis was studied to characterize self-heating of the electrostrictive actuator. A microscopic temperature constitutive model was developed by Hom and Smith for the relaxor ferroelectrics by using hysteresis as the source of temperature generation [32]. This model focused on quantifying saturation polarization and material distribution as function of temperature [32]. The result is an ODE model that predicts nonlinear behavior of the material and hysteresis. Though the model predicts hysteresis with changing temperature, it has to be fitted to the observed data to get the varying parameters. These parameters do not all provide a functional dependency on temperature. Moreover the model is dependent on microscopic parameters that are hard to determine with sufficient accuracy for different PMN-PT composition and phases.

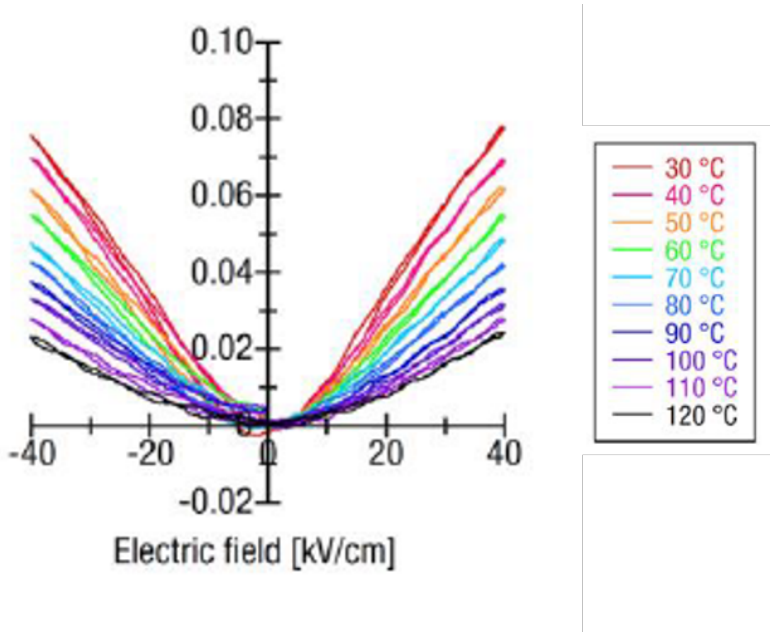

Figure 1-14: Variation of strain-electric field curves with varying temperature for an electrostrictive material [33]

Thermal expansion of electrostrictors is negligible ($<3.5X10{-}6°C^{-1}$) at temperatures between -100°C - 100°C for a wide range of PT composition [34] as shown in the fig. 1-15.

Various important features of the thermal expansion measurements in the selected PMN–PT ceramics

Sample	T_c (°C)	Thermal expansion coefficient ($\times 10^{-6}$ °C^{-1})[a]	Calculates P_s at room temperature (μC/cm^2)[b]
PMN	−10	1.6	72.97
0.8PMN–0.2PT	100	2.0	94.58
0.7PMN–0.3PT	120	2.4	56.33
0.65PMN–0.35PT	175	3.2	54.76

Figure 1-15: Thermal expansion table for wide range of PMN-PT ceramics [34]

The important temperature regions for the paraelectric functioning of electrostrictive materials can be marked using T_m (Maximum dielectric temperature), T_f (frequency invariance temperature) and T_F (freezing temperature) as shown in fig. 1-10. The freezing temperature occurs below T_m and is associated with freezing of domains with respect to thermal perturbations. T_F is defined under quasi-static conditions and the remnant polarization vanishes above this temperature (depolarization) [23]. The freezing temperature is defined at static conditions, under dynamic conditions a temperature called as the depolarization temperature, T_d is used, and its value also changes with the material composition [30]. Above the depolarization temperature (T_d), the material does not have remnant polarization and hence loses all piezoelectric effect.

Electrostrictive behavior (relaxor ferroelectric) is different from normal ferroelectrics due to its broad dielectric maximum peak, resulting in a diffused phase transition. This results in the depolarization temperature shifting from the Curie temperature (T_c), which is defined for normal ferroelectrics, to a new temperature slightly less than T_c. For electrostrictive materials

therefore, T_c is replaced with T_F (or T_d) and T_m which is the maximum dielectric temperature. In normal ferroelectrics like PZT, the Curie temperature and depolarization temperatures are the same due to narrow dielectric maximum peak. The variation of T_d, with respect to T_m, by changing PT content can be seen in fig. 1-16. It is observed that as PT (normal ferroelectric) content increases, the depolarization temperature and T_m approach each other. Operating the electrostrictor above T_d gives a dominant electrostrictive behavior, but operating it above T_m gives reduced hysteresis as mentioned before. Another temperature, as mentioned before in [1-2-2], T_f can be used to denote the absence of frequency dispersion for a certain frequency band. T_f is different for every frequency, hence depending on the operating frequency, the operating temperature should be above the corresponding T_f for low hysteresis and frequency independent material parameters.

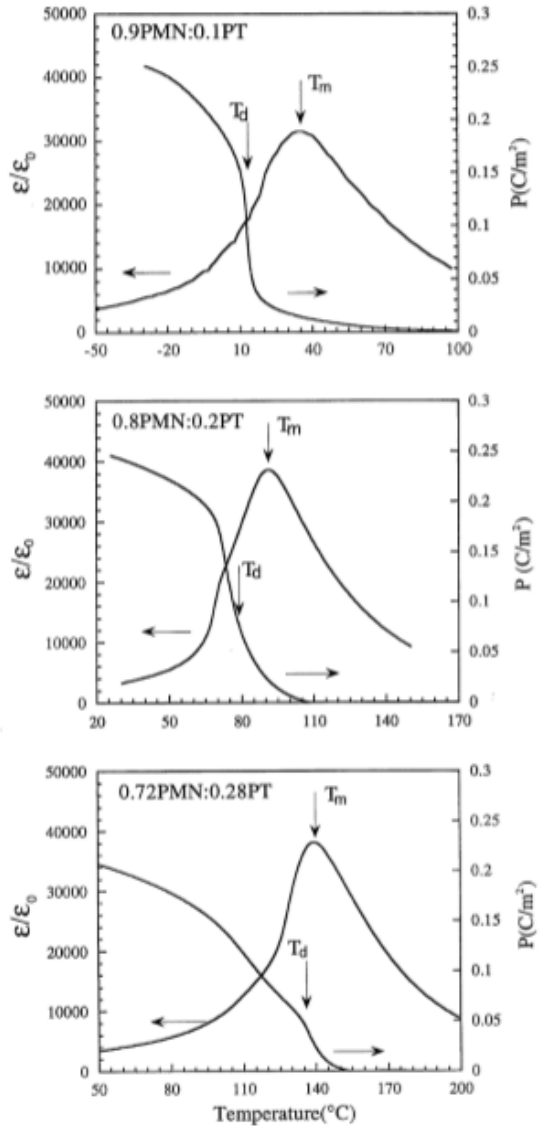

Figure 1-16: Shifting of depolarization temperature towards T_m with increase in normal ferroelectric content (PT) [30]

1-2-6 Effect of Aging

Aging of relaxor ferroelectric materials like PMN-PT is significant concern as it degrades the properties with time. The changes in actuator response can change significantly with aging and the actuator needs to be stable in this region. Investigations showed that amount of aging in the material increases with increasing PT content [35]. The aging process for any material constant (D) of electrostrictive actuator can be modeled using an exponential function dependent on aging rate (τ) and relaxation parameter (ν).

$$D = D_0 + D_1 exp(-\left(\frac{t}{\tau}\right)^{\nu}), \quad [36] \tag{1-13}$$

Considering all the even harmonics of the electrostrictive strain-electric field response, the 2nd and 4th harmonic are the only ones that show minimal aging effects and hence have minimum deviation with time [37]. This is the same as the variation of the first two odd harmonics of polarization response to electric field as shown in fig. 1-17.

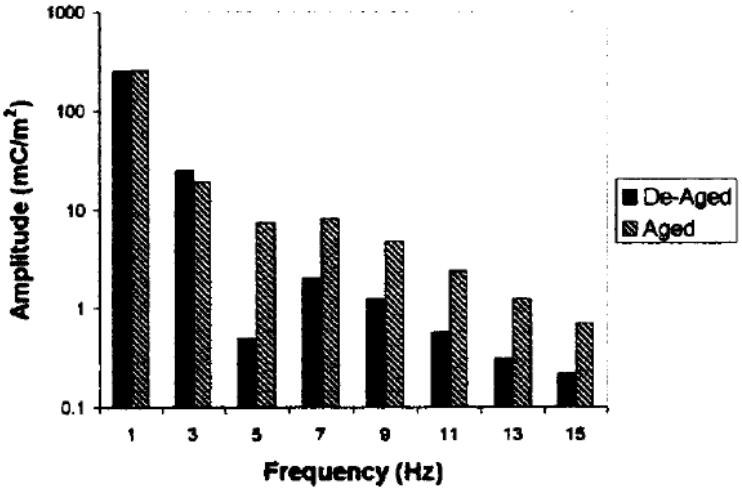

Figure 1-17: Comparison of aged and de-aged polarization harmonic (odd harmonics) responses

At low electric fields, response has negligible contributions of higher harmonic content as understood by the quadratic dependency of strain to electric field [38]. At higher electric fields, the higher harmonics get included to the strain response as seen by the hyperbolic function fit to the strain response data [14]. As the higher harmonics are affected by aging, the response should change at high electric fields. Corresponding polarization-field harmonics to 2nd and 4th strain-field harmonics would include 1st and 3rd. The degradation due to aging can be seen by observing variation of effective piezoelectric coefficient, d_{33} as shown in the fig. 1-19. The data also shows how doping with particular elements that inhibits charge mobility of charges in the lattice structure [36].

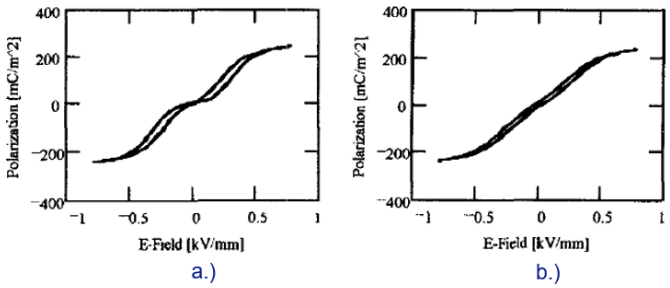

Figure 1-18: Changes in polarization with aging a.) Aged sample, b.) De-aged sample

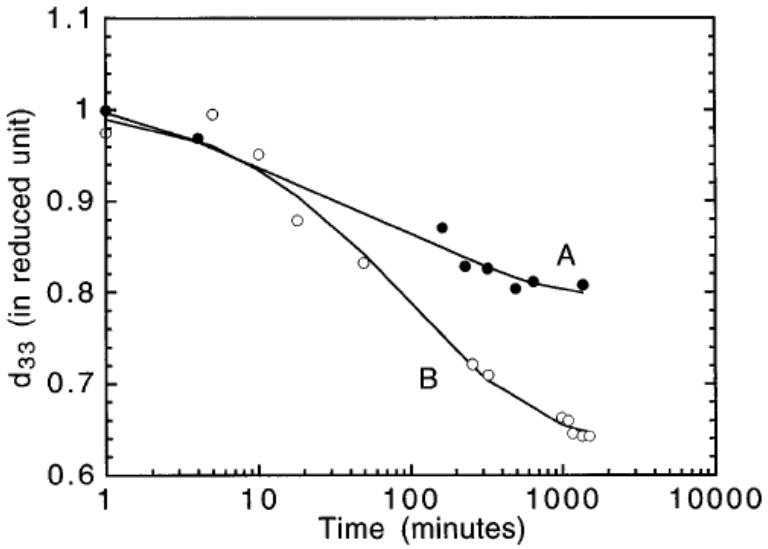

Figure 1-19: Aging data showing reduction effective piezoelectric coefficient, d_{33} fo 0.71PMN-0.29PT. Curve A shows results of sample with Mn doping and Curve B shows sample without Mn doping [36].

The material can be de-aged at temperatures significantly above the maximum dielectric temperature of the material. This temperature can vary but it is usually about 50°C-60°C above the T_m [39]. The dielectric constant of the material decays with time after the material is de-aged and it is important for precision applications that this behavior be modeled and contained. Moreover, the dielectric maximum temperature shifts to the higher temperatures in the case of de-aged samples [40]. The mechanism of aging in relaxor ferroelectrics is quite different from other ferroelectric material and is beyond the scope of this thesis. There are several mechanisms which explain the behavior as discussed by Colla [41] and Shrout [42].

1-3 Measurement Methods

Actuator response analysis for static and dynamic conditions can be done using quasi-static measurements (low frequency input-output measurements), and high-frequency strain-field and impedance measurements respectively.

Quasi-static strain-field measurements have been previously done, by Pilgrim and Williams [20] for harmonic analysis, Ren and Masys [24] for frequency dependence analysis of static model parameters, and Pilgrim [43] for polarization analysis, among others [32],[44],[30]. But none have created a macroscopic temperature dependent model that can be used for position control with electrostrictive actuators. This is probably due to a lack of requirement of such a process, as with position feedback control, temperature compensation would not be needed.

Another measurement method is using High Frequency Impedance measurements. High frequency impedance analysis can give information on actuator behavior and subsequently model parameter variation, without the need for high-precision strain-field measurements. This is handy for getting to know the actuator characteristics with changing operating parameters like voltage and temperature. For this purpose Sheritt and Mukherjee [19] use piezoelectric equations to relate to electrostriction at a DC bias. Robinson and McLaughlin [45] conducted analysis on frequency dispersion of dielectric parameters and electromechanical coupling coefficient. The parameters are compared with frequency and DC bias. Also, it is shown that the parameters above the temperature T_m, do not exhibit dispersion. But still, a temperature analysis and variation of model parameters from high-frequency impedance measurement around resonance frequency, with varying temperature, for position control has not been done.

1-4 Summary and Conclusions

Based on the literature study conducted,

- Above the maximum dielectric temperature (T_m), hysteresis starts to drop rapidly till it saturates to less than 2 %. Avoiding hysteresis is a major advantage as feed-forward control can then be used. Above T_m, hysteresis decreases with increasing temperature. Therefore, a material with T_m below room temperature is needed as an actuator.
- Above certain temperature T_f, the frequency dependence of the material response vanishes and the changes in the model parameters are frequency independent for the corresponding frequency band. Hence, the actuator should be operated in FF above the T_f for a defined frequency band of operation.
- The PT content in the material should be $\leq$15% for minimal hysteresis around room temperature. Moreover, it should always be less than 35% for high performance as shown in fig. 1-13.
- The aging results in changes to higher harmonics of the actuators's polarization-field response and therefore affects the nonlinear strain-field behavior as shown in fig. 1-17. This can be detected by applying Discrete Fourier Transform (DFT) [40],[39] to the

actuator strain response, from which the changes in amplitude of higher harmonics can be measured. Operating the actuator at low electric fields where the contribution of the higher harmonics (>4th for strain field response or 3rd for polarization-field response) is small can lead to stable response if the material is not completely aged. Otherwise actuator must be run in aged condition.

- From saturation effects (fig. 1-9) and hyperbolic relation, it can be inferred that there is a countering effect from 2nd and 4th order harmonic of the strain response (one is negative other is positive). This means that a certain portion of the strain-field curve is expected to be linear within some voltage bound. This should result in a diffused peak of the effective piezoelectric coefficient (d), where a linear operation with small error is possible around the maximum. Moreover, the temperature dependence of this maximum needs to be investigated for compensating the corresponding strain variation.
- To get a quadratic behavior and work with a single parameter, the actuator should be operated at low voltages. This would also help in modeling the response in a linear manner for a DC biased operation as the slope will be linear.
- The variation of k and M is assumed to be independent of voltage in the quadratic and hyperbolic model 1-5. But the invariance is yet to be investigated.
- Impedance resonance response of the electrostrictive material will give information on the material parameters using a suitable impedance response model.

  The state of the art gives an opportunity to investigate temperature variations of electrostrictive response at high frequencies and also position control using with temperature compensation.

1-4-1 Research Gap

The current literature does not give the description of temperature dependent macroscopic model that could be used for position control applications. Moreover, a linearized model, that can also compensate for the temperature induced strain variation, has not been formulated. In addition to a linearized model, a high performance region of actuation in the presence of temperature variations has not yet been investigated. In all such model cases, proper description of working parameters, with bounds on the errors, is needed for precision position control.

1-4-2 Research Objective

The research objective of this thesis is as follows:

Investigate if it is possible to devise useful temperature dependent models for non-linear and linear calibration and position control of electrostrictive PMN-PT material in the presence of temperature induced strain variations.

To achieve this research objective, following sub-objectives have been formulated,

1.) Create one-dimensional impedance model to find the variation of model parameters with temperature using model fit to the data, and verify the actuator impedance.

2.) Analyze the available nonlinear models of the electrostrictive material and derive important conclusions related to parameter sensitivity and its harmonic content from it to help in achieving proper results from quasi-static strain-field experiments, and utilizing those results for further analysis.

3.) Conduct quasi-static strain-field experiments with varying voltage amplitude and temperature. Process the raw results effectively using knowledge from the nonlinear model analysis and literature review to extract useful measurement data.

4.) Fit the nonlinear models to the strain-field experiment results and observe if the variation of model parameters with temperature follow a functional dependency. Analyze the results and make useful conclusions for possible position control and ways to achieve high performance control.

5.) Create feedforward schemes that utilize the resulting temperature dependent electrostrictive models, and show that it can compensated temperature induced strain-variation in real time.

Chapter 2

Model Analysis

2-1 Outline

In this section a linear and non-linear model analysis of the electrostrictive actuator is presented. First, a novel linear model is constructed by linearizing the simplest nonlinear model of electrostriction (quadratic model) around a certain voltage. This would help in getting a good understanding of the underlying electrostriction effect in step wise manner. Using this, an impedance response model is be made that would be used with quick impedance experiments (done in chapter 3) in order to assess underlying electrostriction behavior and variation of model parameters with temperature as discussed in section 1-3. Through this analysis, the non-linear behavior in the electrostrictive actuator is addressed and how the variation of parameters would affect the actuator response. Nonlinear models are then evaluated and analyzed in quasi-static domain. Identification of regions possessing high and low non-linearity in voltage and temperature is done. The goal of this analysis is to get sufficient understanding of electrostriction through voltage based models and validate using experiments.

2-2 Linear Impedance Model

Electrostrictive actuator is a material with very high dielectric constant. This dielectric constant helps it to achieve high degree of polarization (eq. (1-1)). The electrostriction for all insulators obeys quadratic law with polarization (as mentioned in section 1-2). For non-linear dielectrics under low electric field, a linear polarization vs electric field relation eq. (1-1) can be used as the first order approximation of 1-3.

At low electric fields, the actuator shows a quadratic response eq. (1-2). The electrostrictive constitutive equations for the conditions of low electric field can be defined [46] as:

$$x = ME^2 + s^E T \tag{2-1}$$

$$D = \epsilon^T E + 2MTE \tag{2-2}$$

where, s^E is the elastic compliance (inverse of young's modulus) (m^2/N) at constant electric field, T is the stress in the material (N/m^2), D is the displacement current (C/m^2), x is the strain (m/m).

The displacement current is sum of the induced polarization and the electromechanical term $2MTE$ which represents additional polarization in the presence of stress.

For remainder of the analysis, voltage, deformation and force analogues for electric field, strain and stress respectively would be used for ease of analysis with experiment data. The displacement current would also be replaced by charge equivalent using the relation $D = Q/A$, where Q is the induced charge (C) and A is the area of actuator (m^2).

$$z = \frac{MV_p^2}{L} + \frac{s^E f_p L}{A} \tag{2-3}$$

$$Q = \frac{\epsilon V_p}{L} + \frac{2M f_p V_p}{L} \tag{2-4}$$

where,z is the deformation of actuator under applied voltage and stress (m), V_p is the applied voltage (V), f_p is the force (N), A is the area of actuator (m^2) and L is the thickness (m). The charge, Q, in eq. (2-3) can be subdivided into charge induced purely due to capacitance (Q_{C_p}), and charge due to electromechanical coupling (Q_{f_p}). Also, the internal stiffness of the actuator can be represented by $k^E = \frac{A}{s^E L}$ The capacitance of the actuator can be expressed as $C_p = \frac{\epsilon A}{L}$.

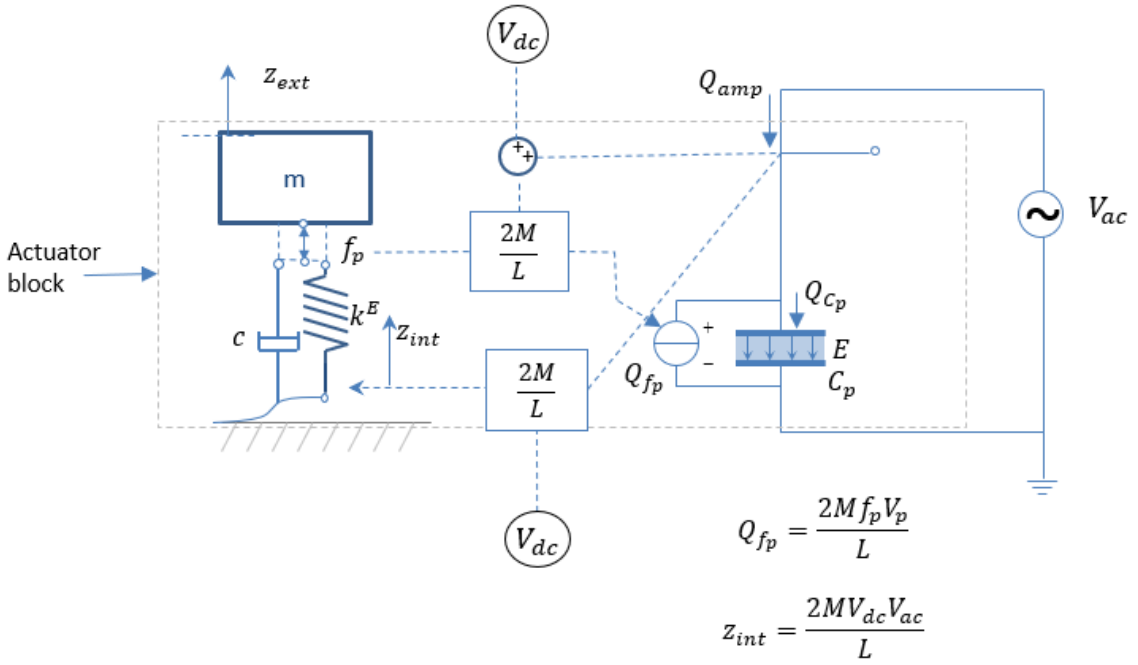

Figure 2-1: Electromechanical model of electrostrictive actuator

For the purpose of linear analysis, the electrostrictor would be operated about a particular DC bias electric field as the slope at 0V is 0, hence it would not yield any dynamic response. Therefore, the applied voltage can be expressed as $V_p = V_{ac} + V_{dc}$.

In such a case, an electromechanical model of the actuator can be created as shown in fig. 2-1. Here the actuator is to be a spring mass system.

In fig. 2-1, k^E is the stiffness of the actuator at constant electric field and can be expressed as $\gamma A/l$ where γ is the Young's Modulus ($\frac{N}{m^2}$). Also, Q_{amp} is the total charge in the circuit. The actuator deformation, z is expressed as z_{ext} to characterize the total deformation. The deformation due to direct polarization is expressed as z_{int}. The external force is assumed to be absent and only the internal force is considered.

The mechanical equation of motion of the actuator can be written as,

$$m\ddot{z} = f_p \tag{2-5}$$

substituting $f_p = (z_{int} - z_{ext})k^E - c\dot{z}$,

$$m\ddot{z}_{ext} + c\dot{z}_{ext} = (z_{int} - z_{ext})k^E \tag{2-6}$$

As discussed before, z_{int} is the position due to direct polarization without the added dynamic effects. At a certain DC bias, V_{dc}, the linearized position can be written as, $z_{int} = \frac{2MV_{dc}V_{ac}}{L}$ (as shown in eq. (1-11).

Using the assumption that $V_{dc} >> V_{ac}$ (so that deformation response could be considered linear for the actuation voltage V_{ac}) for the linear operation and taking laplace transform, we find the position transfer function for electrostriction

$$z_{ext}(s) = \frac{1}{ms^2 + cs + k^E}\frac{2MV_{dc}k^E}{L}V_{ac}(s) \tag{2-7}$$

To conduct electromechanical study, the electrostrictive charge coupling needs to be included in the model. The charge induced in the actuator is composed of two parts: 1.) Charge due to direct voltage induced polarization (Q_{C_p}), 2.) Charge induced due to mechanics of the actuator (Q_{f_p}).

The total charge ($Q_{fp} + Q_{C_p}$) is the charge flowing through the amplifier (Q_{amp}).

$$Q_{amp} = Q_{C_p} - Q_{f_p} \tag{2-8}$$

As mentioned in eq. (2-4), the induced charge due to electromechanical coupling is,

$$Q_{f_p} = \frac{2Mf_p(t)V_p}{L} \tag{2-9}$$

Using the approximation that $V_{dc} >> V_{ac}$, taking laplace transform and substituting the position transfer function, the charge transfer function can be obtained as (for full derivation check appendix A),

$$Q_{amp}(s) = C_p(V_{ac} + V_{dc}) - \frac{M^2c^EV_{dc}^2}{L^2}\left(\frac{6ms^2 + 6cs - 2k^E}{ms^2 + cs + k^E}\right)V_{ac}(s) \tag{2-10}$$

As the charge response is to be obtained only for the AC condition, the DC biased contribution of polarization can be removed the expression eq. (2-10). Compiling the contribution from AC signal results in the transfer function,

$$\frac{Q_{amp}(s)}{V_{ac}(s)} = \frac{s^2(C_pL^2m - 6M^2V_{dc}^2k^Em) + s(cC_pL^2 - 6M^2k^EV_{dc}^2c) + (C_pk^EL^2 - 2M^2(k^E)^2V_{dc}^2)}{L^2(ms^2 + cs + k^E)} \tag{2-11}$$

Current passing through the amplifier can be expressed as , $I_{amp} = sQ_{amp}$. The impedance response transfer function can then be described as,

$$\frac{V_{ac}(s)}{I_{amp}(s)} = \frac{L^2(ms^2 + cs + k^E)}{s^3(C_pL^2m - 6M^2V_{dc}^2k^Em) + s^2(cC_pL^2 - 6M^2k^EV_{dc}^2c) + s(C_pk^EL^2 - 2M^2(k^E)^2V_{dc}^2)} \tag{2-12}$$

The final model parameters are M (electrostriction coefficient), C_p(capacitance), k^E (stiffness) and c is the damping. L (thickness) and m(mass) of the actuator are assumed to remain invariant.

The 4 model parameters are assumed to be independent of applied voltage in the derivation, but they can still vary with temperature.

Assuming the damping to be extremely low and therefore having negligible effect on the resonance and anti-resonance frequency, the impedance resonance frequency can be evaluated using the pole equation of the transfer function 2-12. The resonance frequency comes to be:

$$f_{res} = \frac{1}{2\pi}\sqrt{\frac{C_pk^EL^2 - 2M^2k^EV_{dc}^2}{C_pL^2m - 6M^2V_{dc}^2k^Em}} \tag{2-13}$$

This shows how model parameters and applied DC bias are closely related to the appearance of resonances in the impedance FRF, as the real value of the frequency is dependent on balance of these parameters. Moreover, as the parameters are expected to show variation with temperature, the resonance frequency should also vary with temperature.

The zeros of the impedance transfer are the same as the position transfer function and hence the anti-resonance is the one where the impedance is minimum hence current is maximum. This results in a maxima for displacement.

$$f_{anti-res} = \frac{1}{2\pi}\sqrt{\frac{k^E}{m}} \tag{2-14}$$

There are several things that can be inferred from the model:

1.) At very low frequencies the impedance response is purely first order with -1 slope. From the generic values of electrostrictive parameters (section 2-2), the capacitance is term is almost of the same order as the M^2 term at high DC biases. This makes the slope of the impedance curve dependent on DC. Higher the DC bias, higher would be the offset of the impedance curve.

$\rho(\frac{kg}{m^3})$	L (mm)	A (mm^2)	κ	Q ($\frac{m^4}{C^2}$)	k^E ($\frac{N}{m}$)	V_{dc} (V)
7900	0.5	100	20000	0.013	1.5 x 10^{10}	100

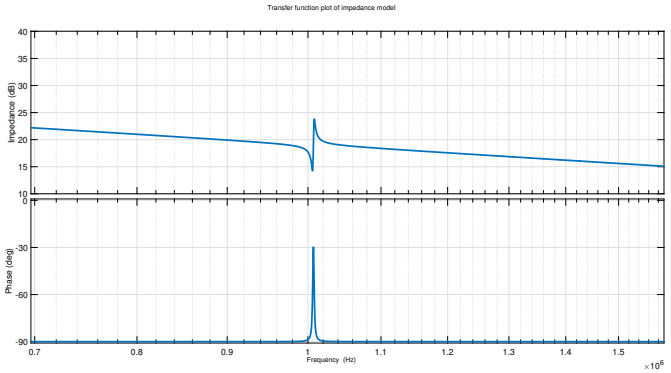

Figure 2-2: Impedance transfer function frequency response under 100V DC bias

$$\frac{V_{ac}(s)}{I_{amp}(s)} \approx \frac{L^2 k^E}{sC_p k^E L^2 - 2M^2 (k^E)^2 V_{dc}^2} = \frac{1}{s\left(C_p - \frac{2M^2 k^E V_{dc}^2}{L^2}\right)} \tag{2-15}$$

2.) As per the electrostriction property, at 0V DC bias, no resonance should be observed as the slope of the strain-field curve is 0, as seen infig. 1-9. At 0V DC bias, the impedance transfer function 2-12 becomes,

$$\frac{V_{ac}(s)}{I_{amp}(s)} = \frac{L^2(ms^2 + cs + k^E)}{s^3(C_p L^2 m) + s^2(cC_p L^2) + s(C_p k^E L^2)} = \frac{ms^2 + c + k^E}{sC_p(ms^2 + c + k^E)} = \frac{1}{sC_p} \tag{2-16}$$

Thus, the impedance response line is just a straight line with slope -1 in the bode plot.

SIDE NOTE: For analyzing the response, the model parameters are borrowed from literature for a certain PMN-0.12PT [47]. As mostly charge based model (1-5) results are available, to get the value of M, linear polarization assumption (1-1) is used for the analysis. Through this , $M = Q\epsilon^2$, where ϵ is the dielectric permittivity. Dielectric permittivity values and Q values are readily available in literature for Hom and Shankar model 1-5. The values used to model the impedance transfer function as shown in section 2-2 (NOTE: Values for dielectric constant (κ) and stiffness (k^E) are rough estimates) and resulting bode plot is shown in fig. 2-2.

The temperature variation should lead to decrease in the value of M as the strain is decreasing for the same applied electric field as seen in the quasi-static curves of fig. 1-14. Assumption is that this decreasing behavior should persist at high frequencies too. The stiffness was assumed to be independent of temperature but in practice it could vary with temperature, and hence sensitivity of impedance to both decreasing and increasing stiffness values would be done. Similarly for capacitance.

To see the sensitivity of involved parameters, variations are used with the original values as reference. As seen in fig. 2-3, with increasing stiffness both the resonance and anti-resonance frequencies shift right as expected. Also, the resonance frequency found to be highly sensitive to changing stiffness.

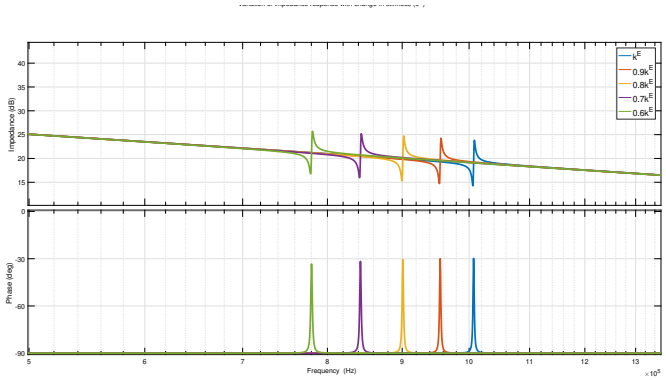

Figure 2-3: Effect of stiffness variation on impedance response

Defining sensitivity coefficient as the ratio of percent change in output (resonance frequency) to percent change in input (model parameters). Sensitivity coefficient for resonance frequency with changing stiffness is about 0.4. For the analysis, the capacitance and the electrostrictive coefficient M are related through the dielectric constant (κ). Which means, decreasing capacitance while keeping either constant does not hold as as both are dependent on the dielectric constant. They are coupled through dielectric constant. The eq. (2-12) will be used to fit it to the impedance experiment data later to find the model parameters.

Effect of thermal expansion To predict the effect thermal expansion would have on the impedance response, the length of the actuator (and therefore associated properties like capacitance) was varied according to the thermal expansion data available in the literature for (1-x)PMN-xPT materials.

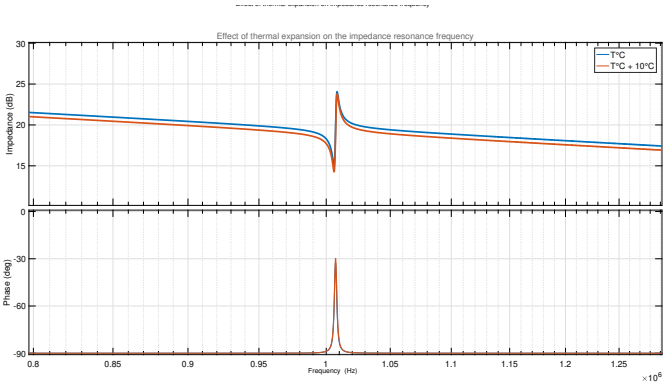

Figure 2-4: Change in the impedance response due to 10 °C rise in temperature

As mentioned before, thermal expansion increases with increase in the PT content (fig. 1-15). Using the thermal expansion value of about 3 X $10^{-6}C^{-1}$, over a 10 $^{\circ}C$ temperature range, we can observe from fig. 2-4 that thermal expansion effects are predicted to be negligible. The variation has been obtained by changing the thickness of the actuator with the new thickness after $10^{\circ}C$ increase in temperature.

Variation of Resonance Frequency with DC bias Using eq. (2-12), the variation of impedance response with changing DC bias can be plotted as shown in fig. 2-5. It can be observed that the resonance/anti-resonance frequency has a negligible shift with changing DC bias. The peak values can be plotted with the DC bias as shown in fig. 2-6.

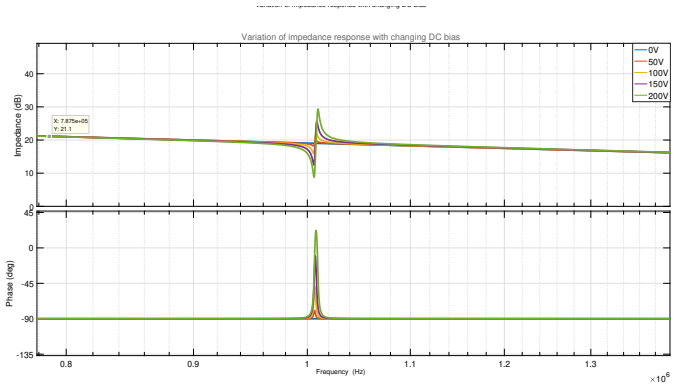

Figure 2-5: Variation of impedance response with changing DC bias

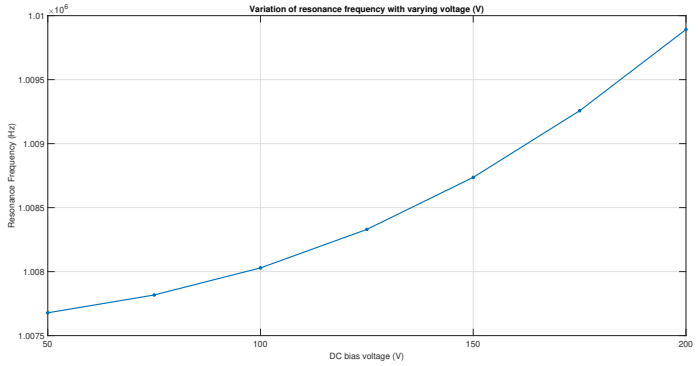

Figure 2-6: Variation of resonance frequency with DC bias

It can be seen that sensitivity of resonance frequency to voltage change is, on an average, just about 13Hz per volt.

2-2-1 Conclusions

An impedance model is created for getting the model parameters from impedance measurements (done later in section 3-3-2) which are relatively simple to do compared to high resolution strain-electric field experiments. The model is formulated for low voltage operation of the actuator. This is the voltage till which higher order even harmonics are negligible and the actuator response remains quadratic. Moreover, the model can only be used for DC biased operation with oscillating voltage under the condition $V_{ac} << V_{dc}$. The exact bounds for this would be evaluated in the next section on nonlinear analysis. The impedance model would be fitted to impedance experiment results to obtain the temperature variation of model parameters.

The limitations of the linear model is that it valid only till the point when the quadratic model can be used to approximate the electrostrictive behavior accurately (bounds and errors discussed in the next section). At high applied voltages, saturation effects occur (as discussed in section 1-2) due to which the linear model can no longer describe the electrostrictive behavior accurately. This limitation can be overcome using nonlinear model approach. Further use of linearization techniques requires analysis into the composition of non-linearity. These aspects would be analyzed in the next section.

2-3 Nonlinear Analysis

In this section, two models for electrostriction, Mason's quadratic model 1-2 and Hom and Shankar hyperbolic model 1-5 would be evaluated. The variation of parameters on the model response would be analyzed in the whole nonlinear region. Further, linearized analysis would be done to determine the DC bias and bounds in which the actuator can be used as a linear actuator. This would be done to understand whether simple feedforward control techniques can be applied for the operation. The effect of temperature on model parameters would be assumed functional. Further, harmonic analysis technique would be discussed and how its properties can be used to get the actual actuator signal from the raw measurement data. This would be then used in filtering the measurement data properly without losing actutor response information.

In the end, conclusions would be made to predict the results from the quasi-static deformation-voltage experiments with varying temperature.

2-3-1 Models

The two stress-free nonlinear models described in section 1-2 are:

1.) Mason's model or Quadratic model:

$$x = ME^2 \quad : \text{Strain-Electric field form} \tag{2-17}$$

$$z = \frac{MV^2}{L} \quad : \text{Deformation-Voltage form} \tag{2-18}$$

2.) Hom and Shankar model

$$x = QP^2 \tag{2-19}$$

$$P = P_s tanh(kE) \tag{2-20}$$

Combining eq. (2-20) and eq. (2-19)

$$x = QP_s^2 tanh^2(kE) \quad \text{Strain-Electric field form} \tag{2-21}$$

$$z = \frac{QP_s^2}{L} tanh^2(\frac{kV}{L}) \quad \text{Deformation-Voltage form} \tag{2-22}$$

The Hom and Shankar model contains three parameter, Q,P_s and k. All these parameters can vary with temperature. Reducing the number of parameters would help in simplifying the

analysis. The hyperbolic model can be expanded using series expansion to get the constituent terms of the expression. As tanh can be decomposed into odd harmonics, for any y$\in$ $\mathbb{R}$,

$$tanh(y) = y - \frac{1}{3}y^3 + \frac{2}{15}y^5 - \frac{17}{315}y^7 + ... \quad (2\text{-}23)$$

Using the expansion in the strain-field expression

$$x = QP_s^2\left(kE - \frac{1}{3}k^3E^3 + \frac{2}{15}k^5E^5 + ...\right)^2 \quad (2\text{-}24)$$

As kE $<$ 1 for low electric fields, we can neglect the higher order terms in the series expansion,

$$x \approx QP_s^2(k^2E^2) = (QP_s^2k^2)E^2 \quad (2\text{-}25)$$

Comparing with eq. (2-18),

$$M = QP_s^2k^2 \quad \text{or,} \quad (2\text{-}26)$$

$$QP_s^2 = \frac{M}{k^2} \quad (2\text{-}27)$$

Substituting the expression for QP_s^2 in eq. (2-21),

$$x = \frac{M}{k^2}tanh^2(kE) \quad \text{Strain-Electric field form} \quad (2\text{-}28)$$

$$z = \frac{ML}{k^2}tanh^2\left(\frac{kV}{L}\right) \quad \text{Deformation-Voltage form} \quad (2\text{-}29)$$

The eq. (2-28) contains only two parameters and is much easier to analyze. Moreover, it can be directly converted to the quadratic model 1-2 on approximation for low electric field. From this point onwards, the term "hyperbolic model" will be used to refer to eq. (2-29) or eq. (2-28).

Analysis To analyze the quadratic and hyperbolic responses, the strain-electric field curves for the quadratic and hyperbolic model are plotted using the parameter values mentioned in section 2-2 for 1 Hz input sine wave. Using a value of k (relaxation coefficient) of about 1 x $10^{-6}mV^{-1}$ [21],

1.) As seen from the fig. 2-7, the quadratic model over-predicts the deformation response with increasing voltage and therefore is only valid for low electric fields.

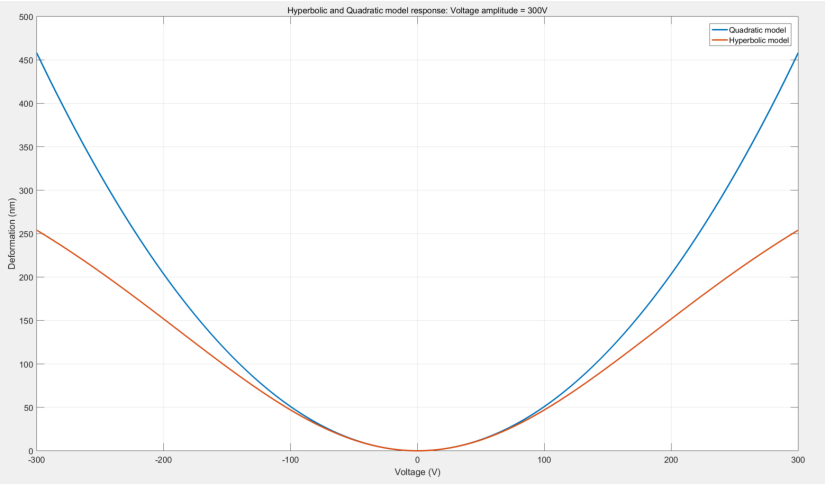

Figure 2-7: Hyperbolic and Quadratic model responses on the same plot for sine wave voltage amplitude of 300V

2.) The error between the two models comes from the increased relaxation time of dielectric domains which translates to a higher relaxation coefficient (k). As this coefficient increases, the response tends to show saturation effect at lower voltages. This leads to increased error between quadratic approximation and the hyperbolic model as seen in fig. 2-8.

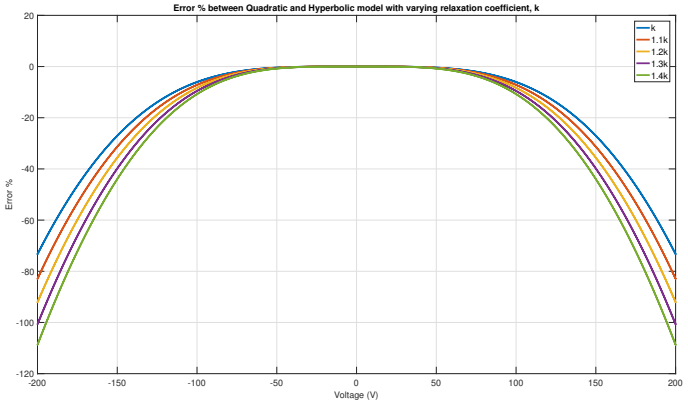

Figure 2-8: Error % between Quadratic and hyperbolic model with varying k

3.) Both parameters, M and k, have different sensitivity effects on deformation. The change in deformation has a diffused effect with changing k, unlike with changing M, as seen in the fig. 2-9. The change is quite small at low voltages but increases exponentially.

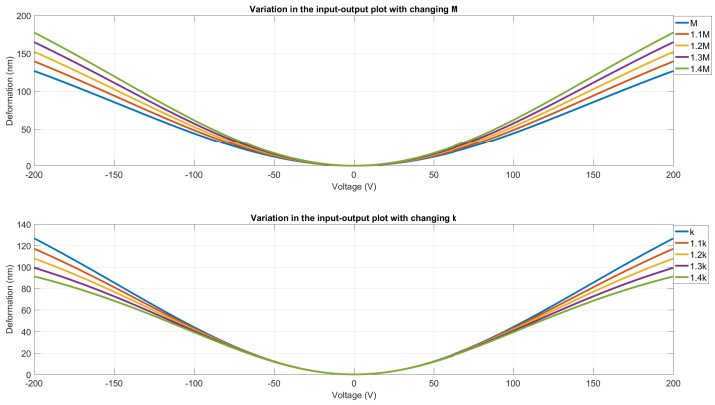

Figure 2-9: Change in deformation-voltage response with varying k and M

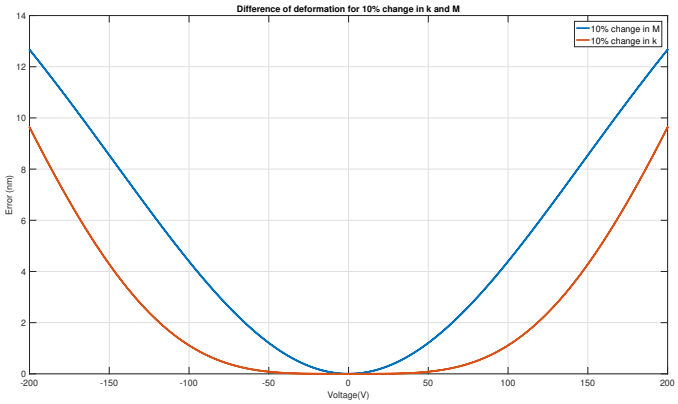

Figure 2-10: Error between the deformation-voltage curves with 10% change in k and M

On expanding the hyperbolic model, a series expansion of even powers of the argument of function, is obtained. This can be written in a expansion form assuming only 2 and 3 terms of the expansion,

$$x = \frac{M}{k^2} tanh^2(kE) \tag{2-30}$$

$$x = \frac{M}{k^2}(kE - \frac{1}{3}k^3E^3 + \frac{2}{15}k^5E^5 - .....)^2 \tag{2-31}$$

Using Multinomial expansion

$$x = ME^2 - \frac{2}{3}ME^4k^2 + \frac{17}{45}ME^6k^4 - \frac{4}{45}ME^8k^6... \tag{2-32}$$

The eq. (2-32) is the Polynomial model of electrostriction. Plotting the different orders of polynomial model shows how it approaches the hyperbolic model scheme with increasing even powers as shown in fig. 2-11.

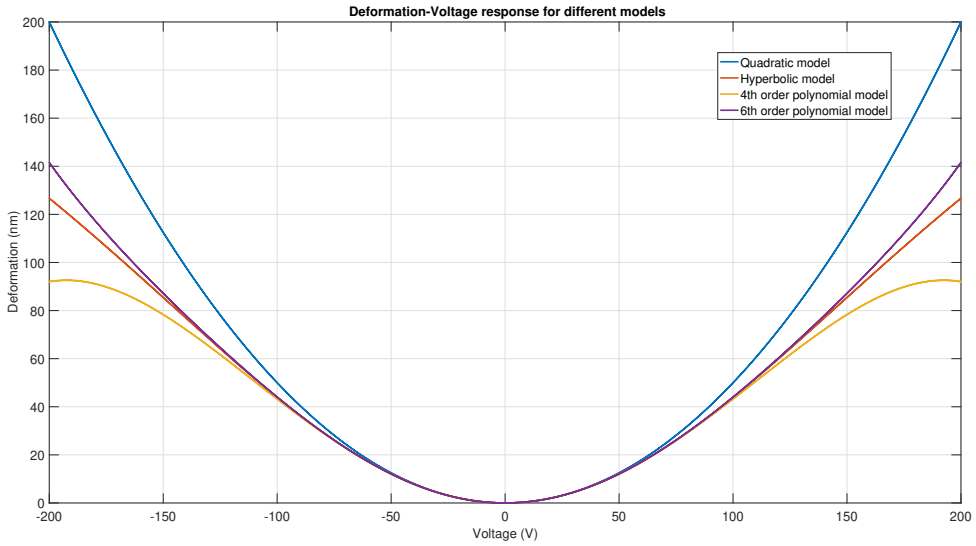

Figure 2-11: Deformation-Voltage curves for Quadratic, Hyperbolic and Expansion models

*

Using the sinusoidal expression for electric field, eq. (2-32) can be used decomposed into constituent harmonics.

$$x = \frac{M}{k^2}(kE_0 sin(\omega t) - \frac{1}{3}k^3 E_0^3 sin^3(\omega t) + \frac{2}{15}E_0^5 sin^5(\omega t)....)^2 \tag{2-33}$$

$$x = A(E_0, k, M) + B(E_0, k, M)cos(2\omega t) + C(E_0, k, M)cos(4\omega t) + ... \tag{2-34}$$

This expansion leads to even powers of the sine voltage which can then be further simplified into harmonics. The eq. (2-34) shows that electrostrictive strain response consists of only even harmonics. As the coefficients, A, B, C, are dependent on the model parameters (M, k), they would vary with temperature. Using the experiment observations in the later section, the temperature effects on different harmonics would then be determined. The analysis would help in identifying optimal control strategies for the actuator depending on the relative magnitudes of successive even harmonics.

2-3-2 Linear analysis using Hyperbolic model

As discussed before in section 2-3-1, the strain response of electrostrictive actuator is composed of even harmonics. Using the hyperbolic expansion as shown eq. (2-30), it can be seen that the higher even harmonics are countering the lower ones. This makes an interesting band of voltage where the actuator displays a diffused behavior in the slope of the strain-electric field curve. The fig. 2-12 shows the slope of hyperbolic model, $\frac{dz}{dV}$, for the voltage range from -350V to 350V using the model parameters as used in section 2-3-1, and plotting it against the corresponding voltage.

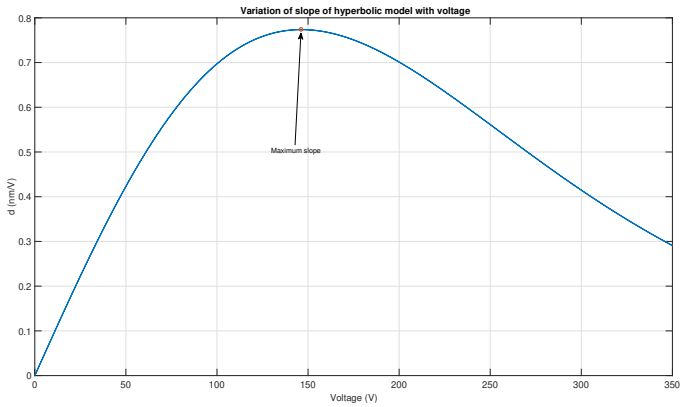

Figure 2-12: Variation of slope of hyperbolic curve with Voltage

It can be seen in the fig. 2-12, that there is diffused maxima peak for the slope. As the slope in the electrostrictive actuator is constantly changing with applied voltage, this diffused peak provides an interesting region where linear actuation can be applied within certain bounds of actuating AC voltage. In such a case, the error for considering the slope invariant of voltage around d_{max} could be within the application error budget and the actuator can be calibrated to operate around the point of maximum slope. This is highly useful as at the maximum slope, the sensitivity to voltage would be highest and therefore the actuation can be carried with maximum performance. In such a case the error for assuming linear actuation against nonlinear model can be calculated for different AC voltages. As experiment data is not available, commenting on the errors and establishing the voltage (and temperature) bounds would be done in section 3-3-3.

2-3-3 Conclusions

Through this model analysis following conclusions can be derived:

1. A one-dimensional impedance model was created that described electrostriction, and the effect of variation of model parameters was analyzed.
2. Thermal expansion shows to have negligible influence on the resonance frequencies.
3. There is little change in the impedance resonance frequencies with increasing DC bias
4. Nonlinear analysis using hyperbolic model shows high sensitivity of M across the entire voltage range, and exponentially increasing sensitivity of k with increasing voltage.
5. The effect of variation of model parameters on deformation response was estimated and trends were identified that would be later used in analyzing experiment results
6. The concept linearized actuation using hyperbolic was put forward. Theoretically using the diffused maxima peak as DC operating point, linear actuation with high voltage range can be obtained.

2-4 Summary

In chapter 2 four models had been described, namely,

1.) **Linear impedance model**
A novel method to model electrostrictive response as an LTI system (2-7) along with the impedance response with temperature dependent parameters (k^E, M, C_p, c). The method is useful when actuator is used with a DC bias and the actuation voltage (AC) is low. As it is derived using quadratic model, it is valid when the applied DC bias voltage is low too. The impedance model is especially useful for getting model parameters using quick impedance measurements instead of highly precision strain-field experiments. Based on the displacement error requirements, maximum DC bias level can be set appropriately using quadratic model analysis (2-3).

2.) **Quadratic model**
This model is borrowed from literature and is an approximation to the electrostrictive response at low applied electric fields/voltage. The model would be useful for temperature compensation as it only has one parameter that describes the temperature dependent behavior of electrostriction (M) at low voltages with sufficient accuracy (2-7). This provides ease of modeling and compensation.

3.) **Hyperbolic model**
This 3 parameter hyperbolic model was adapted from the literature (1-2-2, 2-29), wherein it was modified to have only 2 parameters based on the assumption that it describes electrostrictive behavior accurately (as per literature 1-2-2) and approximates to quadratic model at low voltage levels. Analysis on effect of parameter sensitivity and harmonic composition was done to post-process the experiment data effectively. This model is useful because it describes electrostrictive behavior in full voltage range. The drawback is that it has 2 parameters that could vary with voltage and temperature ,thereby making analysis difficult (shown in chapter 3).

4.) **Linearized hyperbolic model**
This model would be developed further after getting experiment results (in section 3-3-3) thereby making it an empirical model. It is valid in the region around the diffused maximum of the effective piezoelectric coefficient (d_{max}). Using the fact that if the actuator is operated around the voltage at the point of d_{max} (2-3-2), d coefficient becomes independent of voltage and actuator can be operated as a linear actuator. Further, the actuator has maximum performance owing to the fact that the sensitivity voltage at the operating point is highest. The variation of d_{max} and the corresponding DC bias voltage V_m with temperature would be obtained using the experiment results in a later section. A linear variation of these parameters with temperature would make an extremely simple calibration technique that would result in linear operation with high actuation range along with complete compensation of temperature induced strain variations.

The fig. 2-13 gives a graphical overview of the electrostriction models as discussed.

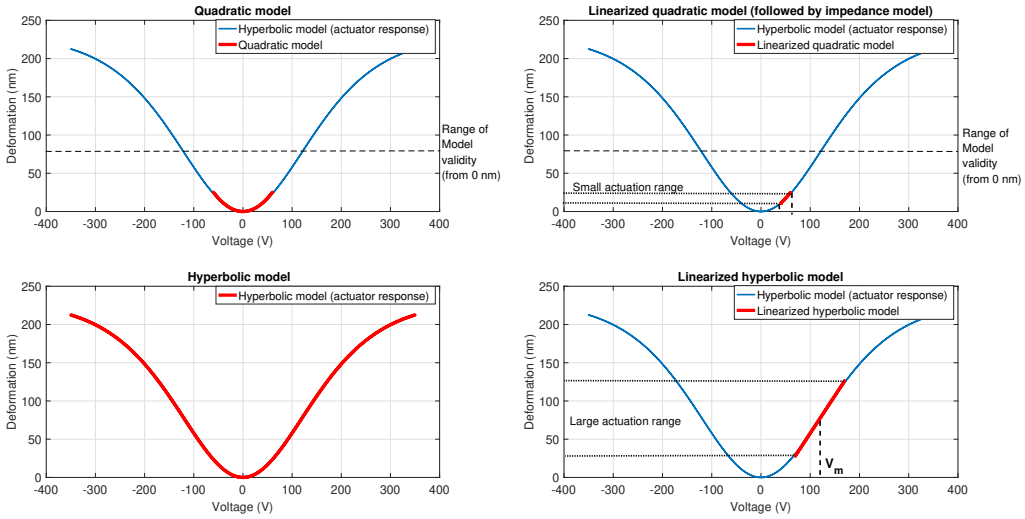

Figure 2-13: Overview of electrostriction models

Chapter 3

Experiments and Analysis

3-1 Outline

In this chapter, high frequency impedance measurements and quasi-static strain field experiments would be carried out in the presence of temperature disturbances in order to characterize the temperature dependency of the actuator. Through this, variation of model parameters would be obtained that would help in making a temperature dependent model. Furthermore, nonlinear behavior analysis done in chapter 2 would be put to use to identify high performance actuation zone. Using this, an optimal voltage region would be identified and another linear model would be created that would also correct for temperature induced strain variations. Lastly, appropriate feedforward schemes would be developed that would use the resultant models to create an effective position control system. The material used for the measurements was 0.85PMN-0.15PT content manufactured by TRS Ceramics. The material has a T_m of about 36-38° C in the frequency range of 1-1000 Hz. This temperature range was chosen to get actuator characteristics around the T_m, and thus validate the electrostrictive behavior discussed in the section 1-2 and chapter 2. The thickness of the actuator was chosen to 0.2mm and 0.5mm. The experiment setup consists of a high voltage delivery amplifier, temperature control devices, data acquisition system, displacement sensor and a signal generator.The functioning and calibration of these instruments are mentioned in appendix B. Moreover the post-processing steps are only briefly explained in this chapter, for more detailed explanation refer to appendix B.

3-2 Impedance Measurement

The impedance resonance frequencies of a square plated 0.85PMN-0.15PT electrostrictive actuator can be calculated using the speed of the acoustic wave through the sample. For transverse and thickness modes [48], the resonance frequencies can be roughly estimated by,

$$f_{trans} = \frac{v}{2W}, \quad v \text{ is speed of sound in the material, } W \text{ is width} \tag{3-1}$$

$$f_{thick} = \frac{v}{2L}, \quad L \text{ is the thickness} \tag{3-2}$$

The velocity of sound in solids is, (3-3)

$$v = \sqrt{\frac{\gamma}{\rho}}, \quad \text{where } \gamma \text{ is young's modulus } (\frac{N}{m^2}),\ \rho \text{ is density } (\frac{kg}{m^3}) \tag{3-4}$$

3-2-1 Experiment Setup

In an impedance measurement, a sine wave voltage signal is applied across the actuator and the resulting current is measured. The current has a magnitude and phase, through which complex impedance can be calculated. The setup for the impedance measurement has a schematic as shown in fig. 3-1.

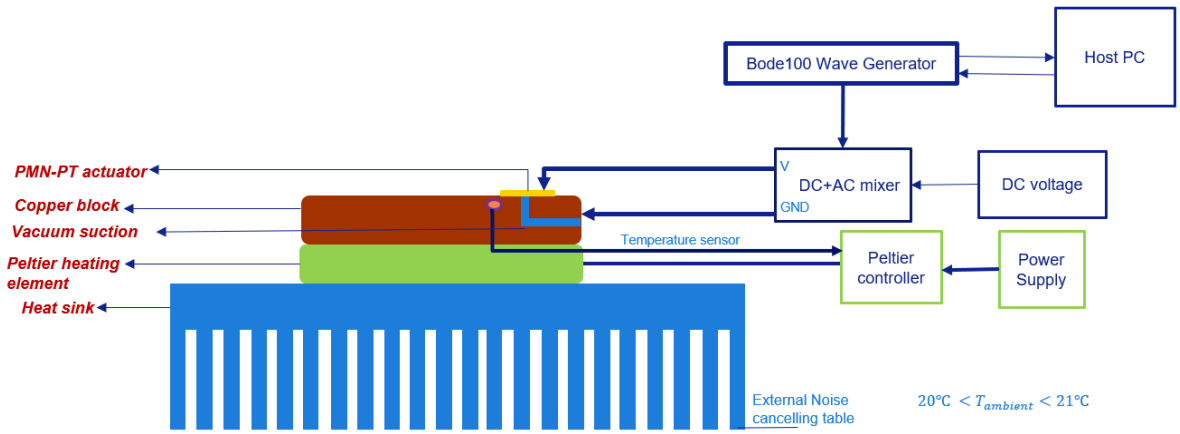

Figure 3-1: Test setup schematic for impedance measurement

The Peltier unit provides the required temperature at its feedback sensor location (which is located just below the actuator). As the actuator is thin, (0.5 mm) with wide surface area, and has a gold plated conductive layer on both sides, temperature of the actuator is assumed to be the same as feedback temperature sensor (NTC(10K)). The copper block acts a support base for the actuator and is connected to the common ground. The Bode100 is a signal generator that produces small AC voltage (< 2 Vrms) with varying frequency and corresponding current to generate impedance response. As the Bode100's output does not give higher voltages, a DC-AC coupler was used to combine DC voltage from a power supply and Bode100's output (as at 0 DC bias electrostrictive behavior is absent at low sinusoidal voltages). The description and data sheets of the Peltier unit, Bode100 and NTC temperature sensor are mentioned in appendix B. To effectively capture the impedance resonance modes across a wide frequency spectrum, the signal generator (Bode100) needed to be calibrated properly. The Bode100 was run with low sampling points and high receiver bandwidth to detect the resonance frequency locations. The range for the resonances was set as 100KHz-10MHz. The signal generator was then calibrated carefully for the this frequency range, with

low receiver bandwidth (300Hz). Lower receiver bandwidth was used to reduce noise in the measurement and detect resonances accurately.

3-2-2 Experiment Results and Analysis

The results of the impedance measurement are shown in fig. 3-3. It can be observed that increasing temperature shifts both, the transverse mode and the thickness mode to higher frequencies.

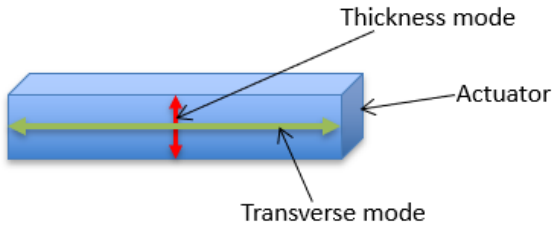

Figure 3-2: Transverse and thickness modes visualized

The transverse and thickness modes can be visualized using fig. 3-2. As discussed before in eq. (3-1), transverse mode would first in frequency spectrum followed by some of its higher harmonics, and subsequently the thickness mode.

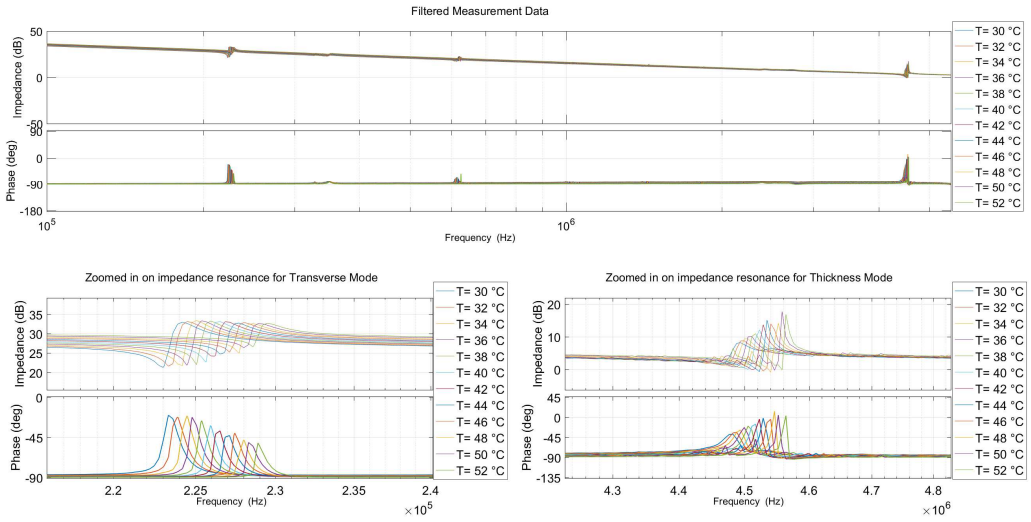

Figure 3-3: Temperature varying impedance measurement between frequency range 100kHz-10MHz at 100V DC bias

The resolution of measurement is less, because otherwise the time required for calibration and measurement was too high. The method to derive the model parameters is by comparing the coefficients of the transfer function of the thickness mode for every temperature. The thickness mode of every temperature measurement is isolated and its transfer function is

Type	M ($\frac{m^2}{V^2}$)	k^E ($\frac{N}{m}$)	C_p (F)	c ($\frac{Ns}{m}$)
Change per °C	1.5064 x 10^{-17} $/°C$	5.8182 x 10^8 $/°C$	1.34 x $10^{-10}/°C$	$4.05/V$
Change per V	1.496 x 10^{-18} $/V$	4.4 x 10^7 $/V$	2.2533 x $10^{-11}/V$	$0.22/$ V

Table 3-1: Sensitivity of model parameters to temperature and voltage

estimated (see matlab code in appendix (cite appendix)). This transfer function's coefficients are then equated with the corresponding coefficients of the impedance model equation (2-12) as derived in section 2-2. This is done by first estimating the transfer function of the thickness mode for each temperature. Both the estimated transfer function and model transfer function, are normalized with coefficient of 's^3'(highest power) in the denominator.

$$\frac{V_{ac}(s)}{I_{amp}(s)} = \frac{L^2(ms^2 + cs + k^E)}{s^3(C_pL^2m - 6M^2V_{dc}^2k^Em) + s^2(cC_pL^2 - 6M^2(k^E)^2V_{dc}^2c) + s(C_pk^EL^2 - 2M^2(k^E)^2V_{dc}^2)} \tag{3-5}$$

Using this approach, 5 equations are formed out of which 4 are independent.

Solving these equations with the thickness mode transfer function gives the values for M, C_p, c and k^E for every temperature at 100V DC bias. The variation of these parameters can be seen in fig. 3-4.

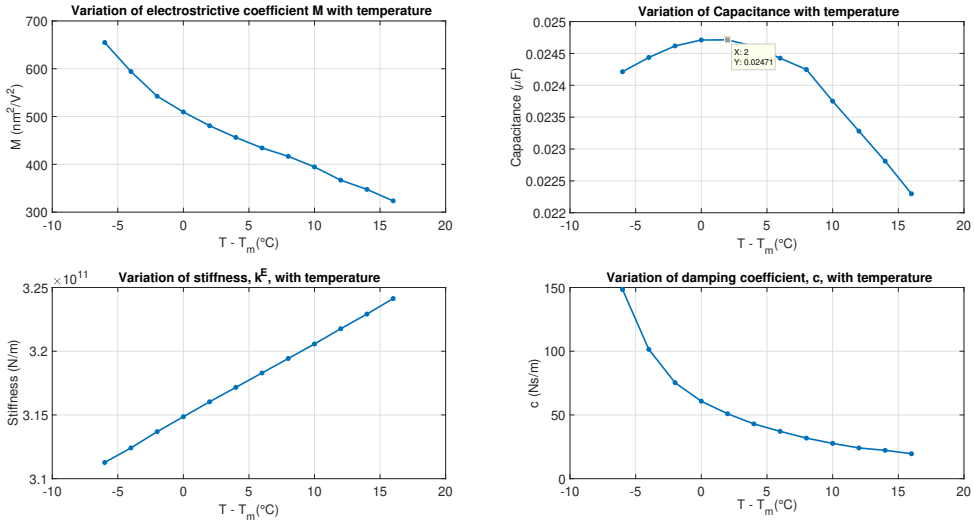

Figure 3-4: Variation of model parameters with temperature for 100V DC bias

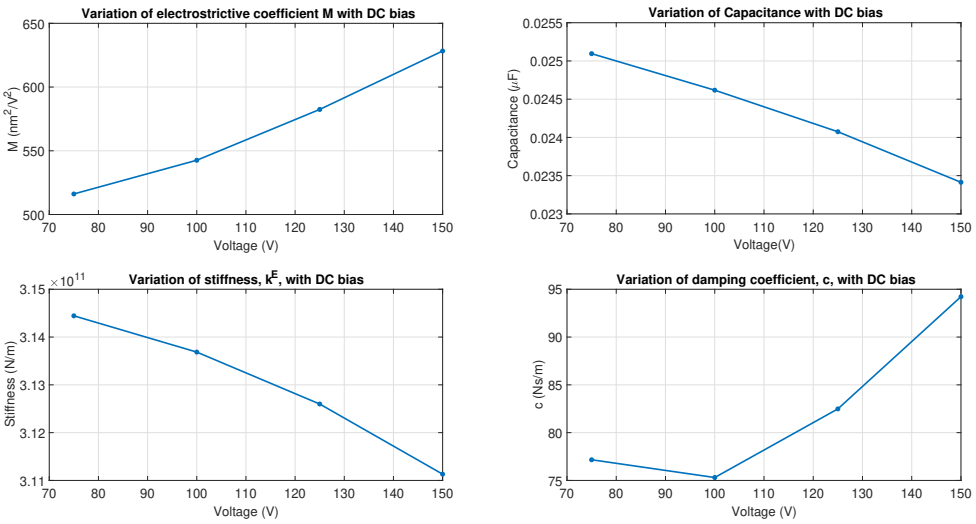

Figure 3-5: Variation of model parameters with DC bias at $34°C$

NOTE: Though the comparison between the percentage change in the model parameters due to temperature and voltage does not make sense without a proper reference or application context. But for the purpose of this thesis, and as per accuracy of results, comparison would be made using change due to $1°C$ and 1V.

Several specific points can be drawn from the results shown in fig. 3-5, fig. 3-4 and table 3-1

1. The changes in the model parameters are much more sensitive to temperature than the DC bias. As the sensitivity to voltage is small,the assumption that model parameters are independent of applied DC bias seems to hold good under the operating conditions and accuracy of experimental analysis.

2. With increasing temperature, M decreases as predicted before in section 2-2. The variation initially has a quadratic behavior but turns linear over after $35°C$. Decreasing M also, characterizes the decreasing distance between resonance and anti-resonance frequencies for every temperature.

3. With increasing temperature, k^E (stiffness), increases. The increase explains the movement of resonances to higher frequencies.

4. The variation of Capacitance with temperature shows a characteristic dielectric maxima at around 36-38$°C$. This the T_m of 0.85PMN-0.15PT (material used for experiments) is obtained at low frequency.

Variation of Resonance frequencies Another important observation that can be made from the impedance results regarding the variation of resonance frequencies with temperature as seen in fig. 3-6. Both the anti-resonance and resonance frequency, in thickness and width mode, vary linearly with temperature. The variation of the resonance frequency with DC

is also shown in the fig. 3-7 that the variation in the resonance frequency with DC bias is negligible as shown in the table 3-2. This means that with increasing voltage/DC bias, the resonance frequency has much less sensitivity to voltage compared to temperature sensitivity. Morevoer, it can be seen that the sensitivities of resonance and the anti-resonance frequency in the width mode to DC bias are almost 0. This observation is in good agreement with the predicted model results as shown in section 2-2. The linear variation of the resonance frequencies can be exploited into detecting the temperature of the electrostrictive element using a high frequency jitter signal (chirp or swweeping sine encompassing the range of the resonance frequencies) on top of the actuation and bias voltage signal. For measuring the temperature, the resulting signal can be filtered using a band pass filter and resulting current can be measured to detect the resonance values. Based on the calibration data (utilizing the linear variation of resonance frequency with temperature), the actuator can be estimated and fed as a feedback to the Feedforward control scheme. The idea is suitable as the operating frequency for the application is between 0.1Hz-100Hz and the resonance frequency is at around 1MHz. Moreover, only a very small amplitude of jitter signal (< 1 V) is needed to measure the resonance frequency and that would have no noticeable effect on the actuator strain.

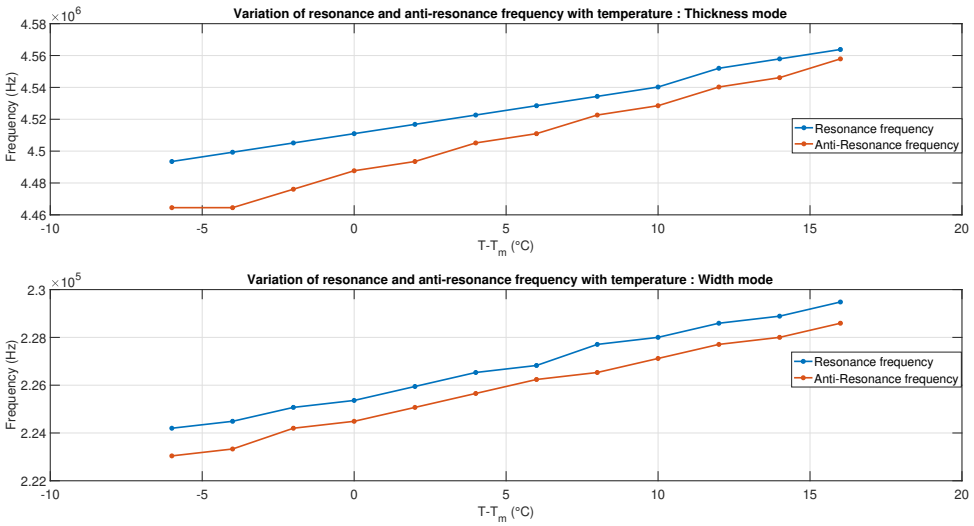

Figure 3-6: Variation of resonance and anti-resonance frequencies at 100V DC bias for Thickness and Width (transverse) mode

Mode	Type	Change with DC bias ($\frac{Hz}{V}$)	Change with temperature ($\frac{Hz}{^\circ C}$)
Thickness	Resonance	- 80	3227
	Anti-Resonance	-226	4227
Width	Resonance	0	240
	Anti-Resonance	8	254

Table 3-2: Sensitivity of resonance and anti-resonance frequencies to DC bias and temperature

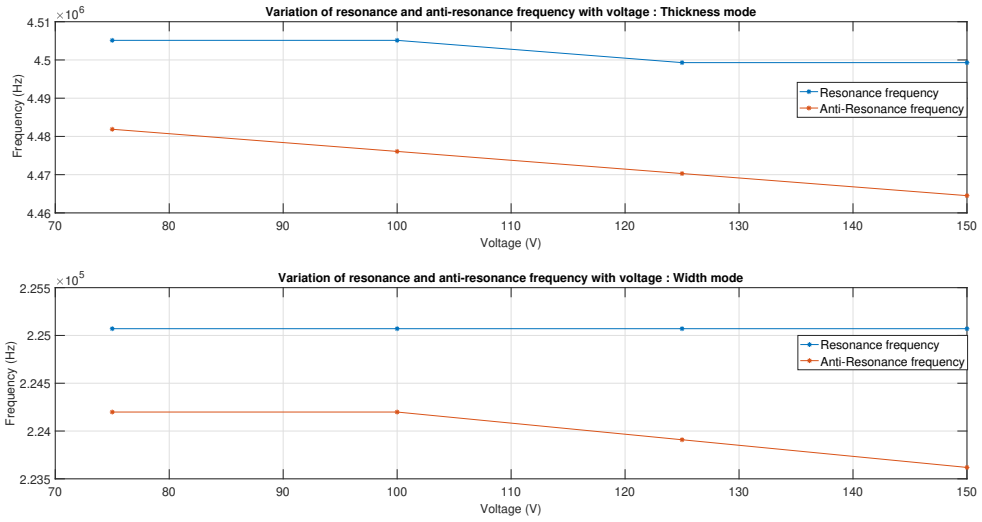

Figure 3-7: Variation of resonance and anti-resonance frequency with DC bias at $34^\circ C$ for thickness and width (transverse) mode

3-2-3 Conclusions

1. The impedance model gives a tentative estimate of the model parameters, most importantly for the electrostrictive coefficient, M. This will later help in verifying the quasi-static measurements that would then be used in the temperature compensating feedforward control.

2. A linear model of the electrostrictive actuator was derived and its properties are compared to the experiment results. The model shows good resemblance of the effects being observed in the impedance response and to the simulated results (section 2-2).

3. As thermal expansion is negligible, the changes in response due to change in temperature, are solely due to changes in the material properties (discussed in section 2-2).

4. This impedance measurement and analysis provides a foundation from which nonlinear response can be understood in a better way.

3-3 Quasi-static strain-electric field measurement

The low frequency measurement were done by directly measuring the deformation of actuator by applying voltage and changing the temperature conditions.These measurements were important for the application but the measurement setup configuration was too time consuming, hence it seemed prudent to do these measurements after doing quick impedance measurements. The quasi-static measurement were also needed to quantify and model the non-linearities associated with voltage and temperature changes. As the application requires low frequency actuation (0.1-100Hz), a better understanding of the actuator's functioning is obtained, moreover these measurements would then be directly used to fit static-model(eq. (1-10), eq. (2-29)) to get temperature varying parameters.

Quasi-static strain-field or deformation-voltage experiments will involve application of a low frequency voltage to the actuator at a controlled temperature. The resulting deformation would then be measured with the help of a displacement sensor. This experiment would be repeated for multiple voltage amplitudes, temperatures and frequencies. After post-processing, a series of plots for the actuator characteristics would be obtained as function of voltage and temperature. Frequency changes would be done for verification of the invariance of response above some temperature above T_m as discussed in section 1-2-3.

3-3-1 Experiment Setup

To measure quasi-static strains in an accurate and precise way, an interferometer was chosen as a desired displacement sensor. Due to highly precise interferometry technique, it could give resolution of upto 1nm under right calibration. The interferometer consists of 2 probes attached to optic fibres that were connected to the central controller of the unit. One probe (main probe) measures the deformation of the actuator to which voltage is applied, the second probe (reference probe) measures deformation of the actuator that is resting freely on top of the copper block. Using this arrangement, the thermal expansion of the setup below the actuators can be cancelled. This invariably cancels out the thermal expansion of the actuator too, but as discussed before in section 1-2-5, the effect is negligible to considered in the measurement. Through the central controller of the interferometer unit, measurements could be taken either through the unit's dedicated software interface or from the analog output behind the controller. Using software, the device calibration was fixed and analog output ports were connected to a separate data acquisition unit's (target PC, Speedgoat) IO board (IO104). The voltage signal from the interferometer was scaled to be between -10V to 10V with the measurement span being -2um to 2um. This resulted in a 5mV change in the voltage signal for 1nm change in displacement. 5mV ($>2\mu$V) was well within the measurement range of the Speedgoat system. (For more information on the interferometer and its functioning refer to the appendix B).

The heating setup with peltier element is similar to the one used in the impedance measurements. In addition, a calibrated NTC 10K temperature sensor was installed next to the PMN-PT actuator with a thermally conductive tape to get real time temperature readings of the actuator as shown in the fig. 3-8. The voltage input to the actuator was sent through the Target PC using Simulink (model can be found in appendix B). This signal was then passed through an amplifier and applied across the actuator. A separate output(voltage monitor)

from the amplifier is taken that gives the voltage output of the amplifier (reduced by factor of 100). According to manufacturer specs (appendix B), for the given capacitive load (about 100nF), the amplifier shows little or no gain decay with for the operating frequency range. This reading was verified with the actual output using an oscilloscope and was found to be accurate to about than 0.1V. All the system were connected to a common ground.

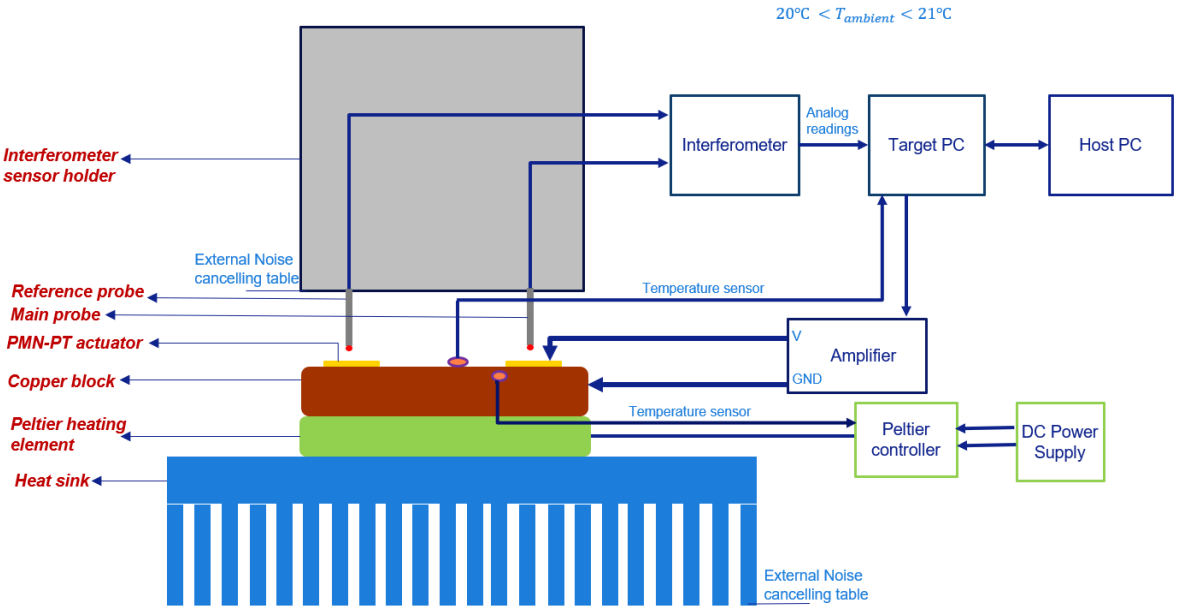

Figure 3-8: Schematic of the experiment setup

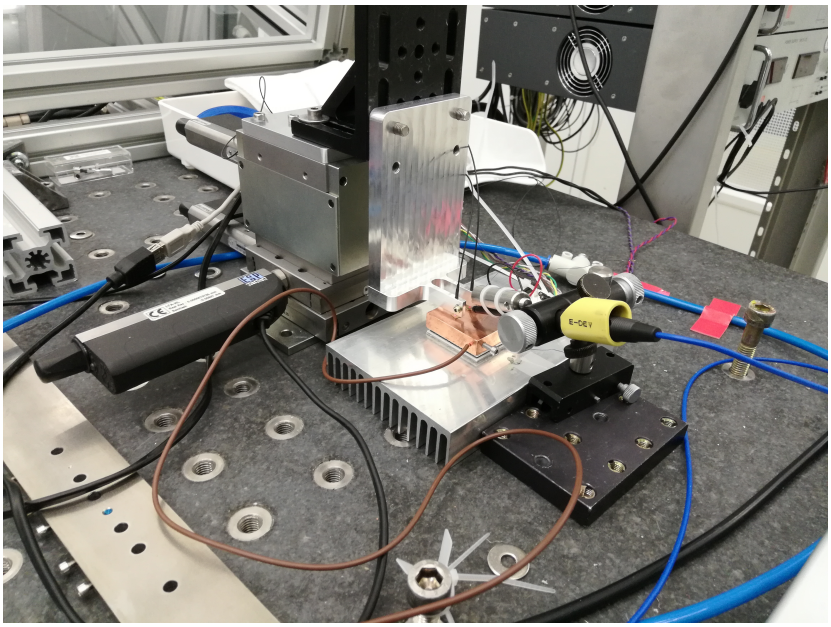

Figure 3-9: Picture of part of the experiment setup (for more pictures refer to the appendix B-2-2)

3-3-2 Experiment Results and Analysis

The voltage data collected from the temperature sensor, interferometer and voltage monitor was fed from the DAQ unit into a file that could be accessed by Matlab/Simulink. The results were obtained after several post-processing steps (please refer to appendix 3 for the detailed post-processing steps).The measurements were taken for several temperature, voltage and frequency points. The averaged deformation-voltage plot with varying temperature and the corresponding averaged deformation plots for different voltage amplitudes are shown in the fig. 3-10, fig. 3-11, and fig. 3-12.

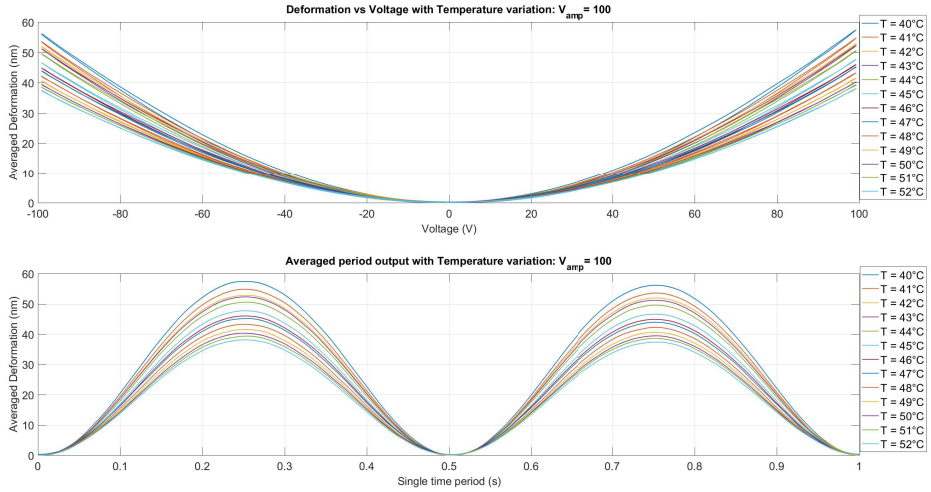

Figure 3-10: Deformation vs Voltage for 100V amplitude

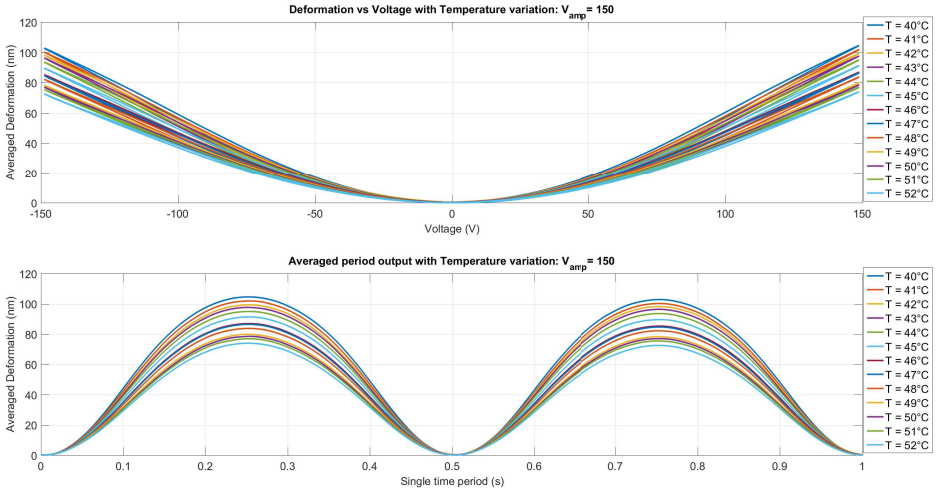

Figure 3-11: Deformation vs Voltage curves with varying temperature for 150V amplitude

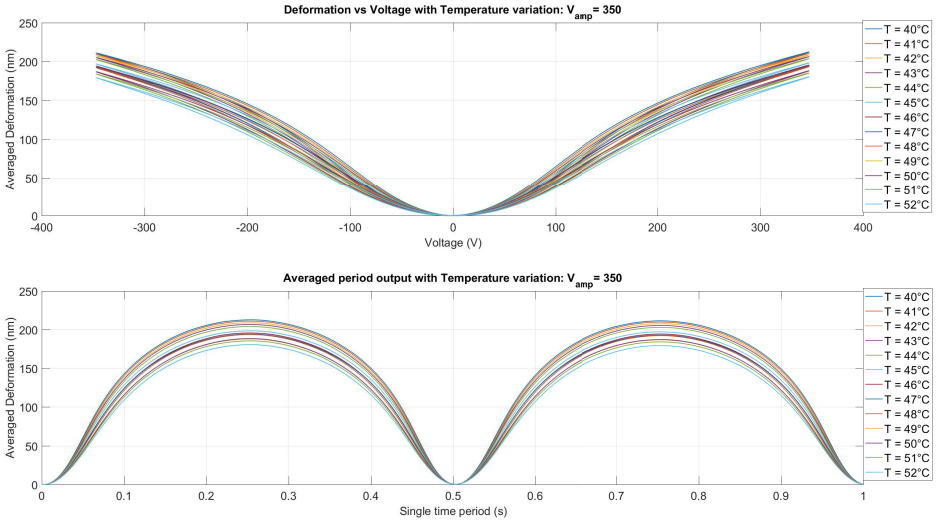

Figure 3-12: Deformation vs Voltage curves with varying temperature for amplitude of 350V

The curves show decreasing deformations with increasing temperature as indicated from the impedance response and literature (section 1-2-5). Also, at higher voltage amplitudes, a saturation effect is seen, as described in section 1-2-2 and section 2-3. This saturation is effect is due to the higher even harmonics in the deformation response of the actuator. Taking FFT of the whole deformation signal, the even harmonics can be observed as seen in fig. 3-13, fig. 3-14 and fig. 3-15 for 100V, 150V and 350V voltage amplitudes.

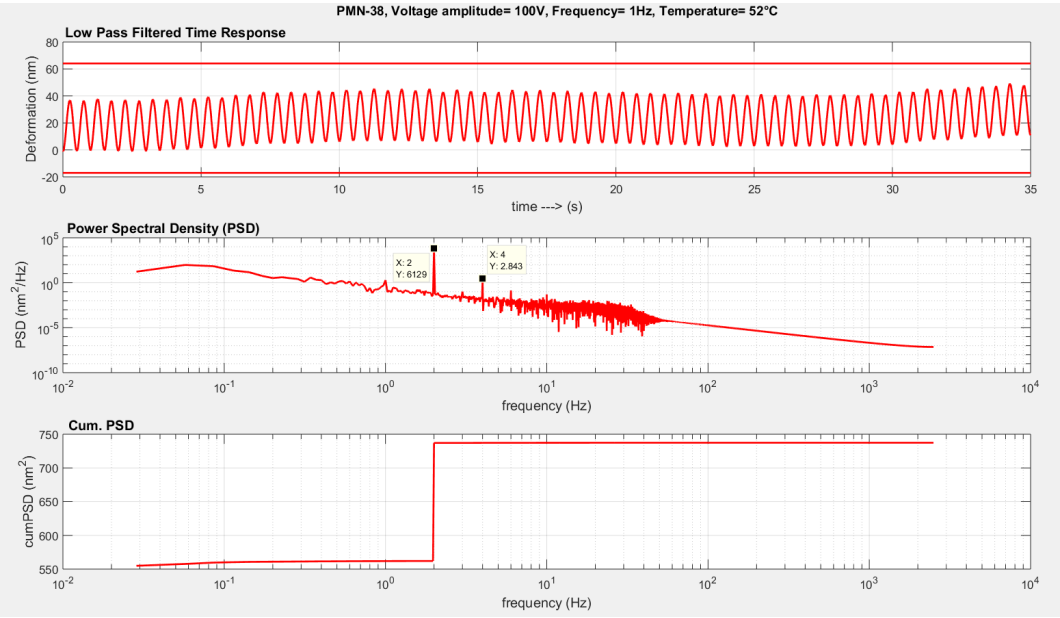

Figure 3-13: FFT response of deformation with 100V amplitude

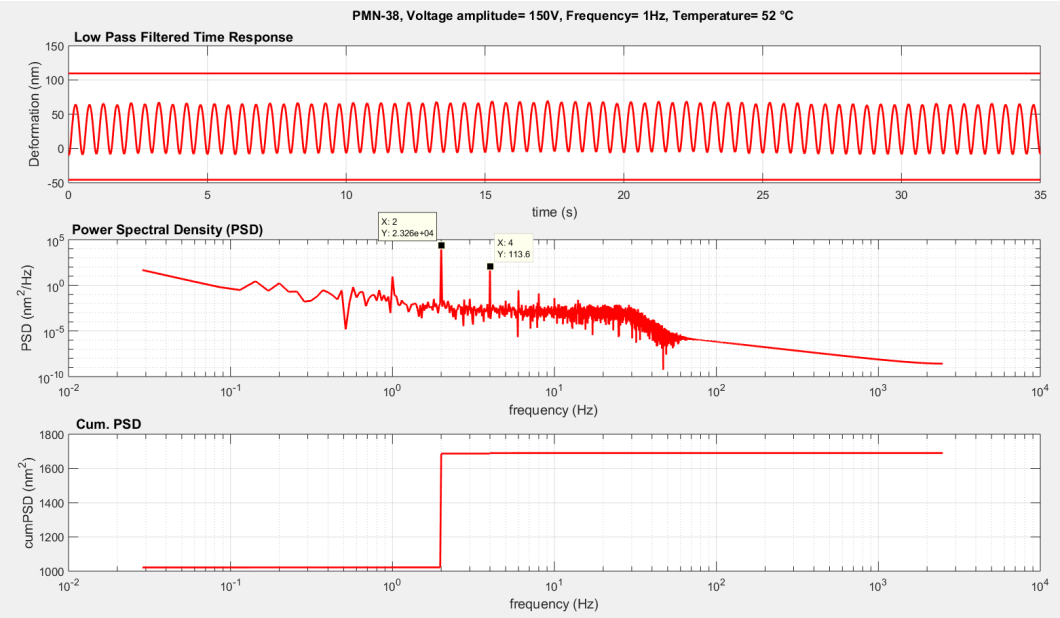

Figure 3-14: FFT response of deformation with 150V amplitude

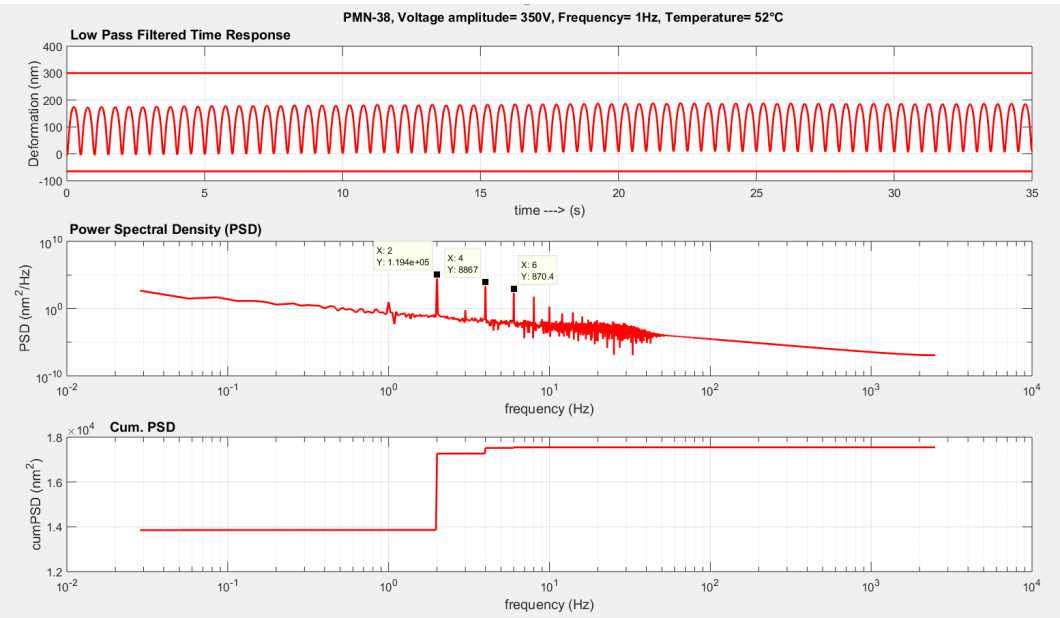

Figure 3-15: FFT response of deformation with 350V amplitude

The plots show the composition of the deformation signal. The higher even harmonics in the deformation response gradually increase with increasing the applied voltage. Also, the harmonic amplitudes decrease with increase in temperature. This can be observed from fig. 3-16, fig. 3-17 and fig. 3-18, that plot the amplitudes of the first four even harmonics in the actual deformation. Due to even response, there is a high zero order harmonic whose amplitude value equals the sum of all even harmonics. At 100V, the deformation response is

highly quadratic, therefore the zero order harmonic and the 2nd harmonic amplitude values have almost the same value.

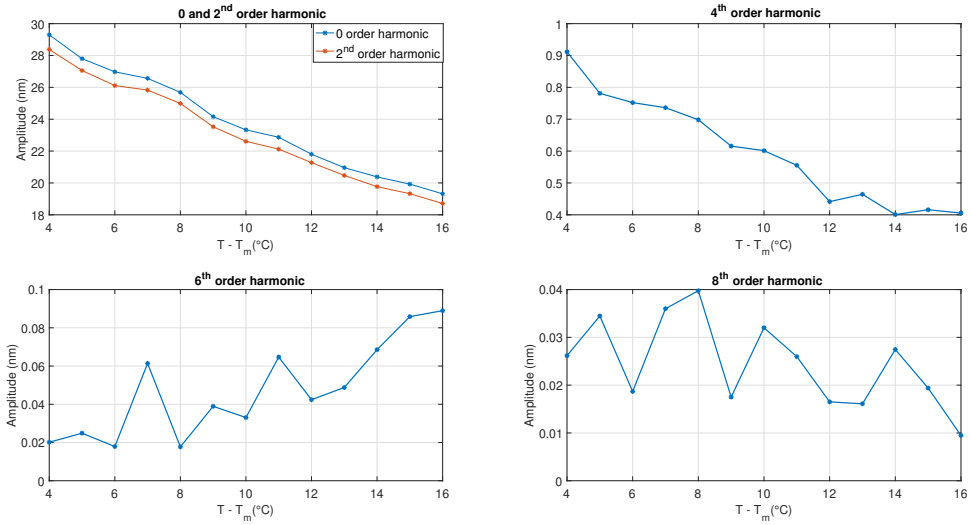

Figure 3-16: Change in harmonic magnitude with changing temperature for 100V amplitude

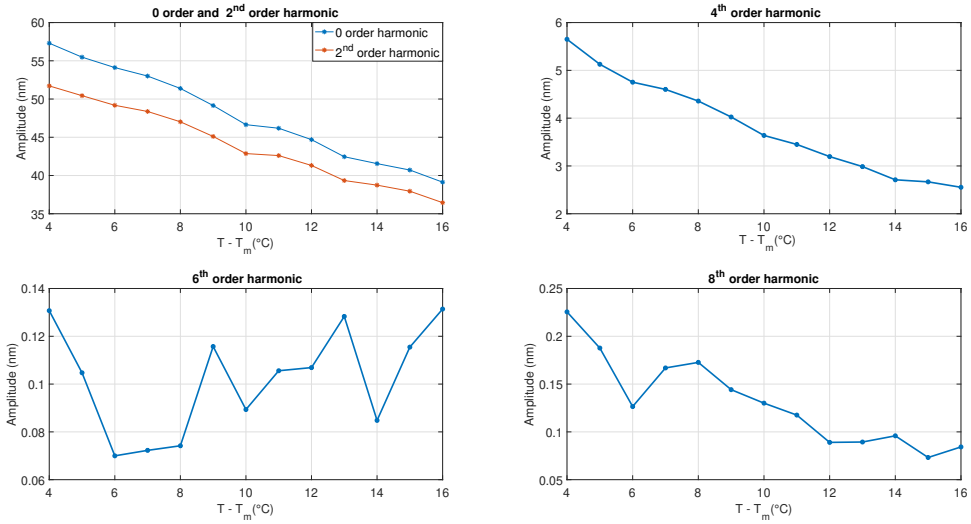

Figure 3-17: Changing harmonic magnitude with changing temperature for 150V amplitude

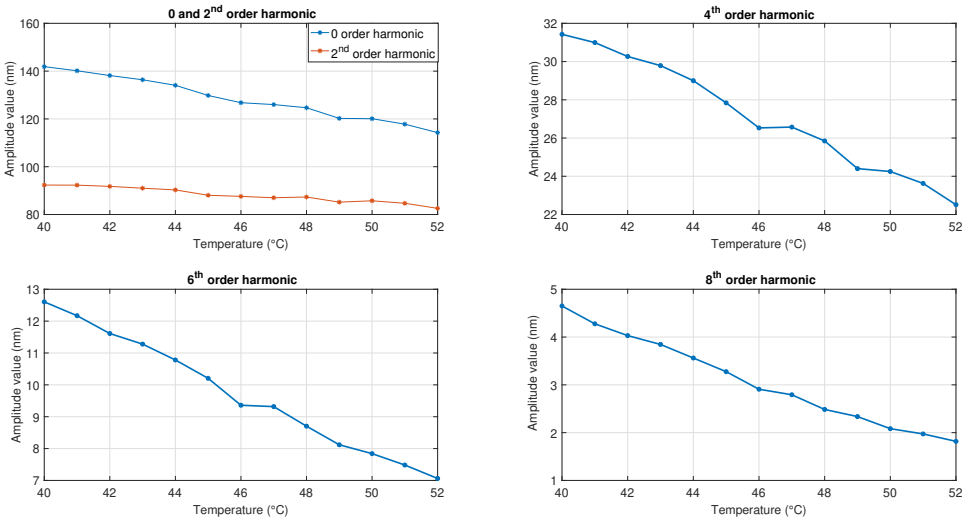

Figure 3-18: Change in the harmonic magnitude with changing temperature for 350V amplitude

The value of the harmonic amplitudes can be used in eq. (2-34) to get the coefficient equations, which could then be solved to get the variation of material parameters.

Fitting the nonlinear models static electrostrictive models (2-29,1-2) to the response curves (3-10,3-11, 3-12) should give the variation of the model parameters, M and k with temperature.

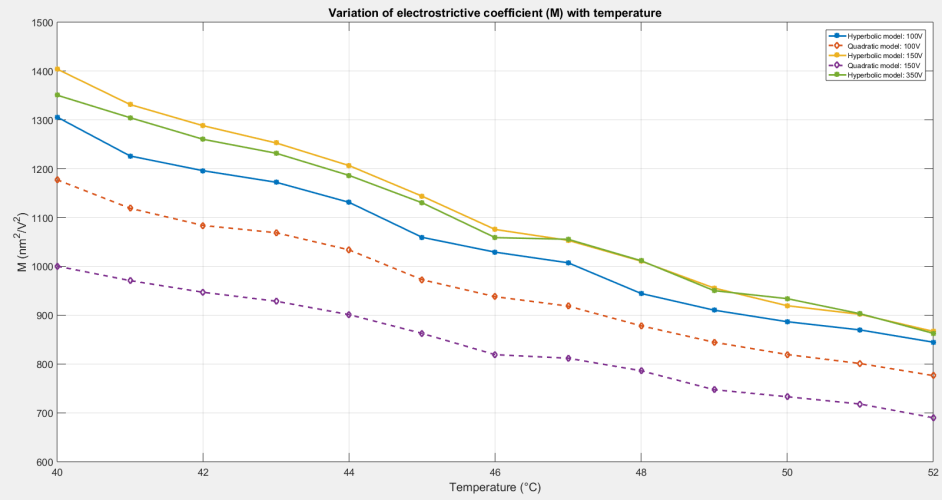

Figure 3-19: Variation of electrostrictive coefficient (M) with temperature for hyperbolic and quadratic model

As seen from the fig. 3-19, the relaxation too varies linearly with temperature in the given temperature range. The curve of k vs T has a lower offset and slope at 100V compared to 150V and 350V. This is due to fitting error and less sensitivity of k at low voltages as discussed in section 2-3-1. Changes in the value of k at low applied therefore have very low effect on the change in the response characteristics. The changing k for 100V actuation from its calculated

value to the one of 350V (keeping other parameters same) changes the deformation response to less than that with $1°C$ change in temperature.

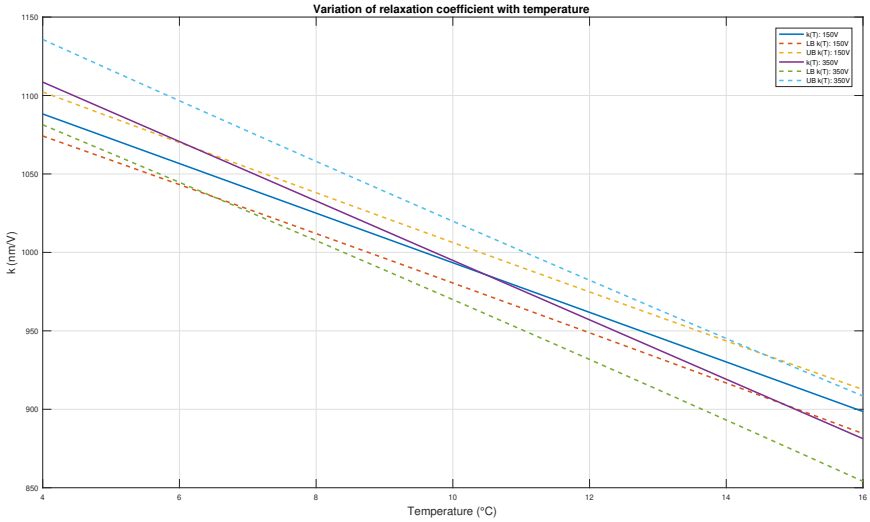

Figure 3-20: Variation of relaxation coefficient with temperature for different voltage amplitudes

The variation of both the model parameters, M and k is quite linear and can therefore have a linear functional dependency with temperature. Using least-squares method a straight line is fitted to get the functional dependencies $M(T)$ and $k(T)$. 95% Predictive bounds are generated using the data and plotted alongside the fitted lines as shown in fig. 3-21. These bounds are quite wide and take into account error following Gaussian distribution. This shows that if another sample is added to the data, it will lie in predictive interval between the dotted lines as show in fig. 3-21.

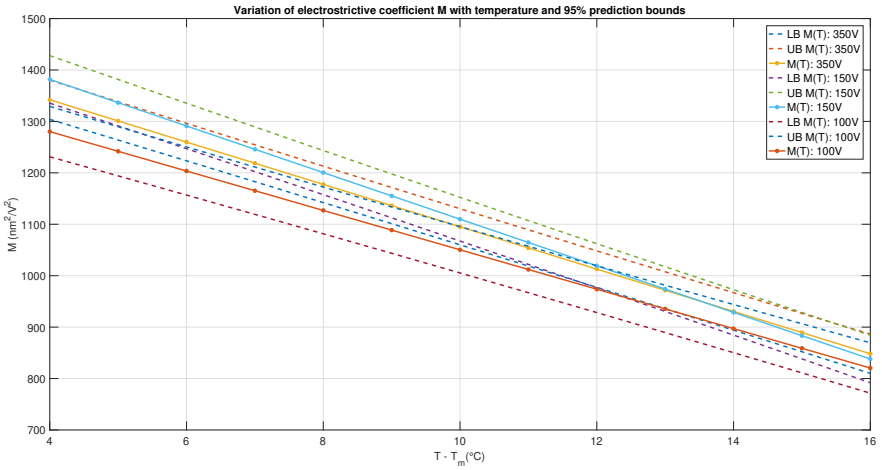

Figure 3-21: Fitted lines obtained from linear regression for electrostrictive coefficient M along with predictive bounds

The model parameters M and k can then be used as functions of temperature with the 95% confidence intervals (shown in the brackets) for the coefficient values:

$$M(T) = m_1 T^* + m_2 \quad (nm^2/V) \tag{3-6}$$

m_1	-41.5	(-48,-35)	$(nm^2/V°C)$
m_2	1504	(1170,1840)	(nm^2/V)

Where, T^* is the temperature difference $(T - T_m)$.

$$k(T) = k_1 T^* + k_2 \quad (nm/V) \tag{3-7}$$

k_1	-17.3750	(-20.7,-15)	$(nm/V°C)$
k_2	1167.5	(1052.5,1322.5)	(nm/V)

These values will change if the operating temperature is lower than T_m. As discussed before, T_m changes with frequency and fraction of PT content in the material.

Using the functional relations $M(T)$ (3-6) and $k(T)$ (3-7), the model equations 2-29 and 1-10 can be represented as functions of temperature.

These temperature dependent models can then be used in feedforward control schemes to get temperature compensation as shown in section 3-4. The basic premise of temperature compensation can be described in fig. 3-22. The idea is to transverse different temperature curves by varying the applied voltage so as to maintain the required set-point.

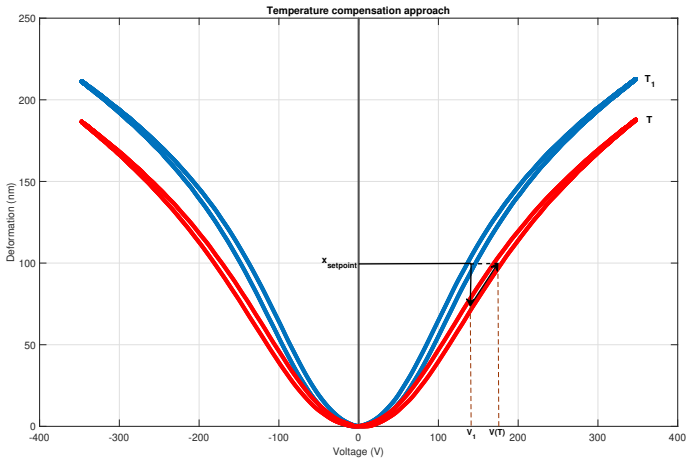

Figure 3-22: Compensation idea

3-3-3 Linearized hyperbolic model analysis using experiment data

In this section, further analysis using experiment data will be built on section 2-3-2. The analysis would be done using the temperature dependent model parameters that display the

electrostrictive effect with minimal errors. In section 3-3-2, the temperature dependence of M and k was shown to be linear to good degree of approximation. But as seen from the (3-23), a quadratic fit better represents the variation of model parameter with temperature for a wide range of temperatures.

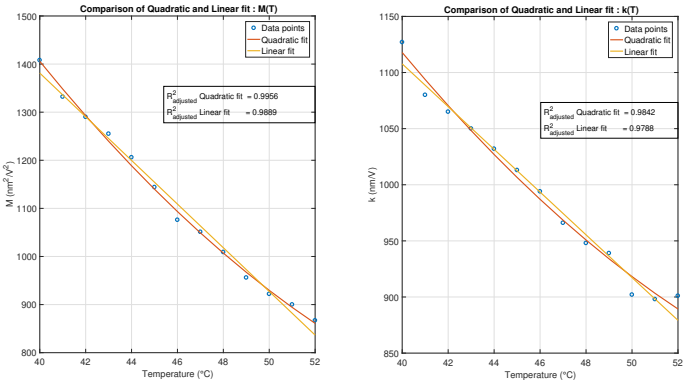

Figure 3-23: Comparison of linear and quadratic fit of M and k with temperature

Using the quadratic fit for these model parameters with temperature , and assuming that the hyperbolic model provides a sufficient degree of accuracy to represent electrostrictive effect, the variation of slope of deformation-voltage curves (from now on to be referred as d) with temperature can be calculated. As explained before in section 2-3-2, the rationale behind this study is that due to the diffused peak of d vs Voltage, the actuator can be operated around the peak voltage value of d vs Voltage curve. In this region, d can be assumed to be independent of voltage using certain AC voltage amplitudes with minimal errors (error analysis described later). Moreover, as the actuator is operated around the maximum d or d_{max}, it will be operated with maximum performance. Moreover, electrostrictive model would be greatly simplified as it will just be dependent on temperature with AC actuation being similar piezoelectric actuation (3-8) around the voltage at d_{max}, V_{max}.

$$z_{AC}(T) = d(T)V \tag{3-8}$$

The slope of the hyperbolic model is mirrored in the region of negative voltage, hence using only positive half of the voltage, the slope of the deformation-voltage curve was shown in section 2-3-2. The variation of the slope(effective piezoelectric coefficient, d)-voltage curve with temperature can now be determined using the functional dependencies of the model parameters. fig. 3-24 shows the variation of d vs Voltage with temperature and also the variation of d_{max} with temperature.

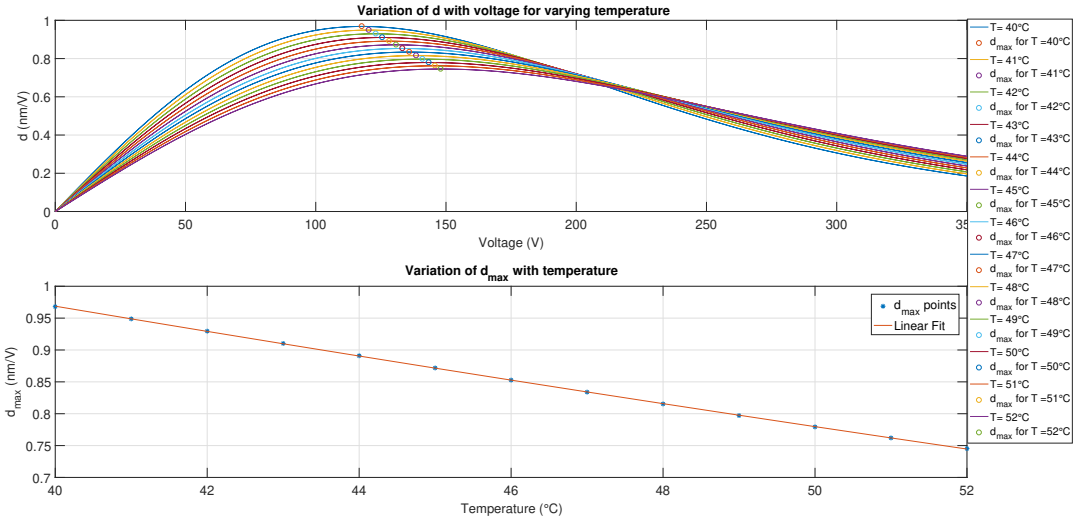

Figure 3-24: a.) Variation of d with voltage at different temperature, b.) Variation of d_{max} with temperature

The linear fit of d_{max} in fig. 3-24 can be used to described $d_{max}(T)$ above T_m as,

$$d_{max}(T) = -0.0187T + 1.714 \quad (nm/V) \tag{3-9}$$

As observed from fig. 3-24, voltage at d_{max} also shifts with temperature. Using this observation, the variation of V_{max} (voltage at d_{max}) can plotted, which also comes out to be linear as observed from fig. 3-25.

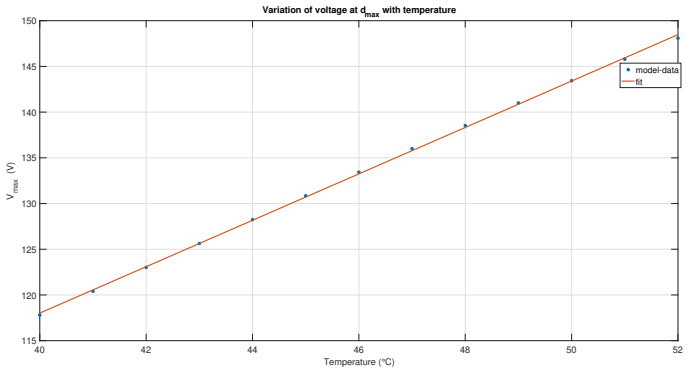

Figure 3-25: Variation of voltage at d_{max} with temperature

The linear fit can be used to describe $V_{max}(T)$ as,

$$V_{max}(T) = 2.54T + 16.5 \quad (V) \tag{3-10}$$

As the shifting d_{max} with temperature corresponds to change in slope with temperature, This may be fully/partially compensating for variation in deformation due to temperature

changes. fig. 3-26 shows the deformation-voltage curves with deformation points at V_{max} for every temperature point, and also the points corresponding to a single voltage. The curves have been obtained by using the hyperbolic model with quadratic functional relations for M and k.

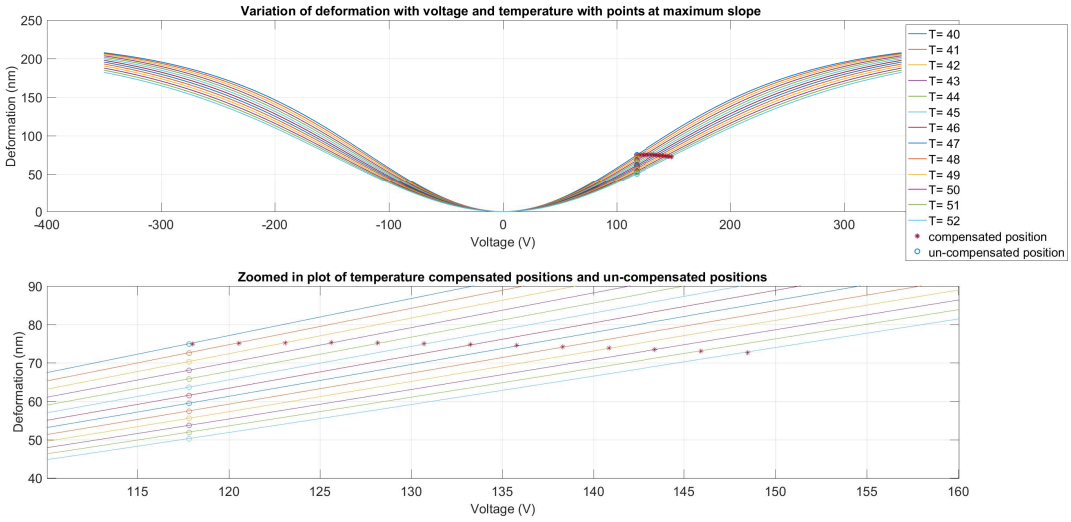

Figure 3-26: Deformation vs Voltage curves with varying temperature along with points at V_{max}.

As seen from the fig. 3-26, the deformation points at V_{max} compensate variation due to temperature quite effectively. The error in compensation shows that the compensation by considering the of relaxation coefficient, k as seen from fig. 3-23. The motivation behind linearizing about d_{max} was due to diffused slope and assuming invariance with actuating AC voltage about the V_{max}. This assumption is valid only if the error with actual deformation curve is small enough for the required application. In fig. 3-27, different AC voltages amplitudes are used for linear actuation around and the error is obtained after subtracting the linear actuation result from the hyperbolic model result for all bias voltages.

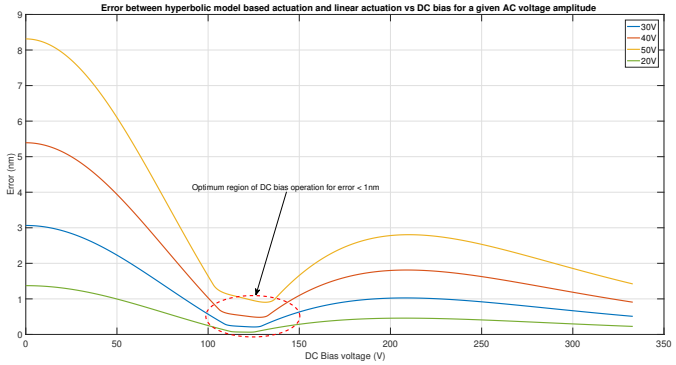

Figure 3-27: Error with different AC voltages around V_{max} for

It can be observed that minimum error in all the AC amplitude cases, is around the same

bias voltage as V_{max}. This shows that according to acceptable error in the actuation and compensation, suitable AC voltages around $V_{max}(T)$ can be used to both steer the actuator to a desired AC setpoint and compensate the temperature induced disturbances.

The error, for assuming a voltage invariant slope, decreases at DC bias = V_{max} with increasing temperature at 30V AC amplitude as seen in fig. 3-28. The error is the maximum error between the hyperbolic model and linear model.

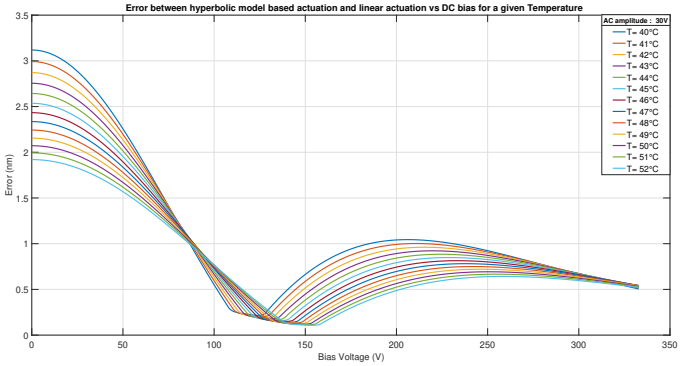

Figure 3-28: Error for assuming voltage independent slope vs DC bias at 30V AC amplitude

3-4 Feedforward Control

The feedforward schemes would use temperature reading as a feedback measure and not the actual position of the actuator. The first scheme involves inverting the plant model and therefore, getting the required setpoint as shown in fig. 3-29.

3-4-1 Inverse Feedforward control scheme

In the control scheme 3-29, P is the plant or the actuator, $\hat{P}^{-1}$ is the inverse electrostrictive model containing temperature dependent behavior, T is the actual temperature of the actuator, V_T is the temperature signal given to the inverse model, z_A is the actual output of the actuator, z_{ref} is the set- point, V_{ref} is the temperature compensating voltage to achieve the desired set-point. A low pass filter is added after the temperature sensor to cancel noise and perturbation above ≈ 0.1 Hz.

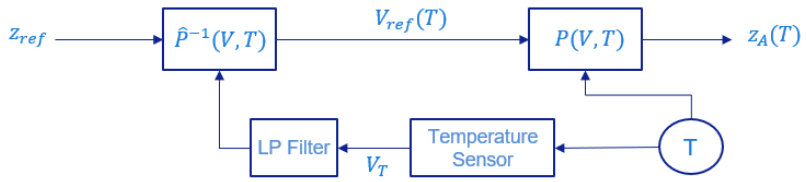

Figure 3-29: Feedforward control: Model inverse based control scheme

The inverse model for feedforward using the quadratic and hyperbolic models can be calculated as,

$$V(T) = \sqrt{\frac{z_{ref}L}{M(T^*)}} \quad \text{(Inverse Quadratic model)} \tag{3-11}$$

$$V(T) = \frac{L}{k(T^*)^2} tanh^{-1}\left(\sqrt{\frac{z_{ref}k(T^*)^2}{M(T^*)L}}\right) \quad \text{(Inverse Hyperbolic model)} \tag{3-12}$$

where z_{ref} is the position setpoint (nm), L is the thickness of the actuator, $M(T)$ is the temperature dependent electrostriction coefficient (nm^2/V), $k(T)$ is the temperature dependent relaxation coefficient and $V(T)$ is the compensating voltage (V) that now depends on temperature.

As the set point will always be positive or have an offset, the quadratic model is always valid, whereas the hyperbolic model is constrained by the domain of inverse hyperbolic tangent function (-1,1). As the function in eq. (3-12) has a square root the domains further reduces to (0,1). This results in a constraint on the set-point that can be given to the model at certain temperatures (when M and k are high). The bound can be calculated using eq. (3-12),

$$0 < \frac{z_{ref}L}{M(T^*)k(T^*)^2} < 1 \tag{3-13}$$

$$0 < z_{ref} < \frac{M(T^*)k(T^*)^2}{L} \tag{3-14}$$

As shown in relation 3-14, knowing the relations $k(T^*)$ and $M(T^*)$ as monotonically decreasing for any particular material composition, setpoint constraints can be obtained for using the inverse hyperbolic model. For example, for the available material PMN-38, the upper bound for set point can be obtained using M and k values at 40 $°C$ or $(T - T_m) = 4°C$,

$$z_{ref} < 223nm \quad \forall \quad T \in (40°C, \tilde{T}) \tag{3-15}$$

where $\tilde{T}$ is any arbitrary temperature above $40°C$ till which material structure does not vary (theoretically called as Burns temperature, T_b refer section 1-2).

3-4-2 Observer based feedforward control scheme

The second way to achieve feedforward control is by using an observer. The observer is the actual electrostrictive model that would take temperature and voltage as its input and generate a deformation output that can be compared to a reference set-point. The error between the reference set-point and the output of the observer can be controlled using a controller. As the observer lacks any dynamics, it is in essence a temperature and voltage varying gain block. The observer based control scheme is shown in the schematic 3-30.

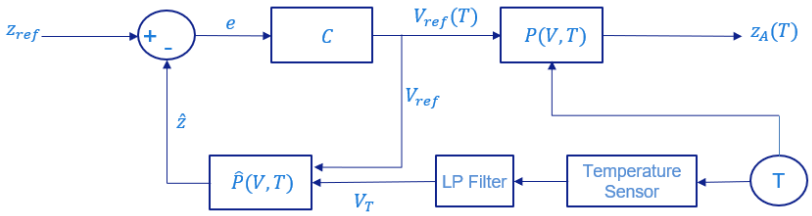

Figure 3-30: Feedforward Control: Observer based control scheme

In the schematic 3-30, C is the controller (PID), $\hat{P}$ is the observer gain (electrostriction model), The control scheme 3-30, can use the full range of the quadratic and hyperbolic model and is valid for all set-points with full-scale temperature range (above the freezing temperature, T_f(refer section 1-2)).

As the dynamics of changing temperature are extremely slow (<0.1 Hz), the observer $\hat{P}$ would be a simple gain block. This will reduce the error signal e in negligible time as shown in fig. 3-31.

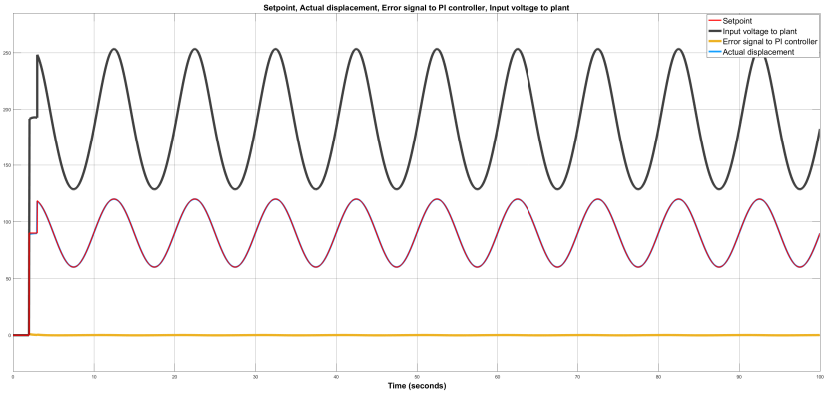

Figure 3-31: Simulation result using observer based scheme and hyperbolic model

3-4-3 Linearized Hyperbolic model based feedforward control scheme

The third way to achieve feedforward control is by using the linearization principles explained in section 3-3-3. As discussed before, the linearized model controls the AC position of the actuator with best performance as it is operating around the DC bias voltage at which the voltage sensitivity is maximum. The added advantage of operating around this point is that the maxima is diffused and hence, the effective piezoelectric coefficient (slope of the deformation-voltage curve) can be considered independent of voltage with very less error (see 3-27, 3-28) by using large AC voltage/actuation voltage amplitudes. A feedforward control scheme that includes summing the changing DC bias voltage and AC actuation voltage (using temperature varying slope and set-point) can be created to control the actuator around maximum slope (d_{max}). As discussed in section 3-3-3, the shifting between different d vs Voltage curves for varying temperature also compensates for the temperature variation thereby maintaining the DC bias setpoint. The AC setpoint (using slope of the linear actuation at DC

bias) is maintained by taking into account the changes in the slope with temperature, which was shown to be linear in fig. 3-24. The control scheme for linearized AC position control is shown in fig. 3-32. In the control scheme, $z_{AC_{ref}}$ is the input AC reference position setpoint and z_{AC_A} is the actual AC position of the actuator.

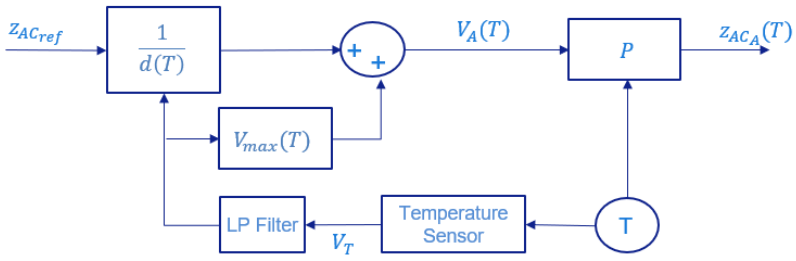

Figure 3-32: Feedforward control scheme: Linearized hyperbolic model

Chapter 4

Results

This section shows the results obtained after applying the feedforward control schemes using temperature dependent electrostrictive models. The expectation is to find the temperature induced strain variation to decrease by substantial amount using electrostrictive parameters as functions of temperature.

The temperature dependent electrostrictive models in quasi-static frequency domain, as discussed in section 3-3-2, are,

$$z_h(V, T*) = \frac{M(T^*)L}{k(T^*)^2} tanh^2(\frac{k(T^*)V}{L}) \tag{4-1}$$

$$z_q(V, T*) = \frac{M(T^*)V^2}{L} \tag{4-2}$$

and the inverse models are:

$$V_q(z_{ref}, T^*) = \sqrt{\frac{z_{ref}L}{M(T^*)}} \tag{4-3}$$

$$V_h(z_{ref}, T^*) = \frac{L}{k(T^*)^2} tanh^{-1}\left(\sqrt{\frac{z_{ref}k(T^*)^2}{M(T^*)L}}\right) \tag{4-4}$$

$$\tag{4-5}$$

4-1 Compensation of strain variation due to temperature change without DC bias

In the first results a pure AC signal is used as a setpoint at 1 Hz frequency, and temperature is varied from $40°C$ to $52°C$ ($T - T_m$ from $2°C$ to $14°C$). The amplitude of the setpoint signal is set to 100 nm. In this way, the setpoint covers the temperature variations from 0-100

nm deformations. The feedforward control using inverse plant scheme (as shown in 3-29) is used for compensating deformation changes due to temperature variation and achieving the desired setpoint using electrostrictive model. In fig. 4-1, 100 nm deformation voltage is estimated to be 100V (at some mean temperature in between 40 and 52 $°C$)from previous experiment results 3-3-2. For this result, the temperature was maintained at discreet points and measurement was conducted at those specific temperature points. The measurement data shows averaged deformations at different temperatures.

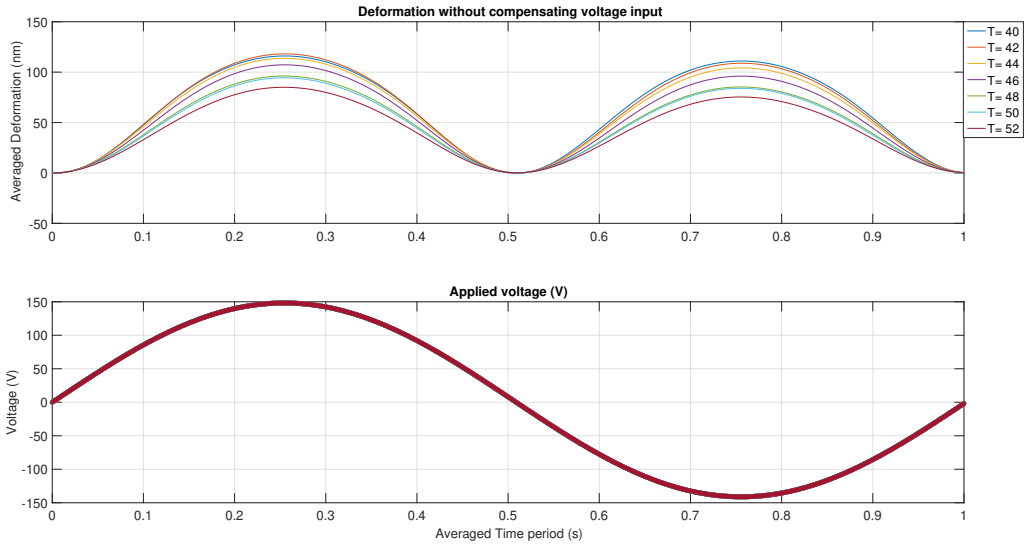

Figure 4-1: Uncompensated signal with voltage amplitude set to 100 V

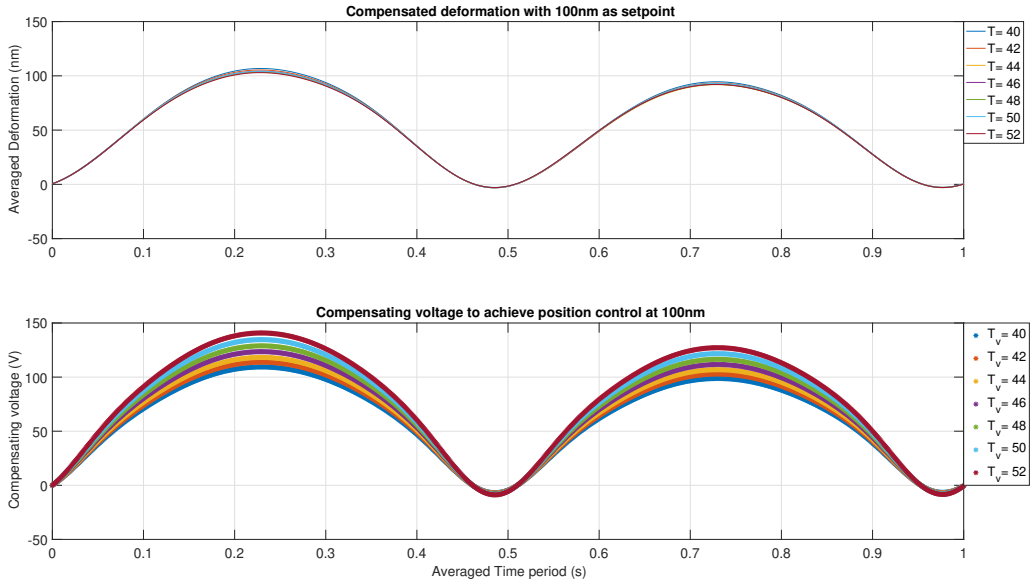

Figure 4-2: Real time: Compensated signal with setpoint amplitude set at 100 nm

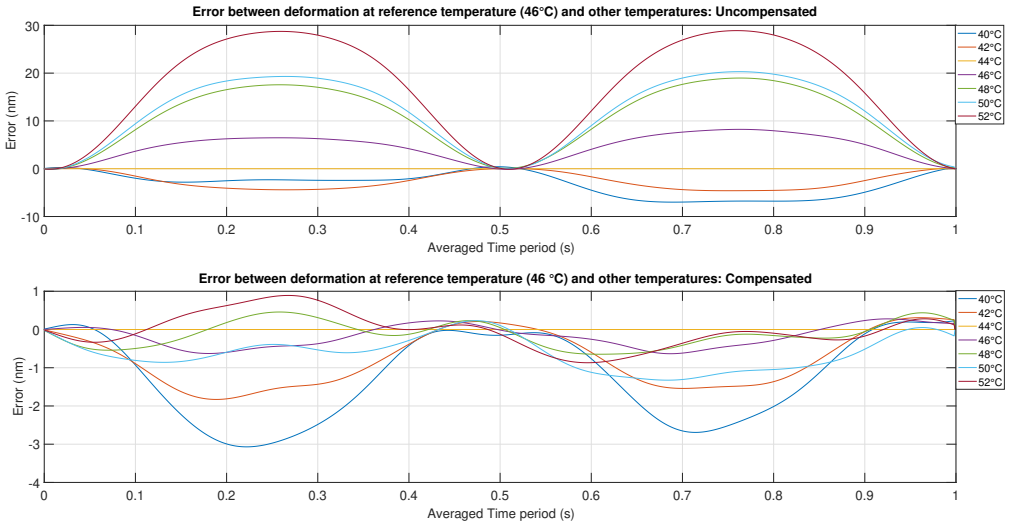

Figure 4-3: Error between a reference temperature output and output signals for Uncompensated and compensated deformations

In fig. 4-1, the compensated result is shown where the voltage is varied with changing temperature(3-11). The bottom graph in fig. 4-2 shows how the applied voltage is varied with changing temperature in order to compensate the temperature induced changes in the actuator deformation.

The error between a setpoint at certain temperature (mean of the range) is calculated by subtracting reference temperature output from output with other temperatures in range as shown in fig. 4-3. The error reduction after temperature compensation is about 87% corresponding to the maximum variations of 4 nm and 32 nm with 12 $^{\circ}C$ change in temperature.

4-2 Compensation of strain variation due to temperature change at DC bias

In this result, a pre-determined DC setpoint is applied (100 nm) to the actuator and a 25 nm sinusoidal setpoint is superimposed on it. The DC set point could not be maintained due to drift effects from varying temperature conditions. Though the DC bias setpoint was not compensated, the changes in the slope (deformation-voltage) due to changing temperature were accurately produced by the feedforward model as shown in fig. 4-6. The results were obtained with temperature variation occurring in real time. Blocks of deformation signals were extracted for each temperature slot with range of approximately $0.2^{\circ}C$. In the time frame of the temperature range, the deformation periods were averaged to get a single period deformation output corresponding to the mean temperature in each slot (standard deviation from averaging was less than 1 nm as shown in Appendix C). The post-processing is explained in more detail in Appendix C. For this result, the temperature was varied continuously from 41 to $51^{\circ}C$ as shown in fig. 4-7. The controller parameters of the Peltier heater were manually tuned to achieve a constant current to change the temperature at the location of its feedback

temperature sensor. This ensured that the copper block (base for the actuator) had minimal influence of higher order thermal modes that might make the block wobble and change its shape. Using the constant current/heat supply at a optimum rate, the block experienced only thermal expansion which was detected using the reference intereferometer probe (as shown in the fig. 3-8).

Using this, several deformation responses corresponding to the temperature slots were plotted. The uncompensated result 4-4 shows variation in deformation for the mentioned temperatures. The compensated result 4-6 shows how the feedforward control scheme using quadratic model eliminates the variation due to changing temperature. The offset and variation in the result from set point amplitude (25nm) can be seen in the error plots in fig. 4-6. The offset variation is due to the quadratic model being used in place of hyperbolic model, nevertheless, the variation due to changing temperature is compensated well by both models due to similar slopes of the M coefficient as shown in fig. 3-19.

Note that the averaged deformation curves are normalized about the DC biased setpoint (which is drifting with temperature). This means that the the DC biased deformation is considered as 0 in the deformations curves in fig. 4-6 and fig. 4-4. The Input-output curves in fig. 4-6 show how the slope changes to maintain the sinusoidal setpoint around the DC biased setpoint (which is set to 0 nm).

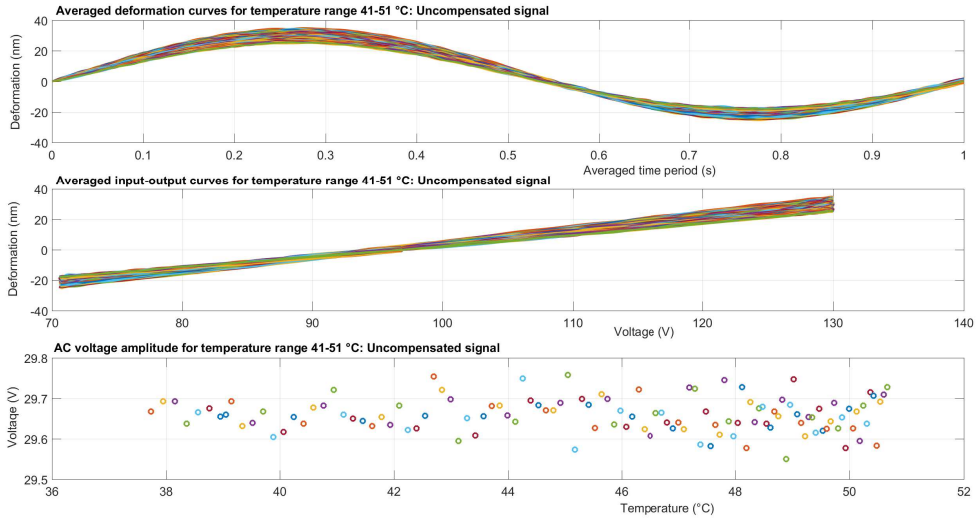

Figure 4-4: Uncompensated signal with DC setpoint as 100 nm and sinusoidal setpoint amplitude as 25 nm

The maximum variation in deformation after compensation is approximately 2.5 nm with 10 $^{\circ}C$ change in temperature, which translates to approximately 75% reduction in temperature variation error from the uncompensated signal (maximum variation of 9 nm). The decrease of temperature variation induced error from 87% to 75% can be attributed to the use of quadratic model for compensation. In the 2nd result, deformation reading is used for for uptill 125 nm. Around this deformation, higher harmonics start getting larger as shown in fig. 3-16 and fig. 3-17. Nevertheless, the quadratic model is sufficient to provide compensation for temperature induced variation in the deformation.

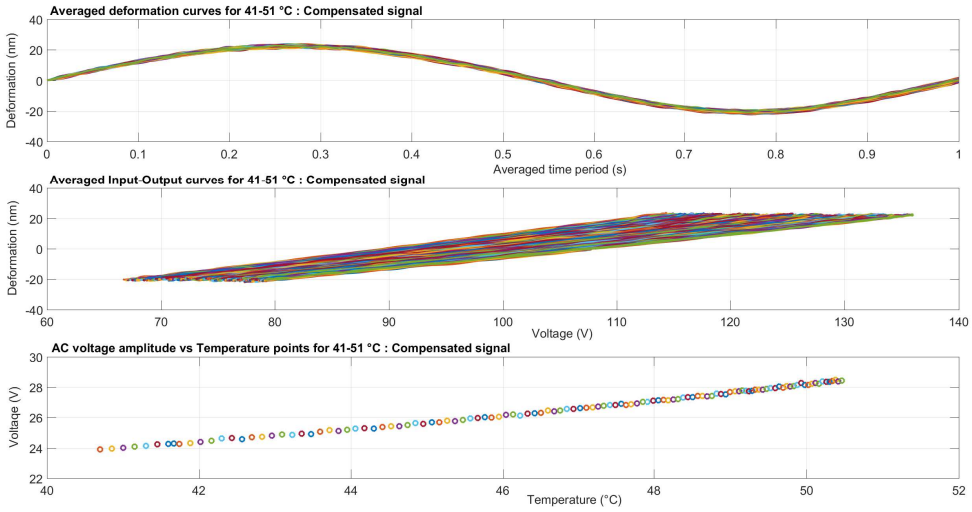

Figure 4-5: Real time: Compensated signal with DC setpoint as 100 nm and sinusoidal setpoint amplitude as 25 nm

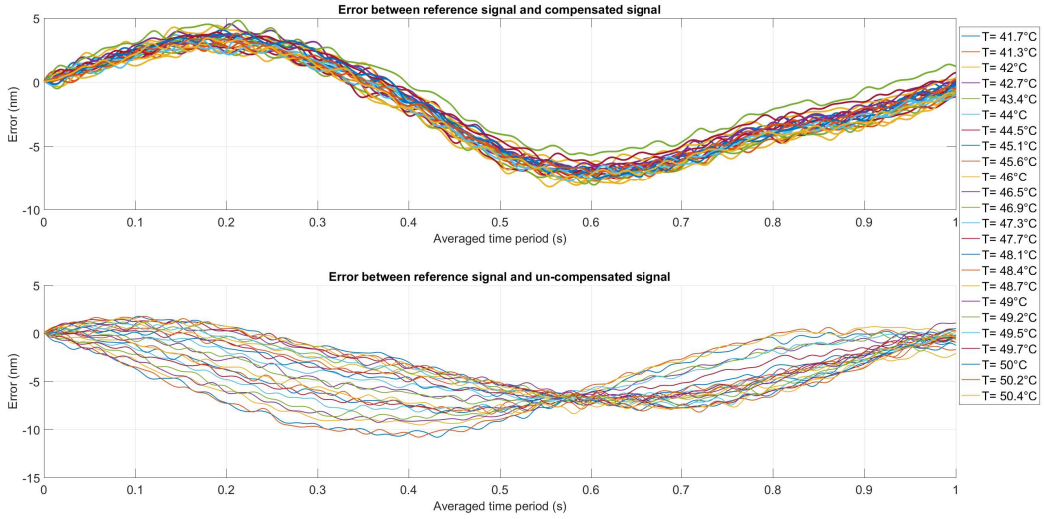

Figure 4-6: Error between the sinusoidal setpoint and deformation curves at different temperatures

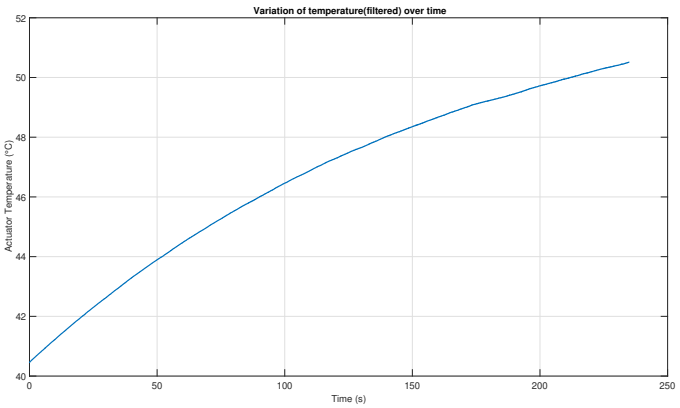

Figure 4-7: Temperature variation used for the results

Chapter 5

Conclusions and Future Recommendations

Electrostrictive PMN-PT has a nonlinear strain-field behavior that is coupled with a temperature sensitive response. The requirement of the thesis was to investigate and characterize the effects of temperature variation and create suitable models that could be used in feedforward control schemes to compensate these variations in real time. To this effort, linear and non-linear models were investigated in section 2-2 and section 2-3 to understand the actuator response to input parameters. The analysis gave important insight and predictions regarding the behavior of electrostrictive response under changing voltage and temperature conditions, that were later verified through High Frequency Impedance (section 3-2) and Quasi-static strain field experiments (section 3-3).

Using experiment data, a functional description of model parameters was obtained. This description was used in the available electrostrictive models to create macroscopic temperature dependent models (3-3). Two feedforward schemes were then used to successfully decrease the temperature induced strain variation by atleast 75%-87% (4). Further variation can be reduced using the temperature dependent hyperbolic model scheme and also using the observer based feedforward model (3-30).

The answer to the Research Objective (1-4-2) can be stated as:
4 useful temperature dependent electrostrictive models have been devised for nonlinear and linear calibration through which precise position control is shown to be achievable using appropriate Feedforward schemes. Using the quadratic electrostrictive model and inverse Feedforward scheme precise position control, in the presence of temperature disturbance, is shown to be achieved in real time.

To summarize, following are the key conclusions of this thesis,

1. Through the literature study it is concluded that proper electrostrictive material composition must be chosen corresponding to the operating temperature in order to get desired low hysteresis and frequency dispersion effects.

2. A linear impedance model (2-2) is useful for finding model parameters and its variation with temperature under low electric field conditions using quick high frequency impedance measurements.

3. Using the experiment results it is shown that the electrostrictive response is accurately described by hyperbolic model whose parameters have good linear functional dependency with temperature as shown in chapter 3.

4. Using experiments, another empirical model for electrostriction is found (section 2-3-2) that is has best performance due maximum voltage sensitivity. The added advantage with this model aside from being linear, is that it gives high actuation-voltage band and compensates for temperature induced variations both in DC position setpoint and actuation position setpoint (AC).

5. Position control in the presentation temperature disturbances was achieved in real time using inverse plant model based FF using quadratic electrostrictive model as shown in chapter 4.

6. Due to deterioration of the electrostrictive samples (electrode layer wore off) and base copper block (erratic thermal and electrical conduction on surface) further real time compensation using other devised models was not achieved, though simulations/analysis show no fundamental problem in achieving position control experimentally.

Future Recommendations

This section includes the scope of future research and applications using this thesis as the background work.

1. The effect of stress on the actuator behavior has been investigated in literature ([14], [49], [2]). But research regarding its application with temperature dependent behavior needs to be investigated. The stiffness is shown to be a linear function of temperature but the sensitivity is quite low. Investigation in the variation of stiffness, and therefore effect of stress, in a band of voltage and temperature is needed to characterize a general response.

2. The impedance results were used to predict the temperature sensitivity and its application as a temperature sensor as briefly explained in section 3-2-2. This aspect is elaborated further in future research. A patent is filed using this idea. Through this, a complete feedforward system, without requiring temperature sensors, can be realized for the deformable mirror application. The temperature self-sensing concept needs to be experimentally verified for position control through feedforward scheme. Moreover, as the main premise of the technique is to detect movement of resonances with temperature, further study is needed to characterize the effects of stress on the movement of resonance frequencies and its incorporation in the impedance model to isolate and measure temperature dependent shifts in the resonances

3. Effect of frequency dispersion of material parameters needs to be accommodated for getting the higher electrostrictive gains below T_f (and above T_m). This should then

be verified using the standard electrostrictive models. This would help in achieving position control over a wide band of frequency and temperature.

4. The temperature self-sensing concept needs to be experimentally verified for position control through feedforward scheme. As the main premise of the technique is to detect movement of resonances with temperature, further study is needed to characterize the effects of stress on the movement of resonance frequencies and its incorporation in the impedance model to isolate and measure temperature dependent shifts in the resonances

5. A more robust experiment setup is needed to eliminate the effects of drift and delay in the measurement so as to characterize the response more accurately. The increased accuracy would help to directly measure and characterize effects like aging. Moreover, a better temperature control environment would minimize dynamic effects of current and therefore make the base of actuator more stable (less effect of higher thermal modes).

Appendix A

Appendix A

Outline In this chapter, the impedance equation for electrostrictive material is derived.

The model's static constitutive equations under no applied force are:

$$x = ME^2 \tag{A-1}$$

$$D = 2MTE \tag{A-2}$$

here D is the electric displacement (C/m^2), E is the applied electric field (V/m), T is stress in the material (N/m^2), x is Induced strain in the material due to applied field, M electrostriction coefficient.

The above equations can be written as a relation between deformation, applied voltage ,induced charge and force as follows:

$$z_{int} = \frac{MV_p^2}{L} \tag{A-3}$$

$$Q = \frac{2Mf_pV_p}{L} \tag{A-4}$$

In the above equations, V_p is the applied voltage, L is the actuator thickness, Q is the induced charge due to internal force f_p under the influence of applied voltage V_p, z_{int} is the induced deformation through applied voltage.

The applied voltage can be written as the summation of the applied DC bias and applied sinusoidal voltage.

$$V_p = V_{dc} + V_{ac} \tag{A-5}$$

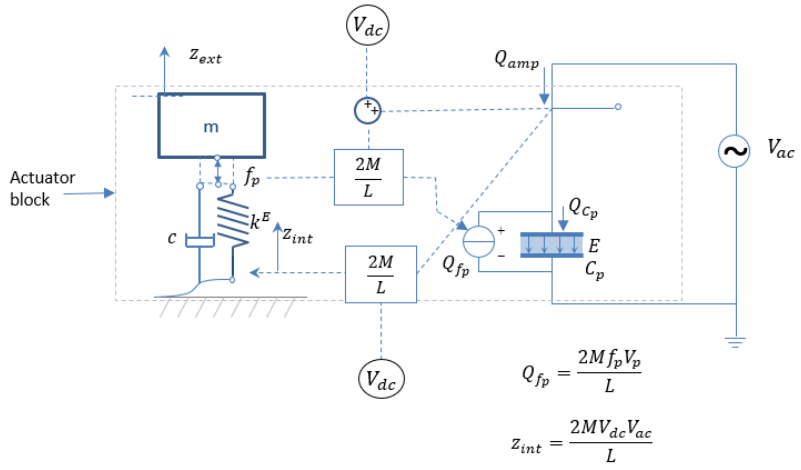

Figure A-1: Electromechanical model

In the fig. A-1, it can be observed that electromechanical coupling model of the electrostrictive actuator in a voltage controlled setting. The external force F_{ext} is assumed to be 0 in this analysis.
The model shows nonlinear relation between applied voltage (V_p) and internal position(z_{int}). The stiffness (k^E) of the actuator is shown by a spring.

The induced charge due to the internal force, f_p is only valid when the actuator has an applied voltage present. This shows that the material behaves sort of like piezoelectric (though with coupled force and voltage) only when under the influence of applied voltage.

Taking into account the dynamics of the actuator. From the free body diagram of the mass, m, we see that,

$$m\ddot{z}_{ext} = f_p \tag{A-6}$$

substituting $f_p = (z_{int} - z_{ext})k^E - cz\dot{e}xt$,

$$m\ddot{z}_{ext} = (z_{int} - z_{ext})k^E - cz\dot{e}xt \tag{A-7}$$

As $z_{int} = \frac{MV_p^2}{L}$, we substitute this into the eq. (A-7),

$$m\ddot{z}_{ext} = \frac{MV_p^2k^E}{L} - z_{ext}k^E \tag{A-8}$$

simplifying,

$$m\ddot{z}_{ext} + z_{ext}k^E = \frac{MV_p^2k^E}{L} \tag{A-9}$$

The eq. (A-9) cannot be directly solved algebraically as we required impedance transfer function and for that we cannot assume some V_p and take the laplace transform of it. We thus expand V_p as $V_p = V_{ac} + V_{dc}$ and assume $V_{dc} >> V_{ac}$ in amplitude. This way we can approximate the electrostrictive behavior as a piezoelectric behavior at a certain DC bias and at the same time incorporate changes in the response with changing DC bias.
We can write,

$$V_p^2 = V_{ac}^2 + V_{dc}^2 + 2V_{ac}V_{dc} \tag{A-10}$$

As, $V_{dc} >> V_{ac}$,

$$V_p^2 = V_{dc}^2 + 2V_{dc}V_{ac} \tag{A-11}$$

Expanding V_p^2

$$m\ddot{z}_{ext} + z_{ext}k^E = \frac{MV_{dc}^2k^E}{L} + \frac{MV_{ac}^2k^E}{L} + \frac{2MV_{ac}V_{dc}k^E}{L} \tag{A-12}$$

Neglecting higher order V_{ac} term as $V_{dc} >> V_{ac}$,

$$m\ddot{z}_{ext} + z_{ext}k^E = \frac{MV_{dc}^2k^E}{L} + \frac{2MV_{ac}V_{dc}k^E}{L} \tag{A-13}$$

Just for reference, we solve the A-13 by taking laplace transform,

$$mz_{ext}(s)s^2 + k^Ez_{ext}(s) = \frac{1}{s}\frac{MV_{dc}^2k^E}{L} + \frac{2MV_{dc}k^E}{L}V_{ac}(s) \tag{A-14}$$

$$z_{ext}(s) = \frac{1}{s(ms^2 + k^E)}\frac{MV_{dc}^2k^E}{L} + \frac{1}{ms^2 + k^E}\frac{2MV_{dc}k^E}{L}V_{ac}(s) \tag{A-15}$$

Assuming a linear response to the applied voltage V_{ac}, the transfer function from V_{ac} to z_{ext} is ,

$$z_{ext}(s) = \frac{1}{ms^2 + k^E}\frac{2MV_{dc}k^E}{L}V_{ac}(s) \tag{A-16}$$

We proceed to the charge calculation for the voltage controlled model

$$Q_{amp} = Q_{cp} - Q_{fp} \tag{A-17}$$

Where, $Q_{cp} = C_pV_p$ is the charge given by the voltage controlled circuit and C_p is the capacitance of the actuator.
The induced charge at a certain DC bias voltage can be represented using the charge equation

of the electrostrictive material,
As,

$$Q_{fp}(t) = \frac{2Mf_p(t)V_p}{L} \tag{A-18}$$

To find the laplacian $[f_p(t)V_p(t)]$, we take the time domain product of f_p and V_p

$$f_p(t)V_p(t) = k(\frac{MV_p^2}{L} - z_{ext})V_p \tag{A-19}$$

$$f_p(t)V_p(t) = \frac{k^E MV_p^3}{L} - k^E z_{ext}V_p \tag{A-20}$$

$$\tag{A-21}$$

Expanding V_p^3,

$$f_p(t)V_p(t) = \frac{k^E MV_{dc}^3}{L} + \frac{k^E M}{L}V_{ac}^3 + \frac{3k^E MV_{dc}^2}{L}V_{ac} + \frac{3k^E MV_{dc}}{L}V_{ac}^2 - k^E z_{ext}V_{dc} - k^E z_{ext}V_{ac} \tag{A-22}$$

As the z_{ext} part contains fluctuations due to V_{ac}, and as $V_{dc} >> V_{ac}$, we can neglect its higher order effect, also, we can neglect the terms that do not contain the V_{ac} component as a linearized response is needed. Therefore,

$$f_p(t)V_p(t) \approx \frac{3c^E MV_{dc}^2}{L}V_{ac} - k^E z_{ext}V_{dc} \tag{A-23}$$

taking the laplace transform of the above equation, we get,

$$[f_p(t)V_p(t)](s) = \frac{3k^E MV_{dc}^2}{L}V_{ac}(s) - k^E z_{ext}(s)V_{dc} \tag{A-24}$$

The charge equation A-18 can then be written as,

$$Q_{fp}(s) = \frac{2M(\frac{3k^E MV_{dc}^2}{L}V_{ac}(s) - k^E z_{ext}(s)V_{dc})}{L} \tag{A-25}$$

substituting the expression for deformation A-16 and $z_{ext}(s)$ in A-25,

$$Q_{fp}(s) = \frac{\frac{6Mk^E MV_{dc}^2}{L}V_{ac}(s) - (\frac{2Mk^E}{ms^2+k^E}\frac{2MV_{dc}k^E}{L}V_{ac}(s))V_{dc})}{L} \tag{A-26}$$

Simplifying,

$$Q_{fp}(s) = \frac{M^2k^E V_{dc}^2}{L^2}(\frac{6ms^2 - 2k^E}{ms^2 + k^E})V_{ac} \tag{A-27}$$

As $Q_{amp} = Q_{Cp} - Q_{fp}$, (charge circulating in the circuit)

$$Q_{amp} = C_p(V_{ac} + V_{dc}) - \frac{M^2 k^E V_{dc}^2}{L^2}(\frac{6ms^2 + 6cs - 2k^E}{ms^2 + cs + k^E})V_{ac}(s) \tag{A-28}$$

The output of the charge response to voltage is considered only from the V_{ac} part at the specified V_{dc}, therefore, compiling only the V_{ac} terms,

$$Q_{amp} = C_p V_{ac} - \frac{M^2 k^E V_{dc}^2}{L^2}(\frac{6ms^2 + 6cs - 2k^E}{ms^2 + cs + k})V_{ac}(s) \tag{A-29}$$

$$Q_{amp} = (C_p - \frac{M^2 k^E V_{dc}^2}{L^2}(\frac{6ms^2 + 6cs - 2k^E}{ms^2 + cs + k^E}))V_{ac}(s) \tag{A-30}$$

$$\frac{Q_{amp}}{V_{ac}(s)} = \frac{s^2(C_p L^2 m - 6M^2 V_{dc}^2 k^E m) + s(cC_p L^2 - 6M^2 k^E V_{dc}^2 c) + (C_p k^E L^2 - 2M^2 (k^E)^2 V_{dc}^2)}{L^2(ms^2 + cs + k^E)} \tag{A-31}$$

As $I_{amp} = sQ_{amp}$

$$\frac{V_{ac}}{I_{amp}(s)} = \frac{L^2(ms^2 + cs + k^E)}{s^3(C_p L^2 m - 6M^2 V_{dc}^2 k^E m) + s^2(cC_p L^2 - 6M^2 k^E V_{dc}^2 c) + (C_p k^E L^2 - 2M^2 (k^E)^2 V_{dc}^2)} \tag{A-32}$$

Appendix B

Appendix B

Outline This appendix includes the description of experiment post processing, data sheets and other calibration techniques used to tune the instruments to get proper results. The chapter starts with the description of the setup and tuning of measurement instruments used in impedance measurements and quasi-static strain field measurements. The section then explains the data acquisition and processing.

B-1 Measurement Instruments and Calibration

In this section, information (data sheet etc) about the measurement instruments used and their calibration would be provided.

B-1-1 Interferometer: Actuator displacement sensor

An interferometer was used as a displacement sensor for the quasi-static strain field experiments. The unit is a Keyence SI series interferometer [50]. It contains a controller, laser probes and a support software. The support software, SI Navigator, was used to calibrate the settings and tune the instrument in the desired displacement region.

The laser is an SI-F01 Micro-Head based probe with the measurement range as 0.05-1.1 mm. The basic principle of the Keyence SI series interferometer is shown in fig. B-1[50]. The SI series interferometer contains two measurement modes: Normal mode and Interferometer mode. The Normal mode is an absolute interferometry and is not accurate enough for the measurement requirement as it considers only the light reflected from the target surface (see fig. B-1).

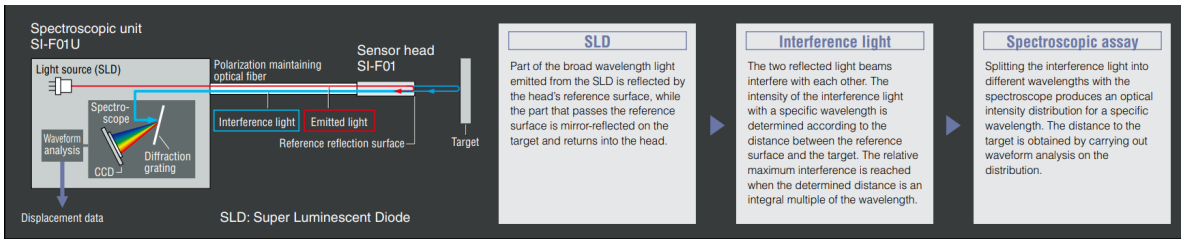

Figure B-1: Working principle of Keyence interferometer

Subsequent waveform analysis of this reflected beam yields the distance to target. The interferometer mode on the other hand uses interference of both the light reflected from the target and the reference reflection surface (see fig. B-1) to measure the resulting intensity, and hence the measures the displacement of the target surface. The resolution attained by the interferometer in this mode is 1nm. Therefore for experiments, the interferometer mode was used. Moreover, for interferometer mode, a relatively shiny surface is required so that the intereference intensity is large enough to get precise reading. As the PMN-PT actuator was gold/chromium plated, it had relatively visible light reflection. As the intensity might change due to the distance of the probe from the actuator surface, the luminosity of the reflected light was observed in the SI navigator software (View Waveform) and the distance to actuator was adjusted to get maximum light intensity (sufficient intensity was confirmed by green light in the Head status). In order to get raw data (so that controlled post-processing could be done later), all the internal signal filtering were turned off in the interferometer controller. Using the analog input/output ports behind the controller (fig. B-2), analog voltage signals were collected and transferred to the SpeedGoat IO104 board (see reference). To get zero the reference measurement for every measurement, a step signal of 5V was passed to the controller from the SpeedGoat 1O104 board to the interferometer controller IO board (fig. B-2). This signal was passed before the start of every measurement.

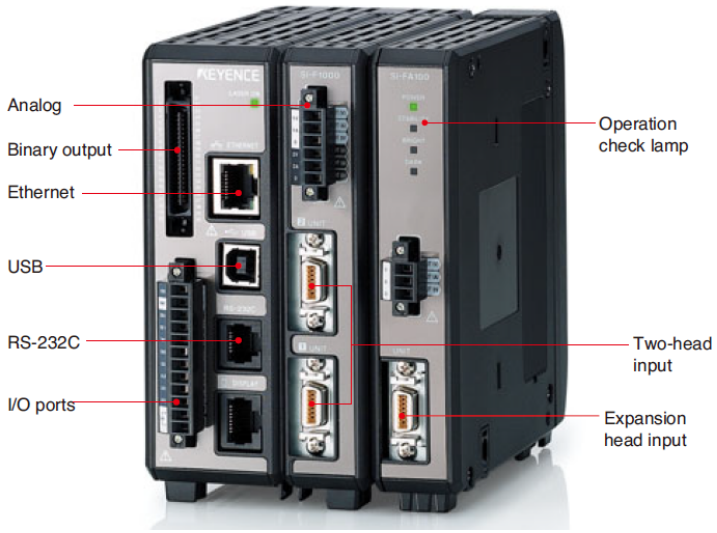

Figure B-2: Interferometer controller data acquisition ports

For analog readings, a Full Scale of (-2μm, 2μm) was used with corresponding voltage range of (-10V, 10V). This resulted in sensitivity of 0.2nm/1mV. As the SpeedGoat IO104 has a voltage detection limit in micro-volts, this sensitivity was sufficient for the measurements. The interferometer probe is resistant to changes in the environment temperature from 0 to 85°C. The variation in displacement reading due to temperature fluctuation for the sensor head is 0.01% of Full Scale per °C. For the mentioned calibration settings, this results in 0.4nm/°C. The actual error would be much less as the variation in temperature for every measurement is kept below 0.01°C through the Peltier heating controller (see reference to Peltier). Further information on the details of the SI interferometer can be found in the data sheets of its website [50].

B-1-2 Peltier Heating/Cooling device

For heating the actuator to a specific temperature with high accuracy, a Peltier Heater [51] along with a suitable controller (TEC-1122, Precision Temperature Controller [52]) was used. The Peltier controller was connected to a 24V DC supply. An NTC 10K temperature sensor was used as the feedback sensor to the controller for maintaining the required temperature at the sensor position. It was connected close to the actuator to achieve the required temperature at the actuator. The controller contains 2 channels for controlling 2 Peltier heaters. In the experiment as only 1 peltier heater was used, only one channel was connected (2nd channel, due to malfunctions in channel 1)to the heater. The settings in the Peltier controller were modified using the TEC service software. The controller had a built-in PID control scheme that could be tuned to achieve required temperature stability and rise time as required. For the experiments, slow dynamics were deemed suitable as they would prevent high current oscillations (that would mean high temperature oscillations) thereby preventing higher thermal modes in the copper block. This means the copper block would only have thermal expansion in the thickness direction without the higher wobbly modes. This expansion would be effectively canceled out using a reference interferometer probe as explained in chapter 3. The dynamics were changed such that the integral time (T_i) was set to 300s and derivative time (T_d) set to 0s and proportional gain was set to just 10%/°C, which is the portion of the normalized heating power that is used to correct the change between the current temperature and required temperature. Using these PID control parameters, the time taken to achieve the 1∘C temperature change was around 1.5 minutes, but the change happened with constant current supply. This resulted in a smooth ramp to reach the required temperature without oscillations for the particular thermal mass of the copper block (approximately equal to the thermal mass of the rest of the system). Other settings in the software were changed based on the temperature sensor in use (NTC 10K sensor), heating or cooling (or both) requirement and Peltier heater specifications [51]. Real time control (using target PC) of the peltier was tried but it required separate interfacing using RS232 port and due to time constraints it was not implemented. Hence, the temperature control was done using the TEC Service software on a separate PC using USB connection to the TEC controller. Required temperature was plugged in the software and resulting temperature was monitored until it reached equilibrium. After that the quasi-static strain field/impedance measurements were started. Further information on the Peltier heater and Peltier Controller can be obtained on the corresponding website [52][51].

B-1-3 Speedgoat Data Acquisition system (Target PC+ I/O board)

Data acquisition and signal transfer from Simulink (for running the experiments) was done using the Speedgoat Target PC. An I/O board (IO104) served as the interface between the target PC and instruments used in the Quasi-Static strain field measurements (NOTE: Speedgoat target PC was not used in the impedance measurements). An SN1997 Speedgoat real-time target PC was used for loading the compiled program from Simulink. The I/O connectivity was done using IO104 board. The I/O board had several driver blocks that were used in Simulink to connect it to the target PC. IO104 is a 16 bit analog module having several analog input and output connections points. A sampling frequency of 5kHz was used for the measurement. Higher sampling frequency was not chosen as each experiment was run for minimum 50s and data files were becoming too large to process in time. Furthermore, the signal received from interferometer was pseudo-analog, meaning, the controller already post-processed the light intensity signal into voltage signal with a sampling rate of 5kHz. Due to these reason 5kHz sampling rate was kept for all measurements. At the beginning of the experiment, the Simulink file compiled the code and fed it into the Speedgoat target PC. At the end of the experiment a data file was generated, from which relevant voltage (from amplifier(seeappendix B-1-4)), deformation(from interferometer (see appendix B-1-1)), temperature (using a voltage divider circuit) and time data was extracted for post-processing. Further information on the Speedgoat target PCs and I/O boards can be found on the respective webpages [53][54],

B-1-4 Amplifier

For amplifying the voltage signal from IO104, a Trek PZD350A amplifier model was used [55]. The amplifier was chosen due to its accurate and high gain at the capacitive loads of the actuator (at 0 Hz frequency, around 0.02μ F). This can be seen in fig. B-3. As the quasi-static experiments were conducted at frequencies lower than 100Hz, the amplifier gain remained stable at voltage amplitudes of $\pm$ 350V.

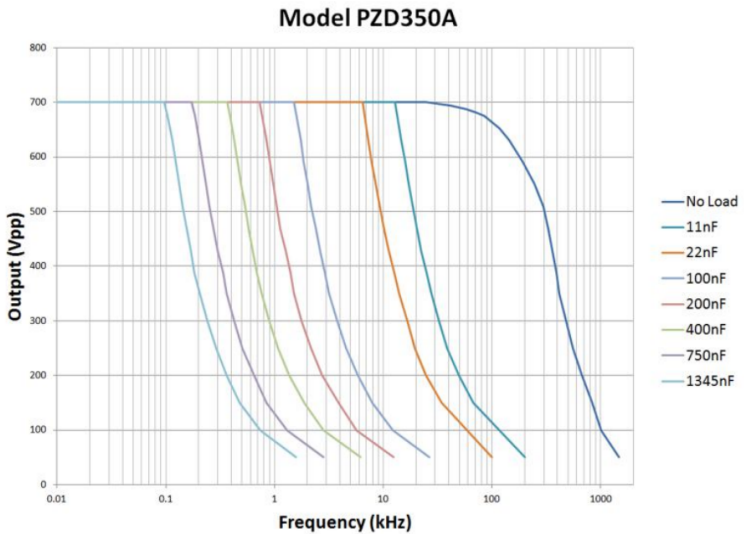

Figure B-3: Frequency response of amplifier output voltage based on capacitive loads

The amplifier also contained dynamic gain adjustment that was tuned appropriately for the specific frequency using an oscilloscope (highly accurate measurement). The output of the IO104 was connected to the input of the amplifier and the gain was adjusted to 100 manually. The actual output voltage of the amplifier was then verified by connecting the output to an oscilloscope. For real time voltage readings, a voltage monitor output (present in the amplifier) was used. The voltage monitor decreased the gain again by 100 times and was fed to the IO104s input pins. This data was used in the post-processing later. For more information on the amplifier check the website [55].

B-1-5 Bode 100 Signal Generator

Bode100 is a type of signal generator that is especially useful for high frequency gain and impedance measurements. The instrument send a low voltage (<0.1V) amplitude chirp signal to the sample to measurement the resulting current and plot the impedance and gain frequency response. The unit requires calibration before use. The calibration is done stepwise for the probe and user requirements(frequency range, resolution etc) using open circuit, closed circuit and a reference impedance (of 50Ω value) configurations.

But as discussed in chapter 3, small AC signal would not generate any dynamics in the actuator even at high frequencies because the voltage sensitivity at 0V DC bias is almost 0 as again shown in chapter 3. Thus, the output of the Bode100 was connected to a DC+AC mixer that also used a DC voltage signal from a power source. The output of this DC+AC mixer was the combination of low voltage AC chirp signal from Bode100 and fixed DC bias from the power supply. This helped in getting impedance response from the actuator at a particular bias(which was varied in the experiments).

As the frequency of interest for the impedance measurements3 was in 1-10MHz range, further tuning needed to be done for getting proper impedance values. This was due to requirement of maintaining a certain voltage and temperature of the actuator. As mentioned in fig. 3-1, the copper block was set as the ground for the voltage signal. This was done due to the constraint that the block was needed to be in full contact with the actuator in order for it to achieve the required temperature. Due to the block and connecting wires, additional inductive and resistive impedance was added to the result that needed to be subtracted from the net impedance result. To achieve this, impedance measurement was conducted to for the setup without the actuator at every temperature. This complex impedance was then subtracted from the overall impedance value of the experiment done with the actuator.

This helped in canceling out the high frequency inductive effects of the wire and temperature induced changes in the resistance of the copper block. Following this approach, the net impedance of the actuator with temperature and DC voltage variation was calculated. This post-processing is mentioned in detail in appendix B-2.

The data sheet of the Bode100 can be found on its webpage [56].

B-2 Post-Processing

B-2-1 Impedance Measurements

For the impedance measurements, additional calibration was needed to remove the high frequency inductance effects from the connecting wires and copper block (mainly resistive due to relatively large size than wires). This was done, as explained in appendix B-1-5, by subtracting the complex impedance of the setup without actuator from the actual impedance readings(with actuator). The raw impedance data for both the cases is shown in fig. B-4.

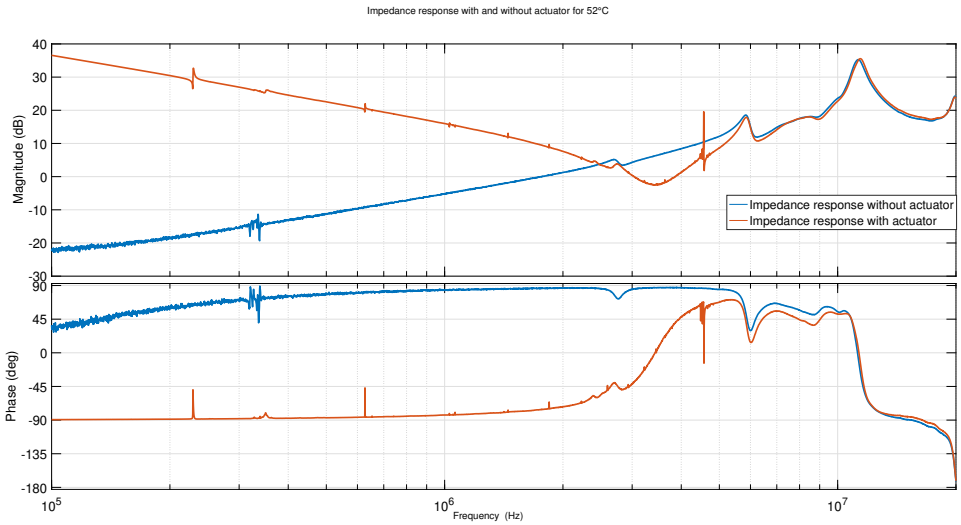

Figure B-4: Impedance response manual calibration with and without the actuator

After getting the impedance data, further post processing involved isolating the thickness and width modes (see chapter 3) and estimating the individual transfer functions for every temperature. The fit for one of the temperatures for thickness mode is shown in (refer figure with the fit and GOF). The coefficients of these transfer were normalized by making the coefficient of the highest power of complex 's' in the denominator. The estimated coefficients were then compared with coefficients of the model transfer function (2-12, which were also normalized about the highest power of 's' in the denominator). This resulted in a set of non-linear equations involving the model parameters. From prior rough knowledge about the order of magnitude of model parameters from literature, it was known that the values fo parameters had difference of 10s of orders of of magnitude. Due to this numerical approach to solve the equations was not used and therefore symbolic toolbox in MATLAB was used to solve the equations algebraically as the equations were polynomial equations and did not contain transcendental functions. The equation set involved 5 equations with 4 unknown variables. To solve for these 4 variables, 4 appropriate equations were chosen (that gave a unique solution for the model parameters). The solutions were calculated for every temperature and then plotted against temperature points to get the required variation estimate.

B-2-2 Quasi-static strain-field measurements

Post-processing of quasi static strain-field experiments involved filtering and extracting useful data from the raw analog measurements obtained via the data acquisition system (Speedgoat target PC). The raw data obtained from the target PC included the raw displacement readings from interferometer (for both the laser probes), voltage input from the amplifier, temperature from the NTC sensor and the time stamp readings (from the clock in target PC). The data was filtered differently for all the signals. The time for the measurements was set to 50s but the first 15 seconds were used for zeroing the interferometer (for reference). In the next 35s the actual measurement was obtained.

Deformation measurement The raw deformation(reference to figure with raw deformation) was first low pass filtered at a cut-off frequency of about 10Hz. This was done to cancel out the noise contribution from the interferometer and setup. From literature survey and later with experiment data analysis, it was known that the higher harmonic contribution of the actuator displacement was negligible after the 3rd even harmonic (8th harmonic). This means for 1 Hz actuating frequency, the contribution of harmonics above 8 Hz was almost null (4 orders of magnitude less than 1st even harmonic in the amount of power contribution as seen from PSD graphs 3-15) for the highest applied voltage of 350V. The 2nd order low pass filter was applied with zero-phase digital filtering that prevented any phase lag in the filtered measurement as seen in fig. B-5.

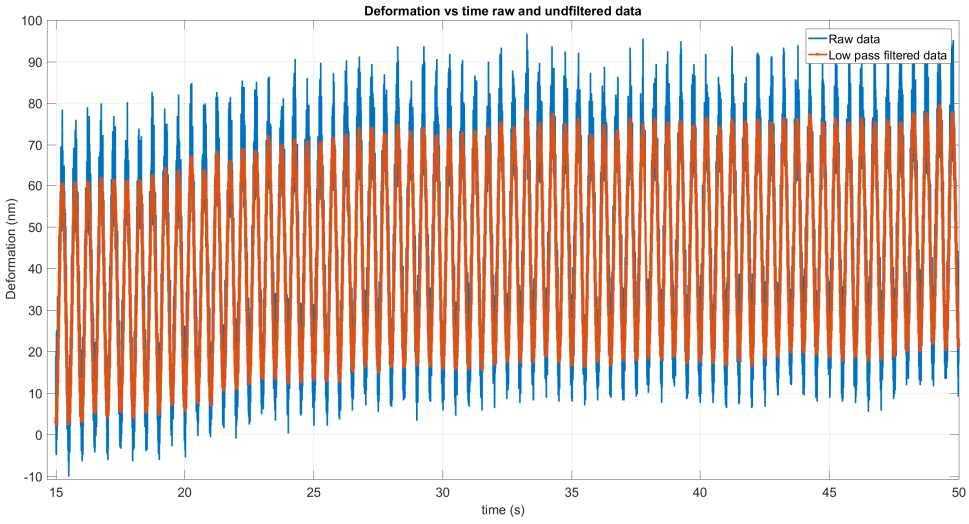

Figure B-5: Deformation vs Time for 40°C temperature

Similar filtering was applied to the deformation readings from the second laser probe (reference probe) that measured gave rough estimate of the overall drift in the setup. This filtered deformation was then subtracted from the main filtered deformation data (B-5). The resulting deformation canceled much of the overall temperature drift in the setup, but still minor drift in few nanometers was left in the resulting data as seen in fig. B-6.

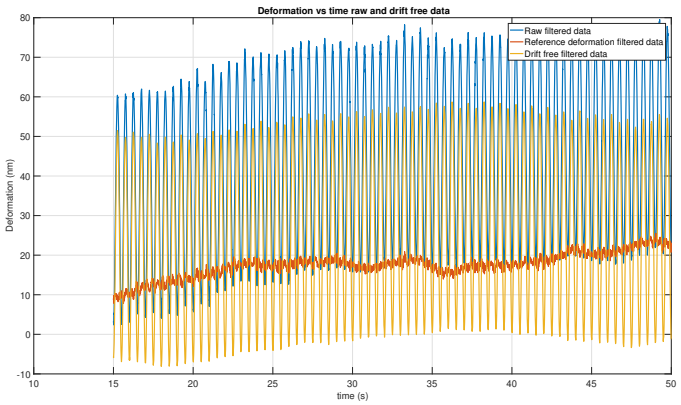

Figure B-6: Reference probe deformation, Raw filtered deformation, Drift free (rough) deformation

The resulting filtered data was then processed for canceling the minor drift effects due to variations in the setup because of temperature change(changes in refractive index of air between actuator and laser probe) (due to long thermal equilibrium times for laser probe holder, copper block, heat sink because fluctuations in room temperature). The drift effects were of much lower frequency that the actuation frequency (lowest frequency of interest). Hence, 1s periods were selected, the first sample was subtracted from that period to cancel the drift effects, and the resulting periods (35 because of 35s measurement time) were then averaged. At certain temperature the 2 standard deviation error between the mean and every period was about 2nm as seen in fig. B-7. This means 95% of all periods had an average error 1.2 nm (average of all 2 sigma deviations(shown in fig. B-7)). This percentage accounted for about 33 periods out of 35 periods that were considered for the measurement. The error in the averaging later translates to error in the fitting of model parameters (see section 3-3).

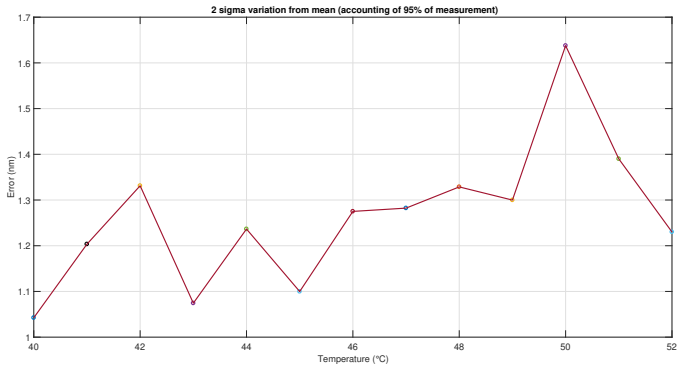

Figure B-7: Averaging error in terms of standard deviation from mean of all periods for a particular temperature

Similar averaging and filtering was done for voltage signal, but due to minor variations, the results did not change much.

Temperature Measurement NTC 10K thermister was used for measuring real time temperature right next to the actuator. The temperature of the actuator was assumed to be the same as that predicted by the temperature sensor. The sensor was calibrated with a reference resistor to verify the voltage reading of the sensor. The sensor was then built in with a voltage divider using a 15KΩ resistor. The resulting voltage across the resistor was used as the signal to the IO104 input. The supply voltage to the voltage divider circuit from IO104 analog output was 5V. Using the Steinhart–Hart equation [57] and by calculating the coefficients of the equation using the manufacturer data-table for NTC 10K thermister, actual temperature in Kelvin (which was then converted to $°C$) was obtained. The data was filtered using a low pass filter at 2Hz because the variations in temperature were assumed to be occurring at frequency less than 0.1 Hz. The resulting data is shown in fig. B-8.

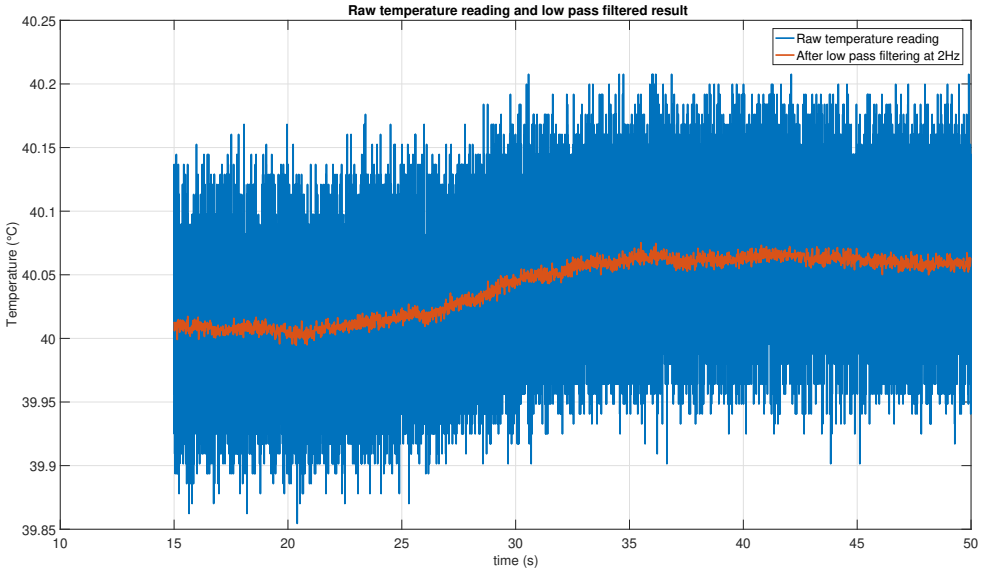

Figure B-8: Raw temperature and low pass filtered data

As seen in fig. B-8 the maximum variation in the temperature is $0.0806°C$.

Delay Compensation Having averaged the deformation, a certain delay was observed in the measurement. The source of delay was not found but the amount of delay was found using step voltage signal (see fig. B-9) and triangular voltage signal induction (see fig. B-10).

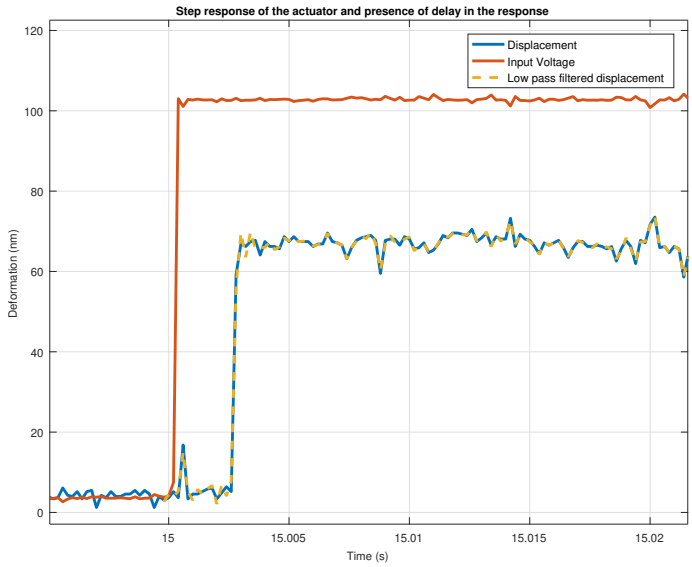

Figure B-9: Step response

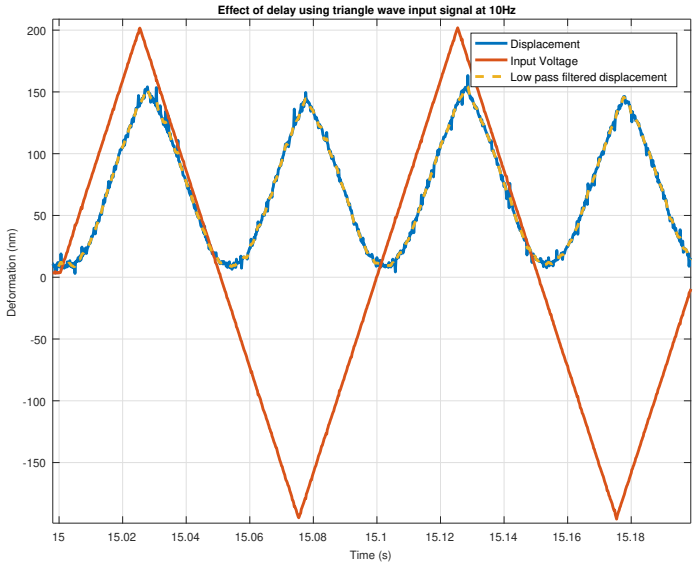

Figure B-10: Triangle wave response

From both B-10 and B-9, delay of 12 samples was observed. This observation was verified at different frequencies (with triangle voltage signal) and found to be the same. For the sampling frequency of 5kHz, 12 samples corresponded to a delay of 2.4ms. The delay was adjusted in the averaged deformation readings for further analysis.

Experiment setup pictures

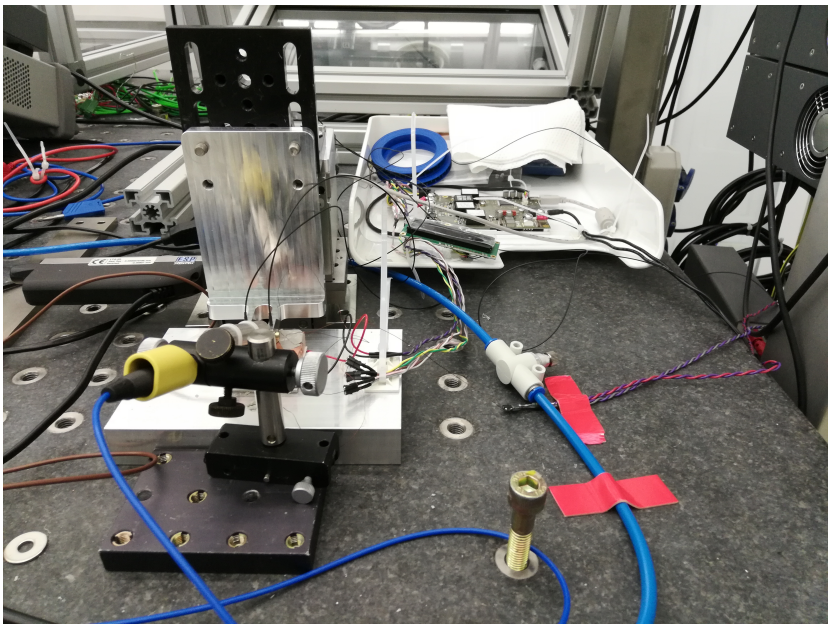

Figure B-11: Front view experiment setup

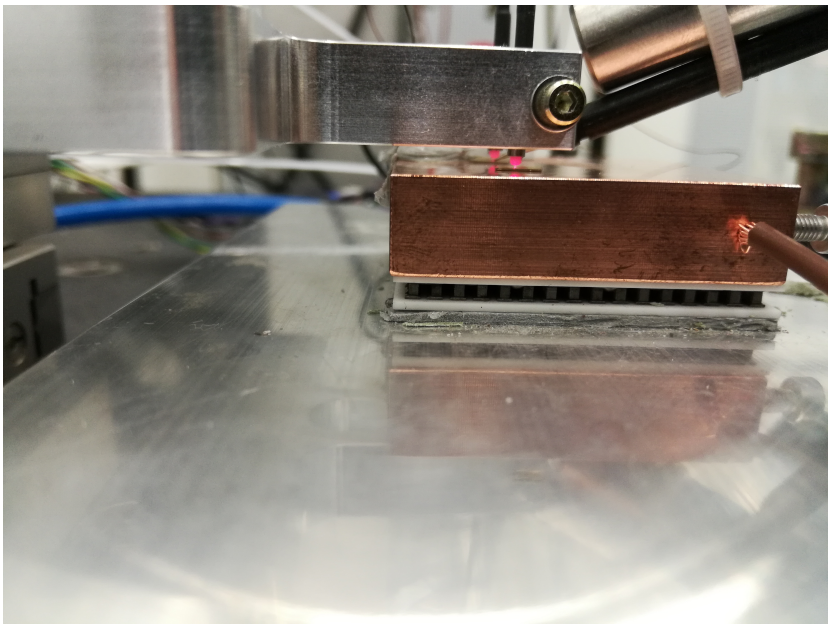

Figure B-12: Zoomed in picture of actuators and laser probes

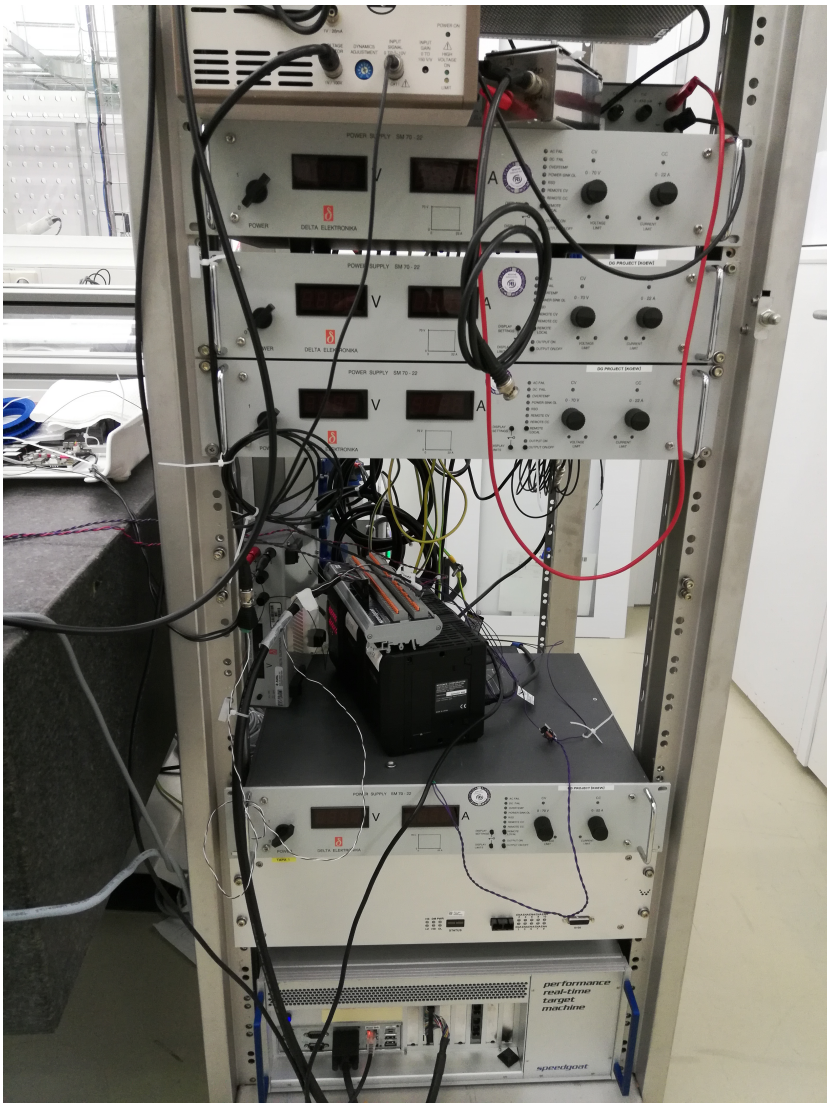

Figure B-13: Other instruments in the experiment setup

Bibliography

[1] "ASML DUV machine." https://www.asml.com/products/systems/twinscan-nxt/tw/s46772?dfp_product_id=11191. Accessed: 2010-09-30.

[2] G. H. Blackwood and M. A. Ealey, "Electrostrictive behavior in lead magnesium niobate (pmn) actuators. i. materials perspective," *Smart Materials and Structures*, vol. 2, no. 2, p. 124, 1993.

[3] D. Guzmán, F. J. d. C. Juez, F. S. Lasheras, R. Myers, and L. Young, "Deformable mirror model for open-loop adaptive optics using multivariate adaptive regression splines," *Opt. Express*, vol. 18, p. 6492, Mar. 2010.

[4] K. Uchino, Y. Tsuchiya, S. Nomura, T. Sato, H. Ishikawa, and O. Ikeda, "Deformable mirror using the PMN electrostrictor," *Appl. Opt.*, vol. 20, p. 3077, Sept. 1981.

[5] C. L. Hom, "Simulating electrostrictive deformable mirrors: II. Nonlinear dynamic analysis," *Smart Mater. Struct.*, vol. 8, pp. 700–708, Oct. 1999.

[6] C. L. Hom and N. Shankar, "Constitutive model for relaxor ferroelectrics," (Newport Beach, CA), p. 134, June 1999.

[7] F. Li, L. Jin, Z. Xu, and S. Zhang, "Electrostrictive effect in ferroelectrics: An alternative approach to improve piezoelectricity," *Applied Physics Reviews*, vol. 1, no. 1, p. 011103, 2014.

[8] V. Sundar and R. E. Newnham, "Electrostriction and polarization," *Ferroelectrics*, vol. 135, pp. 431–446, Oct. 1992.

[9] R. E. Newnham, V. Sundar, R. Yimnirun, J. Su, and Q. M. Zhang, "Electrostriction: Nonlinear Electromechanical Coupling in Solid Dielectrics," *J. Phys. Chem. B*, vol. 101, pp. 10141–10150, Nov. 1997.

[10] F. Li, S. Zhang, T. Yang, Z. Xu, N. Zhang, G. Liu, J. Wang, J. Wang, Z. Cheng, Z.-G. Ye, *et al.*, "The origin of ultrahigh piezoelectricity in relaxor-ferroelectric solid solution crystals," *Nature communications*, vol. 7, p. 13807, 2016.

[11] D. M. Fanning, *Structure property relations in ferroelectric materials*. University of Illinois at Urbana-Champaign, 2000.

[12] Y. Namba and H. Takahashi, "Ultra-precision surface grinding of pmn-pt relaxor-based ferroelectric single crystals," *CIRP annals*, vol. 59, no. 1, pp. 589–592, 2010.

[13] C. L. Hom, S. A. Brown, and N. Shankar, "Constitutive and failure models for relaxor ferroelectric ceramics," (San Diego, CA), pp. 316–328, May 1996.

[14] C. L. Hom and N. Shankar, "A fully coupled constitutive model for electrostrictive ceramic materials," *Journal of Intelligent Material Systems and Structures*, vol. 5, no. 6, pp. 795–801, 1994.

[15] Wikipedia, "Ferroelectricity — Wikipedia, the free encyclopedia." http://en.wikipedia.org/w/index.php?title=Ferroelectricity&oldid=894109069, 2019. [Online; accessed 31-May-2019].

[16] M. A. Ealey, "Standard SELECT electrostrictive lead magnesium niobate actuators for active and adaptive optical components," *Opt. Eng.*, vol. 29, no. 11, p. 1373, 1990.

[17] D. Damjanovic and R. Newnham, "Electrostrictive and Piezoelectric Materials for Actuator Applications," *Journal of Intelligent Material Systems and Structures*, vol. 3, pp. 190–208, Apr. 1992.

[18] F. Craciun, "Strong variation of electrostrictive coupling near an intermediate temperature of relaxor ferroelectrics," *Physical Review B*, vol. 81, no. 18, p. 184111, 2010.

[19] S. Sherrit, G. Catoiu, and B. Mukherjee, "The characterisation and modelling of electrostrictive ceramics for transducers," *Ferroelectrics*, vol. 228, no. 1, pp. 167–196, 1999.

[20] C. B. DiAntonio, F. A. Williams, and S. M. Pilgrim, "The use of harmonic analysis of the strain response in pb (mg/sub 1/3/nb/sub 2/3/) o/sub 3/-based ceramics to calculate electrostrictive coefficients," *IEEE transactions on ultrasonics, ferroelectrics, and frequency control*, vol. 48, no. 6, pp. 1532–1538, 2001.

[21] C. Hom, S. Pilgrim, N. Shankar, K. Bridger, M. Massuda, and S. Winzer, "Calculation of quasi-static electromechanical coupling coefficients for electrostrictive ceramic materials," *IEEE Trans. Ultrason., Ferroelect., Freq. Contr.*, vol. 41, pp. 542–551, July 1994.

[22] Z.-Y. Cheng, R. S. Katiyar, X. Yao, and A. Guo, "Dielectric behavior of lead magnesium niobate relaxors," *Phys. Rev. B*, vol. 55, pp. 8165–8174, Apr. 1997.

[23] C. Stringer, T. Shrout, and C. Randall, "High-temperature perovskite relaxor ferroelectrics: A comparative study," *Journal of Applied Physics*, vol. 101, no. 5, p. 054107, 2007.

[24] W. Ren, A. Masys, G. Yang, and B. Mukherjee, "The variation of piezoelectric and electrostrictive strain as a function of frequency and applied electric field using an interferometric technique," in *ISAF 2000. Proceedings of the 2000 12th IEEE International Symposium on Applications of Ferroelectrics (IEEE Cat. No. 00CH37076)*, vol. 1, pp. 85–88, IEEE, 2000.

[25] R. Wongmaneerung, R. Yimnirun, and S. Ananta, "Synthesis and electrical properties of pb (mg1/3nb2/3) o3–pbtio3 ceramics," *Current Applied Physics*, vol. 9, no. 1, pp. 268–273, 2009.

[26] D.-H. Suh, D.-H. Lee, and N.-K. Kim, "Phase developments and dielectric/ferroelectric responses in the pmn–pt system," *Journal of the European Ceramic Society*, vol. 22, no. 2, pp. 219–223, 2002.

[27] A. Glazounov, A. Bell, and A. Tagantsev, "Relaxors as superparaelectrics with distributions of the local transition temperature," *Journal of Physics: Condensed Matter*, vol. 7, no. 21, p. 4145, 1995.

[28] Z.-Y. Cheng, R. Katiyar, X. Yao, and A. Guo, "Dielectric behavior of lead magnesium niobate relaxors," *Physical Review B*, vol. 55, no. 13, p. 8165, 1997.

[29] G. H. Blackwood and M. A. Ealey, "Electrostrictive behavior in lead magnesium niobate (PMN) actuators. I. Materials perspective," *Smart Mater. Struct.*, vol. 2, pp. 124–133, June 1993.

[30] J. Zhao, Q. Zhang, N. Kim, and T. Shrout, "Electromechanical properties of relaxor ferroelectric lead magnesium niobate-lead titanate ceramics," *Japanese journal of applied physics*, vol. 34, no. 10R, p. 5658, 1995.

[31] N. Shankar and C. L. Hom, "An acoustic/thermal model for self-heating in pmn sonar projectors," *The Journal of the Acoustical Society of America*, vol. 108, no. 5, pp. 2151–2158, 2000.

[32] R. C. Smith and C. L. Hom, "Temperature-dependent hysteresis model for relaxor ferroelectrics," in *Smart Structures and Materials 2000: Active Materials: Behavior and Mechanics*, vol. 3992, pp. 267–278, International Society for Optics and Photonics, June 2000.

[33] K. Abe, "Temperature stability of a pbzmt electrostrictive ceramic," *Japanese journal of applied physics*, vol. 28, no. S2, p. 43, 1989.

[34] R. Wongmaneerung, R. Guo, A. Bhalla, R. Yimnirun, and S. Ananta, "Thermal expansion properties of pmn–pt ceramics," *Journal of Alloys and Compounds*, vol. 461, no. 1-2, pp. 565–569, 2008.

[35] S. Zhang, "Experimental Methods," in *Electric-Field Control of Magnetization and Electronic Transport in Ferromagnetic/Ferroelectric Heterostructures*, pp. 49–74, Berlin, Heidelberg: Springer Berlin Heidelberg, 2014.

[36] Q. Zhang, J. Zhao, T. R. Shrout, and L. Cross, "The effect of ferroelastic coupling in controlling the abnormal aging behavior in lead magnesium niobate-lead titanate relaxor ferroelectrics," *Journal of materials research*, vol. 12, no. 7, pp. 1777–1784, 1997.

[37] C. B. DiAntonio, F. A. Williams, S. M. Pilgrim, and W. A. Schulze, "An investigation into the spectral analysis of dielectric aging in ferroelectrics," *IEEE transactions on ultrasonics, ferroelectrics, and frequency control*, vol. 49, no. 9, pp. 1330–1339, 2002.

[38] W. Ren, A. Masys, G. Yang, and B. Mukherjee, "Nonlinear strain and dc bias induced piezoelectric behaviour of electrostrictive lead magnesium niobate-lead titanate ceramics under high electric fields," *Journal of Physics D: Applied Physics*, vol. 35, no. 13, p. 1550, 2002.

[39] S. P. Leary, "Harmonic Analysis of the Polarization Response in Pb(Mg,/,Nb2/,) (03-based Ceramics-A Study in Aging," p. 7.

[40] C. B. DiAntonio, F. A. Williams, S. M. Pilgrim, and W. A. Schulze, "An investigation into the spectral analysis of dielectric aging in ferroelectrics," *IEEE Transactions on Ultrasonics, Ferroelectrics, and Frequency Control*, vol. 49, pp. 1330–1339, Sept. 2002.

[41] E. V. Colla, L. K. Chao, and M. Weissman, "Multiple aging mechanisms in relaxor ferroelectrics," *Physical Review B*, vol. 63, no. 13, p. 134107, 2001.

[42] T. R. Shrout, W. Huebner, C. A. Randall, and A. Hilton, "Aging mechanisms in pb (mg1/3nb2/3) o3-based relaxor ferroelectrics," *Ferroelectrics*, vol. 93, no. 1, pp. 361–372, 1989.

[43] S. M. Pilgrim, "Electrostrictive ceramics for low-frequency active transducers," *IEEE transactions on ultrasonics, ferroelectrics, and frequency control*, vol. 47, no. 4, pp. 861–876, 2000.

[44] S. A. Brown, C. L. Hom, M. Massuda, J. D. Prodey, K. Bridger, N. Shankar, and S. R. Winzer, "Electromechanical testing and modeling of a pb (mg1/3nb2/3) o3-pbtio3-batio3 relaxor ferroelectric," *Journal of the American Ceramic Society*, vol. 79, no. 9, pp. 2271–2282, 1996.

[45] H. C. Robinson and E. A. McLaughlin, "Frequency dependence of pmn-pt ceramics under electrical bias," in *Smart Structures and Materials 2002: Active Materials: Behavior and Mechanics*, vol. 4699, pp. 532–542, International Society for Optics and Photonics, 2002.

[46] N. Della Schiava, K. Thetpraphi, M.-Q. Le, P. Lermusiaux, A. Millon, J.-F. Capsal, and P.-J. Cottinet, "Enhanced Figures of Merit for a High-Performing Actuator in Electrostrictive Materials," *Polymers*, vol. 10, p. 263, Mar. 2018.

[47] "TRS semiconductors." http://www.trstechnologies.com/Resources. Accessed: 2010-09-30.

[48] S. Sherrit, "Characterization of Piezoelectric Materials for Transducers," p. 45.

[49] Y. M. Shkel, "Electrostriction: material parameters and stress/strain constitutive relations," *Philosophical Magazine*, vol. 87, pp. 1743–1767, Apr. 2007.

[50] "Keyence Interferometers micro-head spectral-interference laser displacement meter." https://www.keyence.com/products/measure/spectral/si-f/index.jsp. Accessed: 2019-06-30.

[51] "Peltier Heater te technology inc.." https://tetech.com/product/hp-199-1-4-1-5/. Accessed: 2019-06-30.

[52] "Thermo Electric Cooling Temperature Controller meerstetter engineering." https://www.meerstetter.ch/compendium/heating-and-cooling-with-a-peltier-controller. Accessed: 2019-06-30.

[53] "Speedgoat Target PC speedgoat." https://www.speedgoat.com/products-services/real-time-target-machines. Accessed: 2019-06-30.

[54] "IO104 module speedgoat." https://www.speedgoat.com/help/slrt/page/io_main/refentry_ref_io104. Accessed: 2019-06-30.

[55] "Trek PZD350A Amplifier trek." http://www.trekinc.com/products/PZD350A.asp. Accessed: 2019-06-30.

[56] "Bode100 signal generator." https://www.omicron-lab.com/fileadmin/assets/Bode_100/Documents/Bode_100_R2_Technical_Data_V1.2.pdf. Accessed: 2019-06-30.

[57] "Steinhart–Hart equation wikipedia." https://en.wikipedia.org/wiki/Steinhart%E2%80%93Hart_equation. Accessed: 2019-06-30.